

ASSOCIATION EURATOM - UNIVERSITY OF LATVIA

AEUL



ANNUAL REPORTS 2007 – 2013

SUMMARY

Riga 2014

TABLE OF CONTENT

1. INTRODUCTION.....	3
2. Year 2007.....	3
3. Year 2008.....	10
4. Year 2009.....	24
5. Year 2010.....	33
6. Year 2011.....	44
7. Year 2012.....	57
8. Year 2013.....	72

INTRODUCTION

This Report summarises the fusion research activities of the Latvian Research Unit of the Association EURATOM-University of Latvia in the period 2007 2013.

The Latvian Research Unit of the Association EURATOM-University of Latvia consists of three Institutes of University of Latvia.

1. IP UL – Institute of Physics, University of Latvia

32 Miera St., Salaspils LV-2169, Latvia.

Phone +371 6 7944700, Fax. +371 6 7901214

ISSP UL – Institute of Solid State Physics, University of Latvia

8 Kengaraga St., Riga LV-1063, Latvia.

Phone +371 6 7187810, Fax. +371 6 7132778

ICP UL - Institute of Chemical Physics, University of Latvia

4 Kronvalda Blvd., Riga LV-1010, Latvia.

Phone +371 6 7033884, Fax. +371 6 7033884

I wish to express my thanks to all those who have assisted the progress of the Association EURATOM-University of Latvia, in particular: EURATOM officers; the staff of the EFDA close support units, the Ministry of Education and Science of Latvia, University of Latvia, members of the associated committees, the administrative staff of the Association, and last,— but not least, the scientists and technicians who have been actively involved in the R&D programme of the Association.

A. Sternberg

Director of the ISSP UL

Head of the Research Unit of the EURATOM - University of Latvia (AEUL)

YEAR 2007

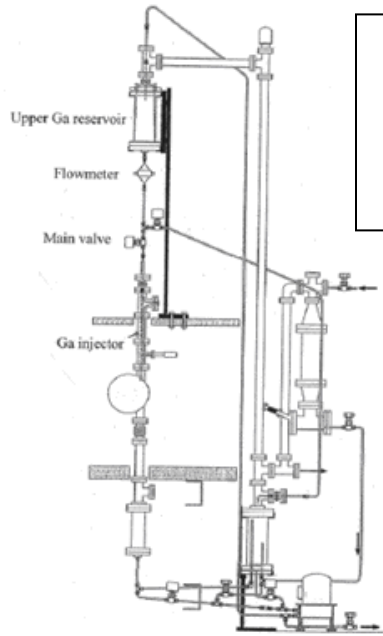
FUSION RELATED LIQUID METAL MHD RESEARCH.

Principal investigator: E.Platacis

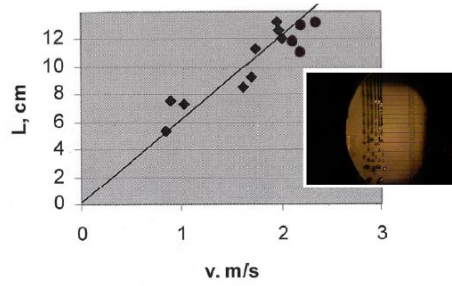
PREPARATION OF A GALLIUM MULTI-JET LIMITER FOR INSTALLATION ON TOKAMAK ISTTOK.

Chapters of the Annual Report: a) Initial conditions for development of multi-jet limiter for ISTTOK; b) Behavior of individual jet in multi-jet injectors; c) Water as a modeling liquid for investigation Rayleigh instability in liquid metals.

Most informative illustrations



Scheme of Ga limiter installed on ISTTOK
Break-up length in the svstem of three InGaSn iets



INVESTIGATION OF METAL IONS IN FUSION PLASMAS USING EMISSION SPECTROSCOPY

Principal investigator: I. Tale

Investigation of single and multiple ionized Ga atoms in the tokamak plasma.

The following experimental setup (Fig.1.) present at ISTTOK was used for the obtaining of the spectral and spatial information of the plasma.

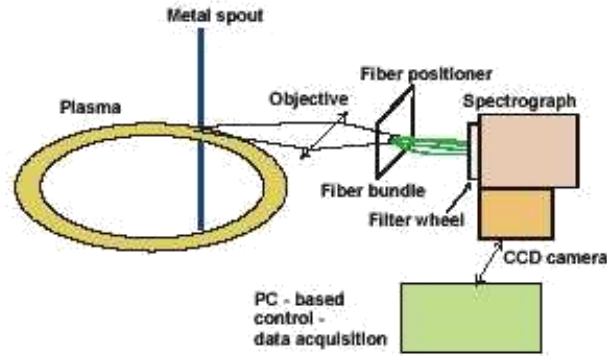


Fig.1. Experimental set-up

Owing to its privileged viewing area with regards to the observation of the light emitted during plasma-liquid metal interaction, the tokamak port has been used to place the collection optics for a multi-channel (7 viewing points in a radial direction) optical fiber relaying radiation to a ½ m imaging monochromator (CVI laser DK480). This apparatus is equipped with a triple-grating turret system, blazed at 300, 500 and 750 nm and 1200 gr/mm each. A spectroscopic CCD (Spectral Products SPH5) camera at the output focal plane of the spectrometer allows the acquisition of line intensities emitted from the plasma in the 200 to 900 nm spectral region. During each discharge it was possible to obtain 4 spectra corresponding to 4 viewing lines of sight radially distributed (due to the magnification ratio of the spectrometer to fiber coupling optics, three end channels of the fiber were lost), and focused on the liquid metal jet poloidal plane where it covers 1.2 cm span. The main advantage of this diagnostic was clearly to identify the presence of gallium (both neutral and ion species) in the plasma.

Fig. 2 a) illustrates a spectrum that shows the characteristic lines of neutral gallium at 417.2 and 403.3 nm. In the same figure it is also possible to identify a few spectral lines produced by gallium ions (both Ga^+ and Ga^{2+}). The analysis of the mentioned spectra, acquired during a shot by shot spatial scan of the plasma, granted additional information on the neutral and ions relative distribution in the radial direction. The results are presented in Fig. 2 b). As expected, the maximum emission for neutral gallium is seen in the vicinity of the jet position while species of higher degrees of ionization penetrate deeper inside the plasmas owing to radial diffusion. In practice since viewing is done along a toroidal direction and ions are transported along the magnetic field lines it should be pointed out that the observed distribution is broadened with regards to the real one. The maximum intensities in the emission profiles are close to each other due to the low ionization potential for the gallium ions (6, 20.5 and 30.7 eV for GaI, II and III, respectively).

The procedure used in the blue region of the spectra has been repeated in the red since several other lines are available for this study to be performed. ($\lambda_{\text{GaI}}=639.7$ nm, $\lambda_{\text{GaII}}=633.4$ nm and $\lambda_{\text{GaIII}}=599.4$ nm). It is important to notice that when the liquid metal jet is not present in the chamber no traces of gallium lines (within the sensitivity of the CCD camera) were observed. In spite of having the data available for the line intensities it has not been possible to obtain density values for the liquid metal reaching the plasma since no absolute calibration has been performed.

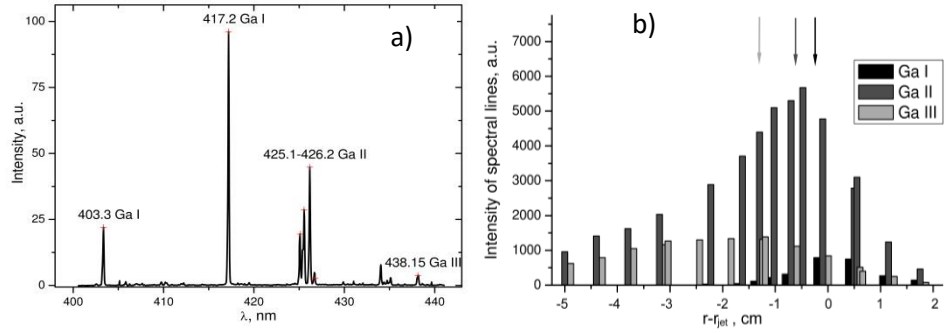


Fig. 2. a) Characteristic spectrum of gallium and b) distribution in ISTTOK plasma with the arrows indicating the maximum emission position.

Based on the experimental results obtained with a single gallium jet system installed at ISTTOK Portugal, the paper regarding technical details of the liquid metal jet system and spectroscopic information of the neutral and ionized Ga species was prepared, submitted and published in Fusion Engineering and Design, **83**, 1, 102-111 (2008):

“Interaction of a liquid gallium jet with the tokamak ISTTOK edge plasma”,

R.B. Gomes, H. Fernandes, C. Silva, A. Sarakovskis, T. Pereira, J. Figueiredo, B. Carvalho, A. Soares, C. Varandas, O. Lielausis, A. Klyukin, I.Tale

PLASMA PHYSICS EU TOPICAL GROUP: TG-MHD

Principal investigator: O. Dumbrajs

Non-complete sawtooth reconnection in the ASDEX Upgrade tokamak has been investigated.

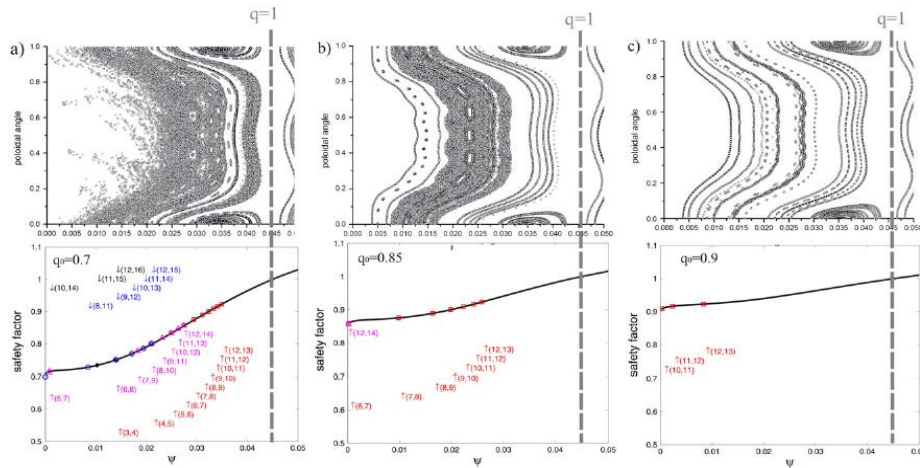


Figure 9. Poincaré plots for the same perturbations (1, 1) + (2, 2) + (3, 3) as in figure 4 but for different safety factor profiles. Note that stochasticization strongly depends on the existence of the low-order rational surfaces which are marked on the safety factor curves. (a) Central q -value is 0.7; (b) central q -value is 0.85; (c) central q -value is 0.9

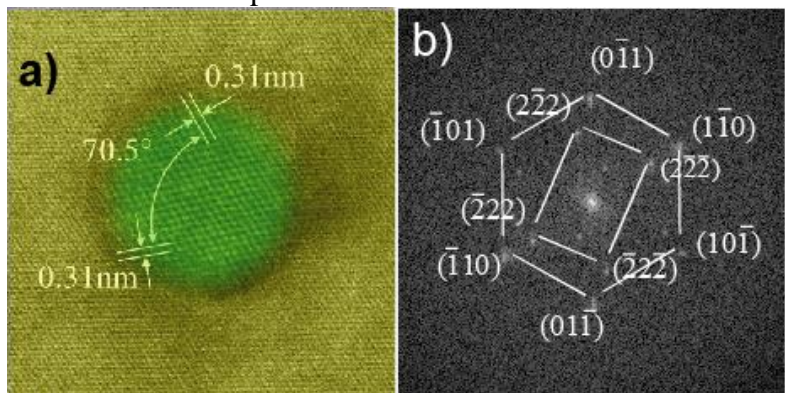
V. Igochine, O. Dumbrajs, H. Zohm, and A. Flaws. “Stochastic sawtooth reconnection in ASDEX Upgrade.” Nuclear Fusion 47, 23 (2007).

MATERIALS MODELING

Principal investigator: E.A. Kotomin

Point defects in fcc-Fe lattice

Reduced activation steels strengthened by Y_2O_3 precipitates are considered as candidate structure materials for future fusion reactors. In particular application of oxide dispersion strengthened (ODS) steels for fusion reactor blanket structure allows increasing its operation temperature by $\sim 100^\circ C$. Both size and spatial distributions of oxides significantly affect mechanical properties and irradiation resistance of oxide dispersion strengthened (ODS) steels. The mechanism of ODS particle formation is still not clear.



HRTEM micrographic image of Y_2O_3 nanoparticle embedded into ferrite matrix (a) and its Fourier transformation (b). The parallel orientation between Fe (110) and Y_2O_3 (111) directions have been confirmed on various small ODS particles. (obtained by M. Klimenkov, KIT / IAM, Karlsruhe).

- Lattice constant of *fcc* Fe has been calculated to be 3.44 Å while cohesive energy is 4.96 eV/atom, qualitatively close to experiments.
- Presence of Fe vacancy noticeably re-distributes the electronic density in iron matrix.
- The vacancy formation energy for 4×4×4 supercell has been found to be 2.37 eV with 0.75% inward relaxation.
- It has been found that O impurities can be located inside the tetrahedral and octahedral interstitials of *fcc* Fe lattice serving as an acceptor of electronic charge (1.3-1.4 *e*) whereas Y atom can only substitute Fe atom in its vacancy serving as a donor (~1 *e*).

FUSION TECHNOLOGY

Principal investigator G. Kizane

The main tasks of the ICP UL in the frame of the Fusion Technology Programme were following:

1. determination of tritium amount and distribution in a divertor materials of the JET;
2. investigation of temperature programmed tritium release from plasma exposed divertor materials and neutron irradiated beryllium pebbles under separate or simultaneous action of fast electrons and magnetic field;
3. analysis of dust and flakes from the JET.

In order to realize the EFDA JET tasks were –

- prepared the working places- the separate laboratory for a sample sawing and cutting
- the work place at the radiation thermal magnetic rig at Salaspils, Latvia.
- arranged storage place for plasma exposed tiles,
- purchased tritium monitors with tritium gas flow detector,
- adapted new analysis methods.

The main facilities used for analysis of the samples were following - electron accelerator ELU-4, radiation thermo-magnetic set up on bases of the ELU-4, a Vance apparatuses, liquid scintillation spectrometer TRiCarb, tritium monitors with gas flow detector, thermal analysis TG/DTA Seiko Exstar 3600TG/DTA, Scanning Electron Microscope SEM – EDAX Hitachi S-4800 and JSM 6490, an X-ray diffractometer (XRD) Bruker D8 Advanced.

EFDA JET tasks from the year 2008-2014 were following:

JW8-FT-1.12 Determination of tritium and analysis of carbon-based plasma-facing components before and after their detritiation with different methods

JW9-FT- 3.46 Analysis of carbon-based plasma-facing components

JW10-FT- 3.62 Post mortem analysis of tritium accumulated in selected plasma facing components

JW11-FT-1.19 AMS and FCM measurements of tritium in laser cleaned tiles and tritium depth profiles in JET divertor tiles

JW12-FT- 1.20 Complete poloidal distribution of tritium retention in JET divertor tiles measured by AMS and FCM+SD analysing methods

JW13-FT-1.21 Analysis of tritium in JET tiles

JW13-FT- 1.23 Preparation for the analysis of long chain hydrocarbon in JET flake/dust material using TGA/DTA coupled to QMS & FTIR

All tasks have been performed in close co-operation with some EURATOM associations - EURATOM-UKAEA, Culham, EURATOM-KIT, Karlsruhe, EURATOM-FOM, Petten, EURATOM-TEKES, Helsinki, EURATOM – MEdC, Bucharest.

The ICP was participant of the EFDA Goal oriented training programmes:

1. from 2008-2012 – in the frame of the EFDA WP08 Breeding Blanket Development for Fusion Reactors on blanket breeder materials, work package WP8 on tritium behaviour in beryllium pebbles
2. from the 2012 is participant of the EFDA WP12 – BeFirst and work package WP5 includes developing methods for analysis of chemical forms of tritium in beryllium.

The ICP realized the grant for the Fusion for Energy (F4E) “Post Irradiation Examination of Be materials irradiated in HIDOBE-01 campaign”, in close cooperation with Karlsruhe Institute of Technology investigated tritium breeding ceramics, lithium orthosilicate.

2007

ICP continued investigations of tritium release from the Be pebbles irradiated in the EXOTIC 8-3/13 experiment. The project objective for the year 2007 was to test the stimulating effect of the simultaneous action of magnetic field (MF), temperature and ionizing radiation on the tritium release from beryllium pebbles and identification of chemical forms of tritium accumulated in the irradiated beryllium pebbles.

In order to realize the task setups and methods for determination of chemical forms of localized tritium and their distribution were optimized and the radiation thermal magnetic rig was tested and adjusted for investigations of tritium release from irradiated Be pebbles under separate and simultaneous action of temperature, radiation and magnetic field.

It should be noted that the EXOTIC-8-3/13 Be pebbles were found to be inhomogeneous with respect to the total tritium activity, A_T , which was found in the range 4-18 MBq/g. This inhomogeneity of the sample limited the accuracy of the determination of the abundance ratios of chemical forms of tritium as the identity of the two samples is essential for this determination, but was detected that the most part of tritium in the EXOTIC-8-3/13 Be pebbles, similarly to the BERYLLIUM pebbles and the JET tile “B”, is localized as molecular tritium T_2 , but the abundance ratios of T^0 and T^+ in the

EXOTIC-8-3/13 Be pebbles are about by a factor of two greater than those in the BERYLLIUM pebbles.

In order to investigate possible effect of MF on tritium release from the Be pebbles irradiated in the EXOTIC-8/13 experiment, they were annealed at a constant rate of temperature increase to 991 and 1123 K and then at a constant temperature for 4 h

Experiments in the radiation thermal magnetic rig show that the electron radiation (TR) and the simultaneous electron radiation and magnetic field (TRM) stimulates the tritium release at annealing in comparison with the action of only temperature of 940 K for 47 minutes. Degrees of detritiation obtained in these experiments show that under similar conditions the detritiation of the EXOTIC Be pebbles proceeded easier than that of the BERYLLIUM pebbles. That can be explained that the EXOTIC pebbles have smaller diameter (\varnothing 0.1-0.2 mm) than the BERYLLIUM pebbles (\varnothing 2 mm) and therefore a larger ratio of free surface to grain boundary surface. A larger abundance ratio of the atomic form T^0 could also contribute to a higher tritium release of the EXOTIC pebbles. A large degree of detritiation of 60% at 940 K for 47 min of the EXOTIC Be pebbles and a less abundance of the molecular form T_2 possibly could explain that facilitating radiation and MF effects on the degree of detritiation of the EXOTIC Be pebbles are relatively less than those on the detritiation of the BERYLLIUM pebbles.

Abundance ratios of chemical forms of tritium in the beryllium pebbles irradiated in the EXOTIC-8-3/13 experiment were determined: T_2 – 65%, T^0 – 23%, T^+ – 12%.

A complete detritiation of these pebbles was achieved at 1123 K for 4 h in a continuous flow of argon, magnetic field (MF) of 2.35 T had no appreciable effect on the tritium release.

At 940 K for 47 min, the degree of detritiation was 60%, 5 MeV fast-electron radiation of 14 MGy/h increased that to 76%, but the simultaneous action of the fast-electron radiation and MF of 1.7 T increased that to 88%.

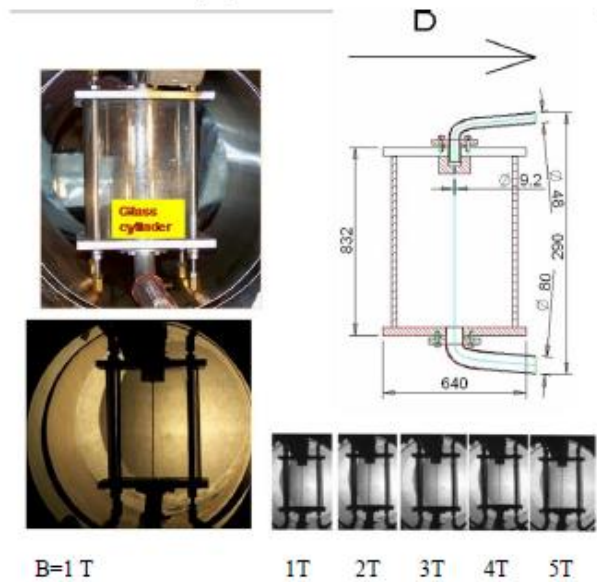
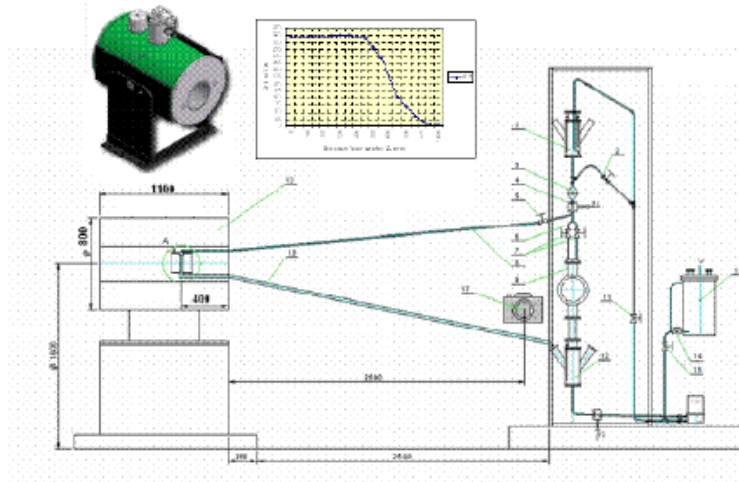
YEAR 2008

FUSION RELATED LIQUID METAL MHD RESEARCH.

Principal investigator: E.Platacis

PREPARATION OF A GALLIUM JET LIMITER FOR TESTING UNDER REACTOR RELEVANT CONDITIONS

Content: a)Abstract; b)Experimental setup; c)Stability of long liquid metal jets; d)Liquid metal jets in strong magnetic fields



Scheme for investigation of jets stability in homogeneous field.
 Test section with jet in a strong homogeneous field.

CHARACTERIZATION OF THE IMPURITY CONCENTRATION, PROFILING AND EROSION IN ITER RELEVANT MATERIALS USING LASER ABLATION

Principal investigator: I. Tale

Development of methodology of laser-induced breakdown spectroscopy for spectral-chemical analysis both the impurity content in TOKAMAK vessel tiles.

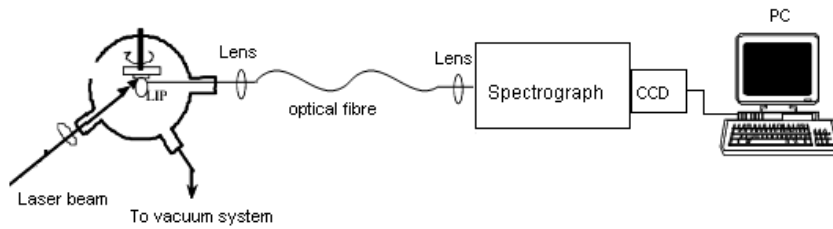


Fig.1 Schematic of the experimental setup

Q-switched Nd:YAG laser (SL-312, EKSPLA), 1064 nm, pulse repetition rate of 10 Hz, pulse width of 135 ps, and tuneable pulse energy up to 250 mJ.

Spectrograph Andor Shamrock sr-303i spectrograph with a grating of 1200 gr/mm. Andor CCD camera. The depth of the craters was estimated by Dektak 150 Surface profiler (Veeco Instruments, Inc.).

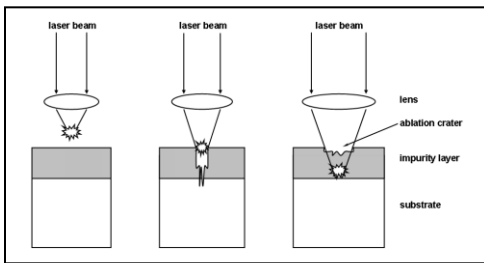


Fig.2. Laser beam focusing

Samples

Two types of samples were used: samples cut from the graphite R6710 divertor of the ASDEX Upgrade tokamak after a boronization process and graphite R6710 samples to provide a reference spectrum of carbon

Results

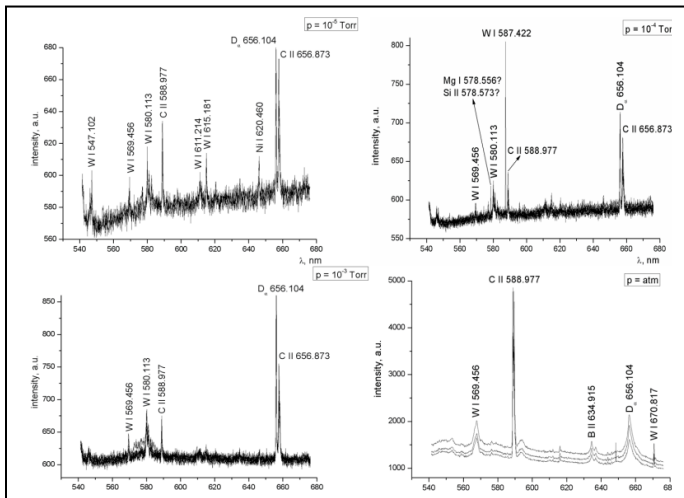


Fig 3. Line spectra of WI, BII , CII, D_{α} , at different gas pressure for ASDEX Upgrade tiles R 6730 after boronization.

Increase of gas pressure from 10^{-5} to 1.0 Torr results in diminish of number of lines and increase of relative intensities due to confinement of plasma at the region next to the surface of ablated material.

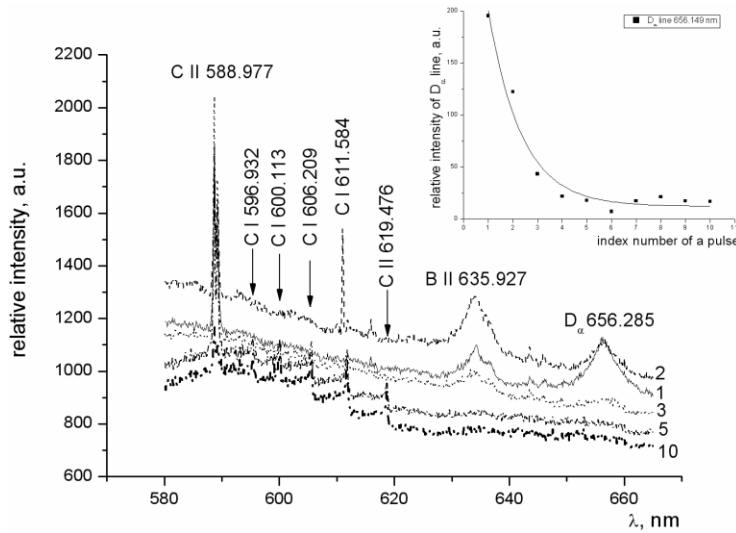


Fig.4. Appearance of D_{α} 656.285 nm line in the laser ablation spectrum of ASDEX Upgrade sample. The numbers on the right side correspond to the index number of the pulse in the sequence. The inset shows the decay of D_{α} 656.285 nm line intensity.

For ASDEX Upgrade sample the average material removal rate was about 0.5 μm per single laser pulse. However, for pure graphite sample this value was close to 70 nm. This is in agreement with the obtained fact, that target reflectance determines the amount of laser pulse power absorbed by the material. Additionally, surface defects are of great importance as they contribute to decreasing the laser intensity threshold required to initiate vaporization of the surface.

D_{α} line appears after the 1st laser pulse. Afterwards, the decrease of deuterium signal in comparison with the carbon line is observed. D_{α} line has nearly vanished after applying the 2nd laser pulse. The inset demonstrates that by the end of the series of laser treatment the intensity of D_{α} line has decreased almost two-fold compared to that after the 1st pulse. After a sharp decreasing of the intensity of deuterium line, the signal becomes practically equal to the background level

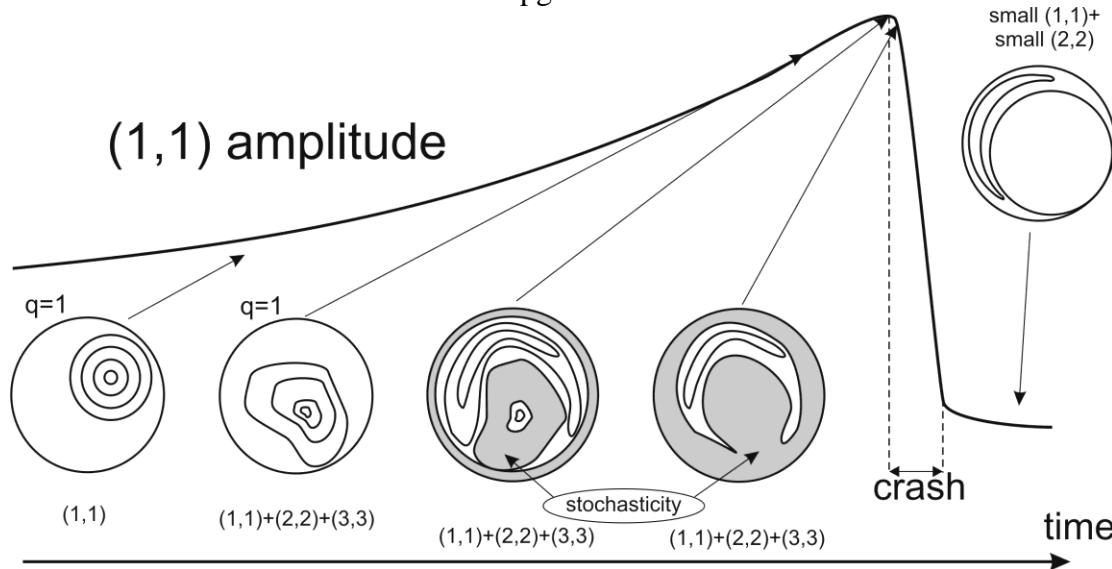
Conclusions

Qualitative elemental analysis of ASDEX inner wall tiles was performed by laser-induced plasma spectroscopy. The main advantages of this method are: its simplicity, its ability to simultaneously monitor all elements in plasma, that no sample preparation is required, and that it is able to analyse any material, irrespective of its physical state. The thickness of the ablated layer in the case of the PFM was around 0.5 μm per laser pulse, but for the polished reference sample about 70 nm. The spectra show a decrease of deuterium signal and an increasing signal of the substrate during the layer-by-layer ablation process. These results show that laser-induced breakdown spectroscopy is a potential method of analysis of migrating materials and co-deposited layers of PFMs. The quantitative characteristics of this effect will be the subject of further investigations. Additionally, laser scanning can be used as a procedure of deuterium removal from co-deposited layers.

PLASMA PHYSICS EU TOPICAL GROUP: TG-MHD

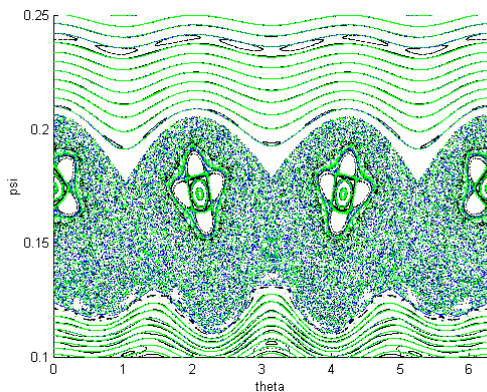
Principal investigator **O. Dumbrajs**

Heat diffusion coefficients in a stochastic magnetic field have been determined in the case of frequently interrupted regime of neoclassical tearing modes and of incomplete sawtooth reconnection in the ASDEX Upgrade tokamak.



O. Dumbrajs, V. Igochine, and H. Zohm, "Diffusion in a stochastic magnetic field in ASDEX Upgrade", Nucl. Fusion 48, 024011 (2008).

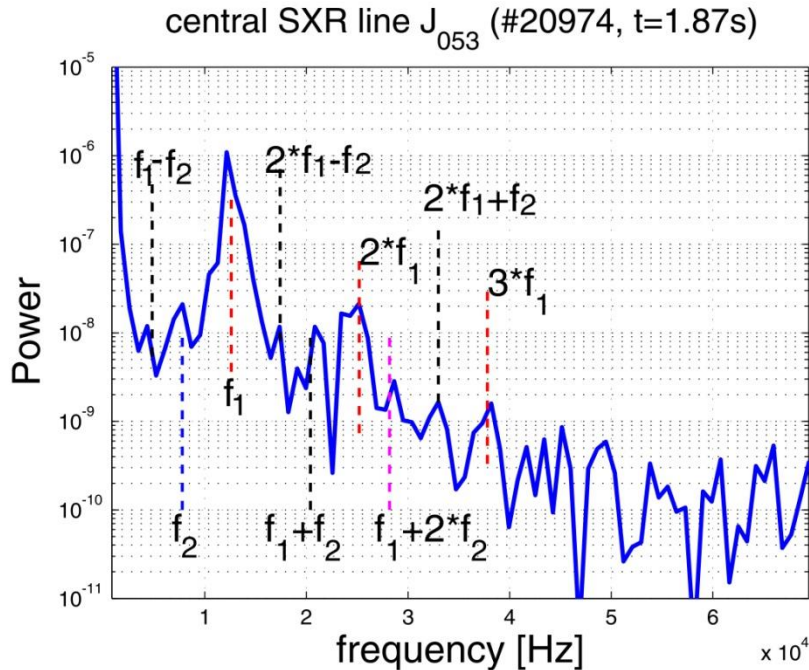
The optimum time stepping in some models for the study of magnetic field in tokamaks is determined by using local criteria. A special attention is given to the analysis of stochasticity produced by the time discretization.



Phase portrait.

D. Constantinescu, O. Dumbrajs, V. Igochine, and B. Weysow, "On the accuracy of some mapping techniques used to study the magnetic field dynamics in tokamaks," Nucl. Fusion 48, 024017 (2008).

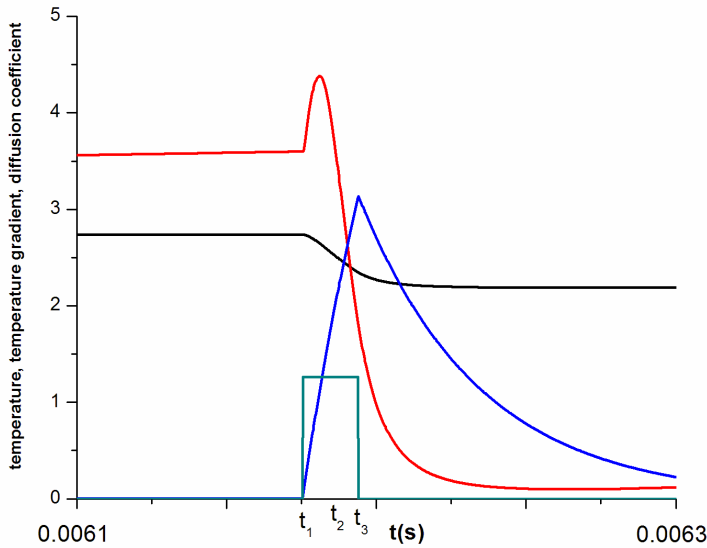
It has been demonstrated that during the pre-crash phase the quasiperiodic transition to chaos occurs.



Power spectrum in slightly quasiperiodic stage before the sawtooth crash. Low frequency part of the spectrum consists only from two incommensurable frequencies and their linear combinations. A relation between the primary frequencies is the golden mean ($f_2 = f_1(\sqrt{5}-1)/2$).

V. Igochine, O. Dumbrajs, and H. Zohm, "Transition from quasiperiodicity to chaos just before sawtooth crash in the ASDEX Upgrade tokamak" Nucl. Fusion 48, 062001 (2008).

A hysteresis model is used to describe experimental data on sawtooth crash in ASDEX Upgrade tokamak.



Hysteresis in sawtooth crash. Temperature gradient (red curve) rises until the instability threshold at $3.6\text{keV}/m$. At this moment $t = t_1$ the instability is turned on by switching the function Q (green curve, arbitrary units) to χ_{\max} . The central temperature (black curve) begins to decrease and diffusion coefficient (blue curve, arbitrary units) begins to increase. During further evolution due to hysteresis the function Q is switched back to χ_{\min} not at $t = t_2$ when temperature gradient passes again the instability threshold, but at $t = t_3$ when temperature gradient becomes equal to $\beta k = 1.8\text{keV}/m$.

O. Dumbrajs, V. Igochine, H. Zohm and ASDEX Upgrade Team, "Hysteresis in sawtooth crash in ASDEX Upgrade tokamak," The Open Plasma Physics Journal 1, 9-13 (2008).

GYROTRONS TOPICAL GROUP: TG-H&CD

Principal investigator O. Dumbrajs

Specific examples of hysteresis with respect to variation of magnetic field, current, electron beam radius and beam voltage are given.

O. Dumbrajs and T. Idehara, "Hysteresis in mode competition in high power 170 GHz gyrotron for ITER" Int. J. Infrared Millimeter Waves 29, 232 (2008).

Two continuous frequency tunable coaxial gyrotron oscillators are considered.

Z.C. Ioannidis, O. Dumbrajs, and I.G. Tigelis, "Linear and non-linear inserts for Genuinely wideband continuous frequency tunable coaxial gyrotron cavities," Int. J. Infrared Millimeter Waves 29, 416 (2008).

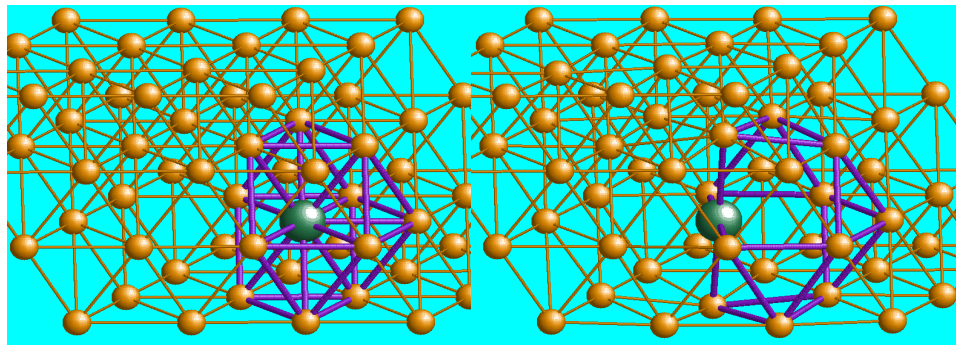
Mathematical formulation and numerical results for the resonant characteristics of the TM modes in a coaxial cavity with longitudinally corrugated insert is presented.

Z. C. Ioannidis, G. P. Latsas, I. G. Tigelis, and O. Dumbrajs, "TM Modes in Coaxial Cavities with Inner Surface Corrugations" IEEE Trans. Plasma Sci. 36, 2613 (2008).

MATERIALS MODELING

Principal investigator: E.A. Kotomin

MIGRATION OF IMPURITY ATOMS IN FCC-FE LATTICE



The model of Y substitute atom and vacancy migration in the *fcc*-Fe lattice.

- A barrier for oxygen atom migration between the nearest O and T positions has been found to be 1.1 eV (*cf.* 1.72-1.75 eV, according to various experimental studies).
- The formation energy of the Y-substitution defect in the γ -Fe lattice is estimated to be 0.48 eV
- The calculations on the interaction between the Y substitutional atom and Fe-vacancy at different inter-distances have been performed first. The results of these calculations clearly show that the attraction is found for the 1-NN, 3-NN and 4-NN configurations while the repulsion is observed for the 2-NN configuration. The relative displacement of Y atom towards Fe vacancy in the 1-NN configurations is the most significant (1.25 Å) as far as Y occupies intermediate position between two vacant lattice sites and the binding energy for this configuration is the largest (1.67 eV). The repulsive interaction between Y atom and Fe vacancy at 2-NN site might be caused by the two iron atoms which are positioned at 1-NN sites relatively to both point defects leading to the displacement of this Y atom away from the both neighboring iron atoms and Fe vacancy.

JW8-FT-1.12. DETERMINATION OF TRITIUM AND ANALYSIS OF CARBON-BASED PLASMA-FACING COMPONENTS BEFORE AND AFTER THEIR DETRITIATION WITH DIFFERENT METHODS

Principal investigator G. Kizane

A new project proposal “Determination of tritium and analysis of carbon-based plasma-facing components before and after their detritiation with different methods” has been prepared for the EFDA JET Technology Work programme 2008 and accepted as Task JW8-FT-1.12.

At the same time ICP continued investigation of tritium release from beryllium pebbles Exotic 8/8-13.

In the frame of the task JW8-FT-1.12. analysis of selected samples of plasma-facing components (PFCs) in order to support particle transport studies and development of in-situ detritiation methods

Investigations of properties of the tritium trapped in the deposited films, in the surface layers and in the bulk of CFC tiles with respect to temperature, radiation and magnetic field contribute to the development of detritiation methods.

.The workplace for mechanical treatment of carbon-based tiles used for this study was arranged in Salaspils. Samples for tritium analysis were prepared by core-drilling method. In order to determine the tritium content in the carbon samples, we use the combustion technique proposed by Vance. Three set-ups of Vance apparatuses were placed in a fume hood for full combustion method of a sample. The tritium was collected in two bubblers, 98-99 % of tritium was collected in the first bubbler. The time of a complete combustion, 10 h, depends on thickness of the carbon-based disc being combusted. After each combustion water aliquots were taken for analysis for total tritium determination with a TRiCarb 2910TR counter. Conditions for the combustion of carbon-based samples were checked by thermogravimetric method. The combustion reaction reaches its maximum rate at 803-808 °C.

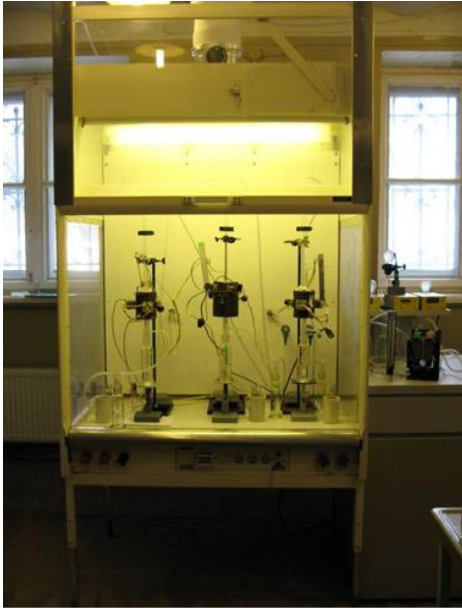
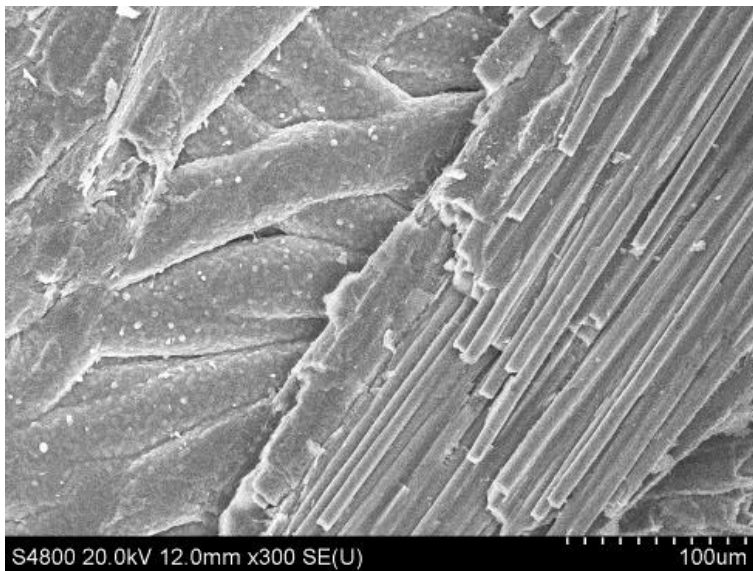


Figure 1. General view of fume hood with set-up of 3 Vance apparatuses

Scanning electron micrographs shows coarse fibres of different orientations. Interfibre porosity was observed, fibre diameter can be estimated to be about $40\ \mu\text{m}$, a multi-layered concentric structure of the fibre around a core of diameter about $7\text{-}10\ \mu\text{m}$ was visible.



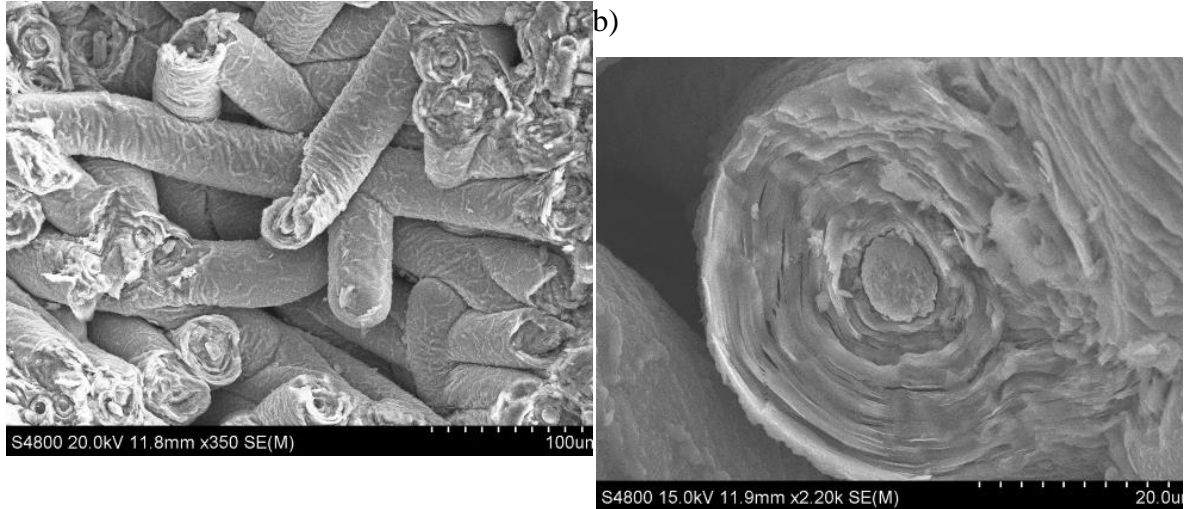


Figure 2. Scanning electron micrographs of a sample from an inner part of CFC tile 3BW G4A

Tritium distribution was analysed for carbon-based tile 3BWG4A, it has been taken out of the MkII Gas Box divertor of the JET, operated during the years 1998-2001. This cylinder was core drilled out of the tile and cut into discs in the Tritium Laboratory Karlsruhe. These discs were analysed on tritium activity in our laboratory at the University of Latvia. Distribution of tritium activity in cylinder 11 of tile 3BWG4A is unequal, 99.9% of tritium is located in the first disc of cylinder 11 of tile 3BWG4A, the mass activity of the plasma-facing surface disc - was 0.6 GBq/g, but that of the next discs - was 0.17 MBq/g and 96 kBq/g accordingly. Then the tritium activity gradually increases in the sequence of discs A3 to A17 and finally to the rest of the cylinder, i.e. for disc A17 – 0.17 MBq/g and for the rest – 0.32 MBq/g.

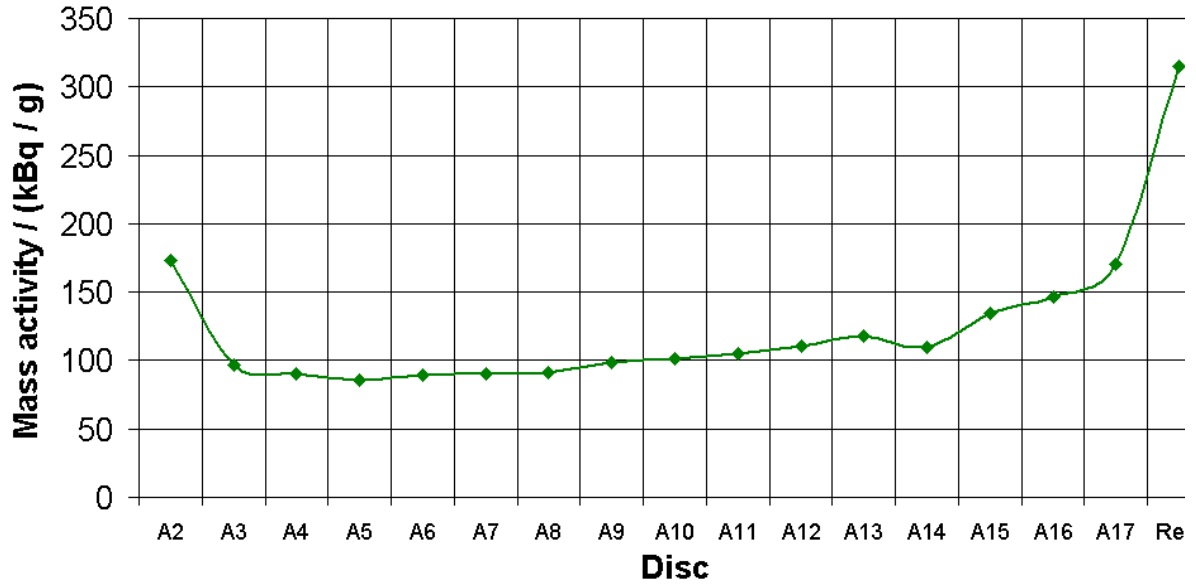


Figure 3. Mass activity of tritium for discs A2-A17 and the rest of cylinder 11 of tile 3BWG4A, divertor MkII Gas Box

Tritium release by thermal desorption

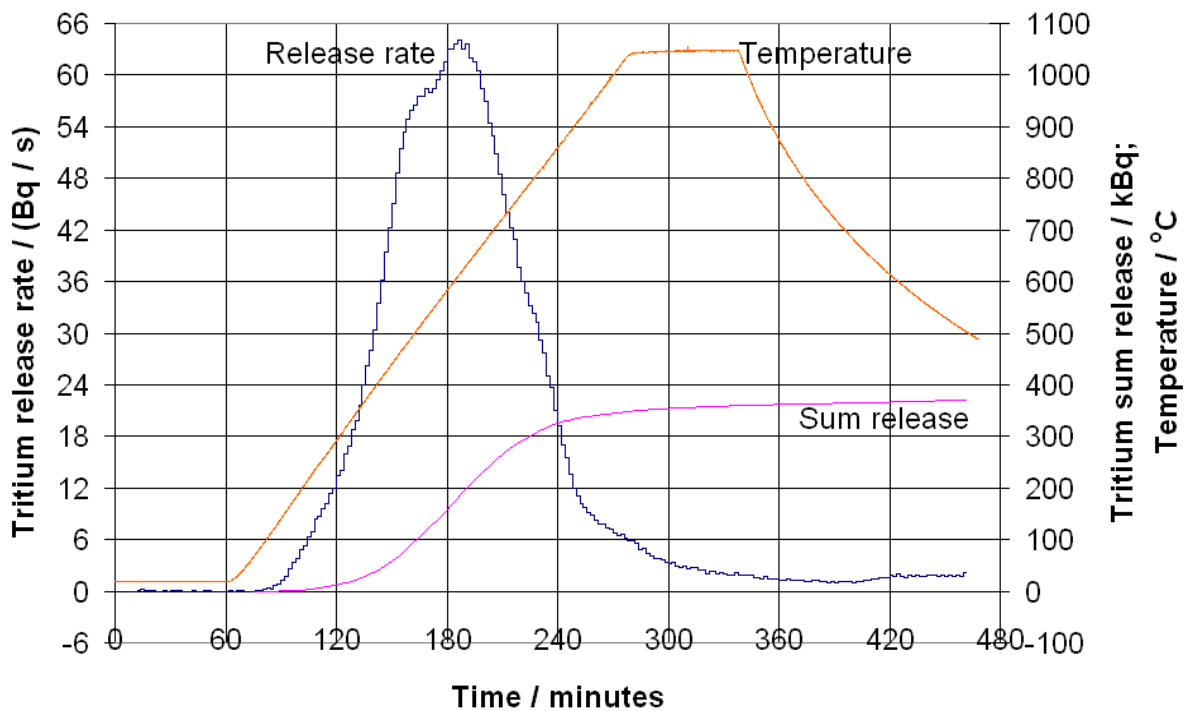


Figure 4. Tritium release by thermal desorption from plasma surface sample of cylinder 4 of tile 14BWG4B

Curves of tritium release at annealing of disc A1 of cylinder 4 of tile 14BWG4B at a rate of 5 °C/min to 1050 °C in a flow of He + 0.1% H₂ at a rate of 15 L/h are shown in Fig 4. The tritium release started at 140 °C, and its rate reached a maximum at 620 °C. At the end of the experiment, the total release of tritium was 0.37 MBq corresponding to the mass activity of tritium of 2.7 MBq/g.

Main conclusions for the task JW8-FT-1.12.:

Amount of tritium in the cylinder 1 of tile 14BWG4B gradually decreased from 1st to 3rd disc and then remained constant. 99.9 % of tritium is located in the first disc of cylinder in plasma exposed side of 3BWG4A tile. The tritium activity gradually increases in the sequence of discs A3 to A17 and finally to the rest of the cylinder, i.e. for disc A17 – 0.17 MBq/g and for the rest – 0.32 MBq/g.

Second task 2008 Behaviour of tritium in EXOTIC 8-3/13 and PBA (Pebble Bed Assembly)

The beryllium pebbles irradiated in the EXOTIC 8-3/13 and PBA (Pebble Bed Assembly) experiment were investigated in year 2008. The irradiation programme EXOTIC (EXtraction of Tritium In Ceramics) and PBA was carried out in the High Flux Reactor (HFR) in Petten, the Netherlands. EXOTIC 8-3/13 pebbles of a diameter 0.1-0.2 mm have been manufactured by spraying molten beryllium in an inert atmosphere (inert gas atomization process, IGA) at Brush Wellman Inc. Their grain size is 40 to 200 µm. The main impurities are 3400 ppm BeO, 100 ppm Mg. The Be pebbles were irradiated for 449.8 days in the HFR at temperatures 800-900 K with a neutron fluency of 2.7×10^{25} n m⁻² ($E > 0.1$ MeV) of a fast fission spectrum. The ⁴He content of 285 appm and the ³H content of 1.16 appm (i.e. 138 MBq·g⁻¹) at the end of the irradiation in the year 2000 were calculated on the basis of the irradiation history. The PBA pebbles of a diameter 0.9-1.1 mm were irradiated 294 full power days in the HFR.

Tritium release at annealing 553 and 770 K

Annealing of Be samples about 9-13 mg was performed in a continuous flow of the purge gas He + 0.1% H₂ of the rate 14-15 L/h without and in MF of 1.7 T and/or 5 MeV fast-electron radiation of the dose rate $P=14$ MGy·h⁻¹ in a special rig.

Tritium release at temperatures ≤553 K

Tritium release from the EXOTIC 8-3/13 Be pebbles was realized at the temperature ramp of 5 K/min to 553 K and then at 553 K for 3 h both without and in MF of 1.7 T. Under the given conditions, tritium was released in a single broad peak starting with a steep increase at 410 K, reaching its maximum at 480-553 K, and then declining like an exponent towards a background level. The samples of the pebbles were found to be dissimilar with respect to the initial total tritium activity 2.5-4.5 MBq·g⁻¹ and to the tritium fractional sum release at the annealing 10% - 19%

Under the electron radiation, tritium was released in a single comparatively narrow peak starting with a steep increase shortly after the switching on of the electron radiation, reaching its maximum at <500 K, and then declining like an exponent towards

a background level. The initial total tritium activity of the pebble samples was 2.6-4.6 MBq·g⁻¹, and the tritium fractional sum release was 17% - 26%

Tritium release from the EXOTIC 8-3/13 Be pebbles under the simultaneous action of electron radiation of 14 MGy·h⁻¹ for 3 h and MF of 1.7 T was realized without any additional heating. The samples investigated in this series were comparatively similar with respect to their initial total tritium activity 4.7-5.3 MBq·g⁻¹. The tritium fractional sum release from these samples was 21% - 29%.

It is worth noting that the dissimilarity of the batch of the EXOTIC 8-3/13 Be pebbles investigated may be characterized by the fact that the batch contained also some coarse agglomerates of the pebbles containing 10-19 MBq·g⁻¹ of tritium, having also a high tritium fractional sum release about 50% at annealing at 553 K for 3 h without radiation and without MF.

Tritium release at temperature 770 K

Tritium release from the EXOTIC 8-3/13 Be pebbles at the temperature ramp of 5 K/min to 770 K and then at 770 K for 1 h both without and in MF of 1.7 T show two distinct peaks on the curves of the tritium release rate. The initial total tritium activity of the pebble samples was found to be 3.6-5.3 MBq·g⁻¹, and the values of the tritium fractional sum release are 17% - 24% without MF and 25% in MF of 1.7 T.

Tritium release from the EXOTIC 8-3/13 Be pebbles under the action of electron radiation of 14 MGy·h⁻¹ for 3 h and the temperature programme but without MF the values of the tritium fractional sum release were found to be in the range 19% - 71%. The tritium release spectra illustrate dissimilarity.

Tritium release from the EXOTIC 8-3/13 Be pebbles under the simultaneous action of electron radiation of 14 MGy·h⁻¹ for 3 h, the temperature programme and MF of 1.7 T shows the two distinct peaks, the values of the tritium fractional sum release were found to be in the range 32% - 37%.

Analysis of chemical forms of tritium in the be pebbles allow say that the abundance ratios of the separate chemical forms in the pebbles change after tritium release at annealing the pebbles under action of radiation and magnetic field separately and simultaneously. In the case of annealing under action of radiation (R, T), we can conclude that the fast electron radiation in experiments cause radiolysis of a fraction of T₂ in bubbles (T₂→T^o+T^o), but temperature is too low for larger release of tritium. In the case of annealing under action of all the three factors simultaneously (R, MF, T), residual amount of molecular tritium reduces much more because the magnetic field can cause spin transformation (S→T) in the pairs of radicals generated by radiolysis; the efficiency of recombination of atomic tritium decreases, and diffusion of tritium in form of atomic tritium T^o increases.

The main form of tritium in the PBA Be pebbles is molecular tritium T₂. Untreated PBA Be pebbles contain molecular tritium T₂ – 90-95 %, atomic tritium – 2 - 5 % and ionic form of tritium T⁺ – 2-5 %, the activity of tritium in 1 gram of PBA Be pebbles is 2-4 GBq/g.

We can conclude a trend that the electron radiation causes a higher fractional release of tritium than a simple thermal treatment of a longer duration and a higher temperature or a similar temperature programme without the electron radiation and a trend that at a given

temperature programme the simultaneous action of the electron radiation and MF of 1.7 T causes a higher fractional release of tritium than a similar electron radiation of the same duration but without MF. A similar trend was observed for the tritium release from neutron-irradiated beryllium pebbles and for the detritiation of D-T-plasma-exposed beryllium tiles from JET.

Main conclusions

The samples of the EXOTIC 8-3/13 Be pebbles investigated were found to be dissimilar with respect to the initial total tritium activity and the tritium fractional release under the given conditions. A trend that the electron radiation causes a higher fractional release of tritium than the same temperature programme without the electron radiation was observed. A trend that the simultaneous action of the electron radiation, the temperature programme and magnetic field of 1.7 T causes a higher fractional release of tritium than the simultaneous action of the electron radiation, the temperature programme but without magnetic field can be concluded.

YEAR 2009

FUSION RELATED LIQUID METAL MHD RESEARCH.

Principal investigator: E.Platacis

DEVELOPMENT OF A GALLIUM JET LIMITER (GJL) AS A SYSTEM FOR PROTECTION OF PLASMA FACING COMPONENTS ENSURING THE REMOVAL OF THE DEPOSITED HEAT AND IMPURITIES.

Content: a) Introduction b) Experimental background; c) Design proposal; d) Mock-up of the liquid metal installation for FTU



Mock-up of the jets entrance region.
Three d=3mm liquid metal jets.



**WP09-PWI-01-02/UL/PS/BS
LIBS SPECTROSCOPY OF THE IMPURITY CONCENTRATION DEPTH
PROFILE IN WALL TILES**

Principal investigator: I. Tale

1. Preparation of samples

Three types of tile materials have been used for investigation

Graphite R6710 tile #1 for reference studies

AUG post mortem graphite:

Tile #2.1 Experiments from year 2003

Tile #2.2 Divi.o., x/6/8, D2, 2003

AUG post mortem W-coated graphite:

Tile #3 HS, C4, S14, 2002

2. Ablation crater formation

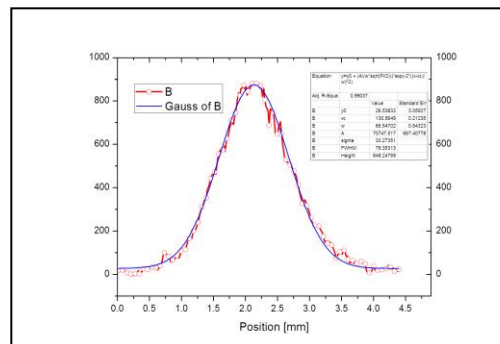
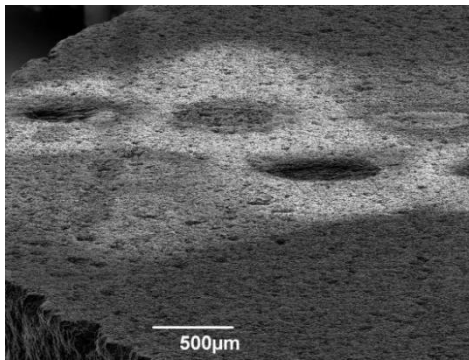


Fig.1 SEM image of an ablated target #2.

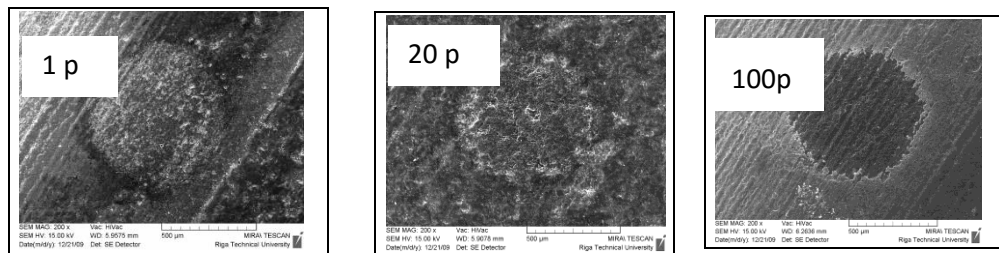
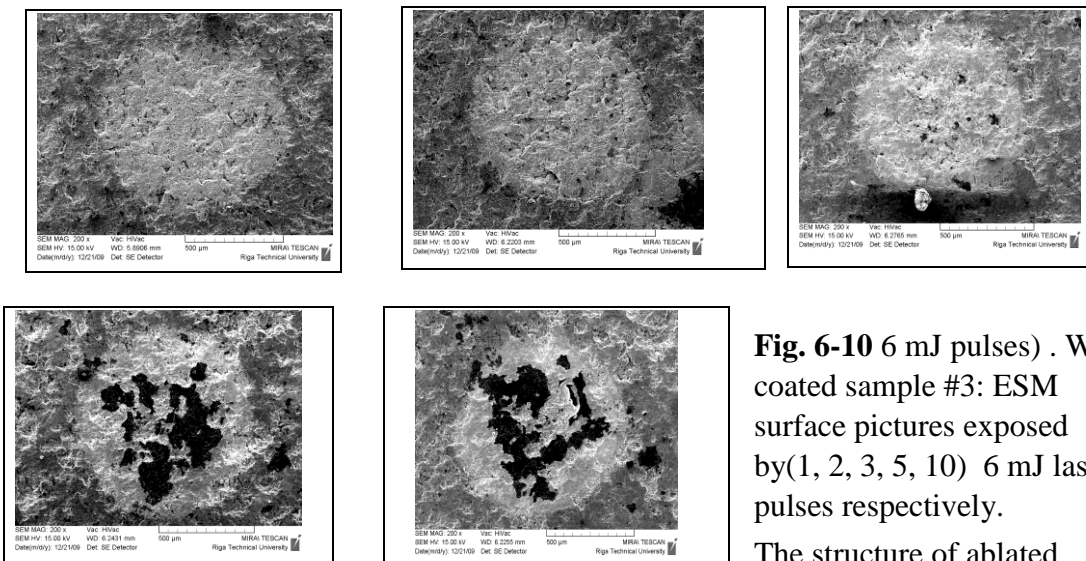


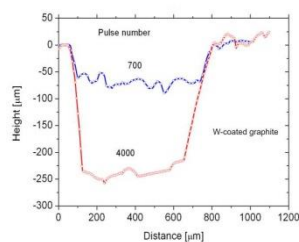
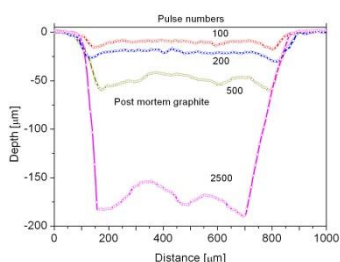
Fig2.. Laser pulse intensity distribution

distribution

Figs. 3-5 crater evaluation graphite sample #2.2 by using 6 mJ energy pulses.



The structure of ablated surface part remains the same as the initial one. A number of more brighter spots are present The 3-rd shot results in creation of dark spots. They are expanded by next shots indicating that part of the W-layer is removed from the sample.



Figs. 11, 12 The crater depth profile at different number of laser shots at pulse energy 10 mJ: Left: sample #2.2; right sample #3.

3. Plasma plume spectra measurements and line analysis

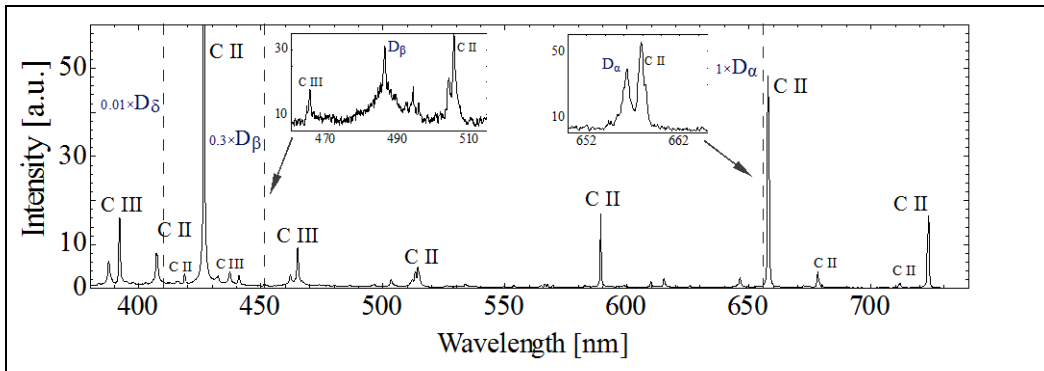
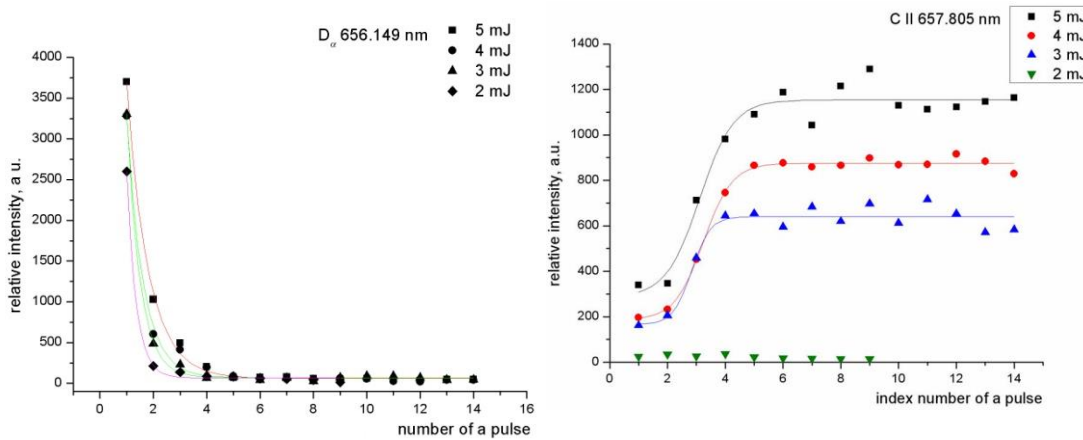


Fig. 13. The D_{β} , D_{α} and D_{α_1} -lines in the carbon tile #2.1.

4. Post-mortem analysis of carbon plates from ASDEX Carbon tile #2.1



Figs 14, 15 Depth profiles of D_{α} line ($\lambda=656.15$ nm), $C II$ ($\lambda=657.805$ nm) at different energies of laser pulses. The index number of a pulse in the sequence is shown on the X axis. The estimated thickness of the ablated layer according to the crater depth profile $\lambda=190-220$ nm.

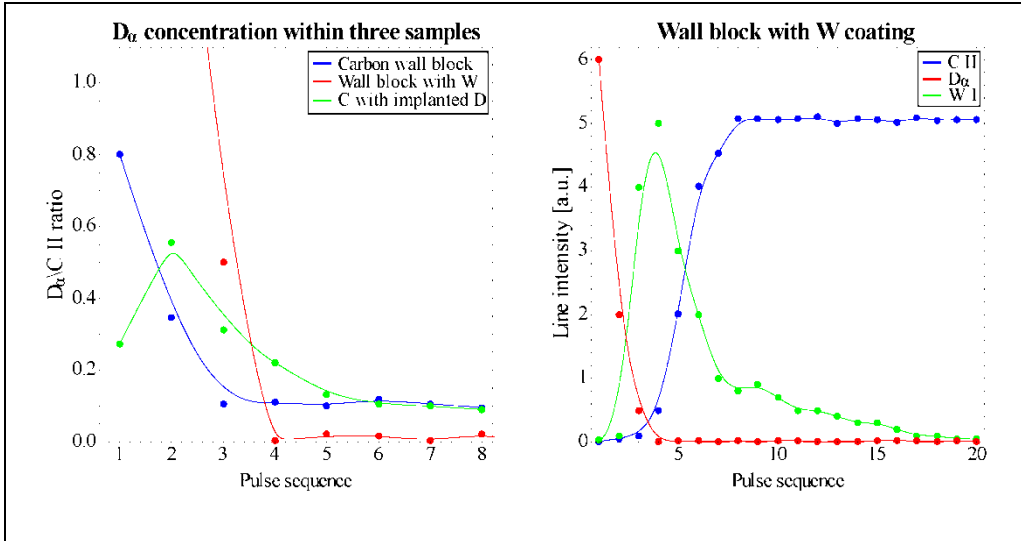


Fig. 16 summarizes the depth profiles of deuterium in carbon based and W-coated carbon tiles of AUG as well as the characteristic depth profile of deuterium, carbon and tungsten in the sample of W-coated tile.

5. Solutions for *in situ* out of vessel LIBS spectroscopy

For *In situ* implementation of LIBS spectroscopy only one common optical port can be available for access to the wall. Assumed, that the diameter of the optical window will be at least 100 mm.

Distance from the optical port to the opposite wall of vessel can reach from about 4 m to about 10 m.

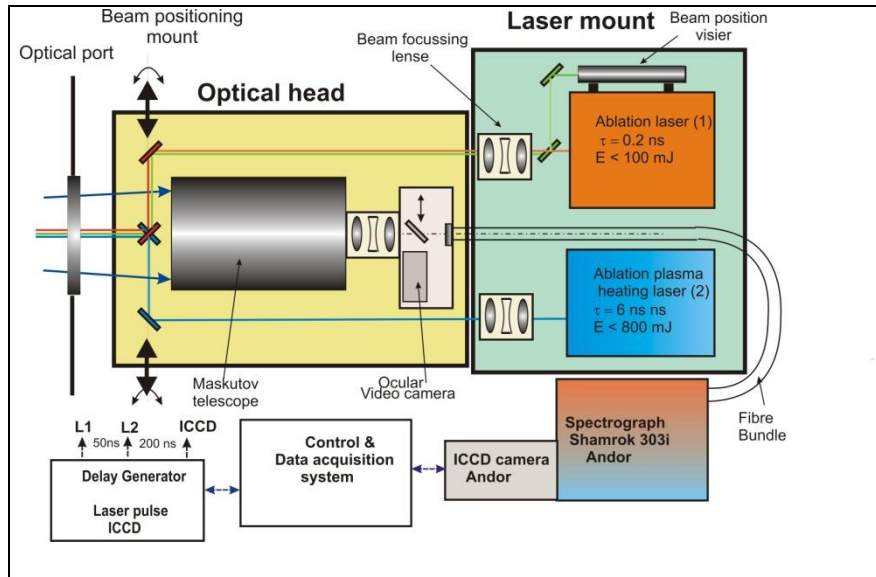
Implementation of LIBS spectroscopy reduces to the two main problems:

Methods to focus and position the laser beam(s) on the wall surface;

Methods both to enhance the efficiency of plasma emission by the laser heating technique and to eliminate the plasma thermal emission background from the spectral line emission of plasma atoms and ions.

The objective has been successful tested for objective – target distance from 3.5m to 10m.

Sketch of the equipment for in situ double



2010
Task WP10-
PWI-05-04-
01/ULV/PS
*Spectroscopy
of Ga multijet
vapor
concentration
and
dynamics in
tokamak*

plasma

The liquid Ga metal limiter experiment involves collaboration between Associations: ENEA Frascati, Italy, IST Lisbon, Portugal AEUL, Latvia.

According to the final plan the Ga multijet experiments at IST tokamak ISTTOK during 2010 will not be performed. Present task is focused in development of advanced technique for multi-jet liquid metal experiments at FTU ENEA Frascati.

Following the analysis of experience of the Ga-vapor spectroscopy at experiments at ISTTOK the preferred direction for investigation of the Ga vapor distribution is the poloidal plane of tokamak. The liquid Ga jet will be injected in the underneath part of vessel. The aim of project is development of equipment for investigation of dynamics of metal vapor distribution in poloidal plane during the plasma pulse and equipment for spectroscopy and the spectra acquisition systems. plane of tokamak.

GYROTRONS TOPICAL GROUP: TG-H&CD

Principal investigator O. Dumbrajs

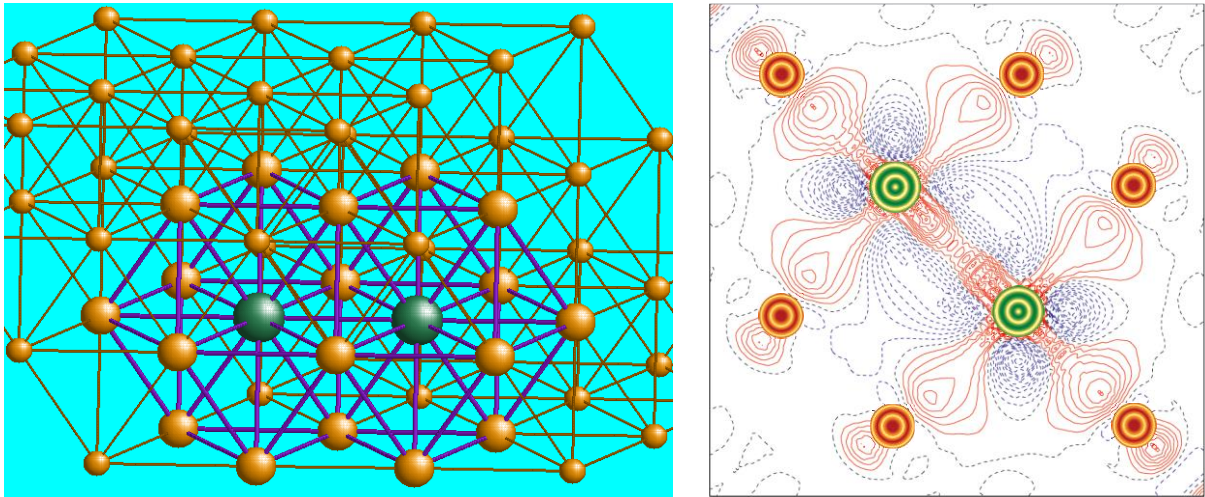
The analysis of electron interaction process in the course of gyrotron switching from one mode to another is presented.

O. Dumbrajs, Y. Kominis, and G.S. Nusinovich, "Electron dynamics in the process of mode switching in gyrotrons" *Phys. Plasmas* 16, 013102 (2009).

MATERIALS MODELING

Principal investigator: E.A. Kotomin

SMALL CLUSTERS CONSISTING OF Y IMPURITY ATOMS IN FCC-Fe LATTICE



The model of the γ -Fe crystalline lattice with 2 Y substitute atoms in the 1st nearest neighbors positions (a) and the corresponding charge redistribution around the 2 Y substitutes inside the (110) splitting plane (b).

The interaction between two Y substitutional atoms at different separation distances (1-NN, 2-NN, 3-NN and 4-NN) has been calculated. No binding has been found between the two yttrium atoms in the iron lattice at any distance. Since we have observed a light repulsion between the single Y substitute atom and surrounding Fe atoms some enhancement of the electron density between Y-Y pair can be visible as compared to the configuration of yttrium atom and iron vacancy, *i.e.*, the repulsion between the two Y substitute atoms is smaller than that between Y and Fe atoms.

JW9-FT-3.4. ESTIMATION OF THE TRITIUM DISTRIBUTION IN THE CARBON BASED TILE.

Principal investigator G. Kizane

This study is carried out according to EFDA JET Technology Task JW9-FT-3.4. In this task tritium distribution, thermodesorption and the effect of the structural changes on that

has been analysed in the selected tile of the JET Mark II SRP divertor. The analysed tile was from JET MkII Septum Replace Plate (SRP) divertor used in 2001-2004 operation periods of JET.

During the operation period the divertor temperature was held at about 200°C. In the year 2003 Trace Tritium Experiment had been performed with an introduction of 380 mg tritium into the vacuum chamber, is estimated that 66 g of deuterium input retained in the vessel, what is approximately 4 % of total deuterium and neutron flux was $3.6 \cdot 10^{14} \text{ n} \cdot \text{cm}^{-2}$.

Since the tritium accumulation dominates on the inner divertor shadowed areas, tile No. 4 14BWG4B from MK II SRP has been selected for this investigation.

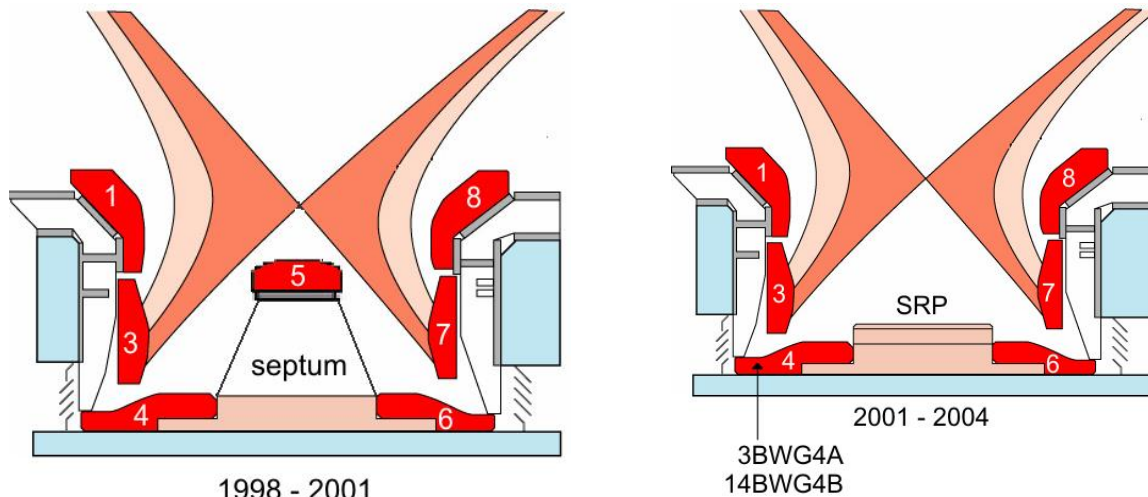


Fig. 5. Configurations of JET divertors Mk-II-GB of the Gas-Box type with a septum (left) and a septum replacement plate (SRP) (right).

The distribution of tritium with depth through the tile has been measured at different toroidal and poloidal positions. A high concentration of tritium was found in the discs at the plasma facing surface. At some tile positions (e.g. at the inner divertor corner shadowed from the plasma) up to 98-99% of the T can be in the surface slice, whereas in other poloidal positions there can be more T in the bulk than at the surface. The tritium distribution in the toroidal and poloidal directions is not uniform; concentration of accumulated tritium strongly depends on the location of the tile. The changes in position and ratio of the carbon lines (1588 cm^{-1} and 1355 cm^{-1}) in the Raman spectra with depth through each core indicates the degree of disruption of the carbon lattice. The structural changes of the tile material close to the plasma facing surface are considerable and correlation with the tritium accumulation has been observed.

The highest surface activities of tritium were found in the shadowed part of the tile. For instance, the mass activity of the surface slice of Cyl10 was $0.156 \text{ GBq} \cdot \text{g}^{-1}$, while in Cyl 2 representing the SRP part it was only $0.006 \text{ GBq} \cdot \text{g}^{-1}$. Tritium activity in the surface layer can be described as a variable proportional to the thickness of deposition layer and inversely proportional to the energy deposited on a tile since tritium accumulate.

Diffusion of tritium into the bulk of a tile is expected at high temperatures as is clearly demonstrated in the results from the sloping part where the tritium mass activity of the bulk was found to be about an order higher than in other parts of the tile.

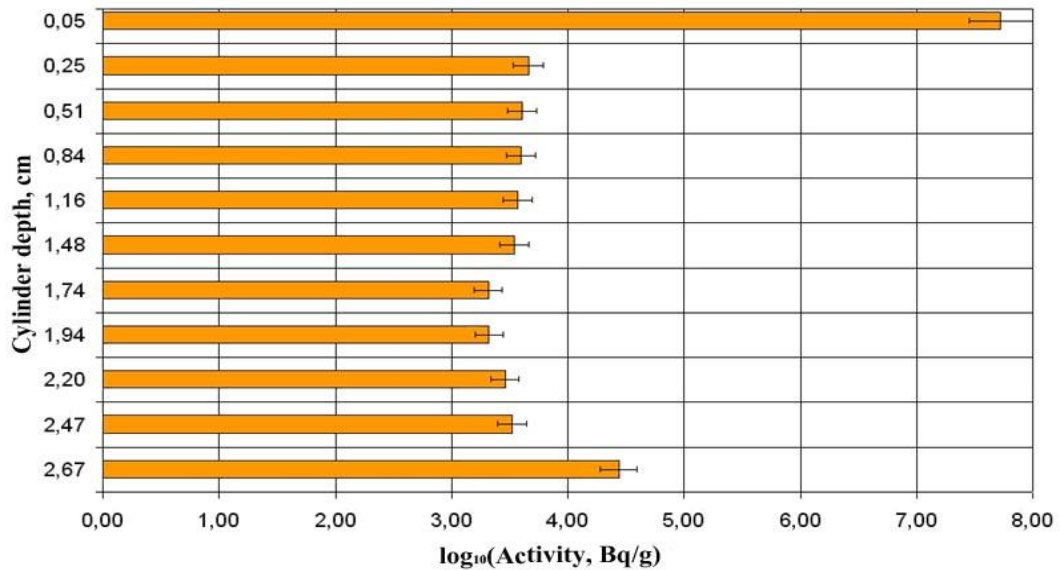


Figure 6. Depth profiles of mass activity of tritium in cylinder 10 of tile 14BWG4B.

To estimate the changes of the material structure the carbon fibre modifications were analyzed. An increase of the fibre diameter close to the backside surface was observed to be up to 30%

Increase of fibre diameter can be caused by neutron irradiation as a result of formation of extra graphite planes or interplanar voids. However, the neutron flux in the JET is not sufficient to cause such changes ($3.60 \cdot 10^{14} \text{ n} \cdot \text{cm}^{-2}$ for the 2001-2004 operation periods) and neutron damage would be uniform through the tile: the largest modification was observed at the backside of the tile. This might mean that fibre modifications have been caused by some other reason, e.g. mechanical forces due to the method of mounting the tile in the divertor. The tile is mounted by pulling down on a central bolt with the tile supported at the corners, so that the backside is in tension. Therefore, there are no extra graphite planes but existing planes have separated as a result of the deformation, and extra space for tritium to diffuse has appeared.

Main conclusions

Depth profile of the tritium shows high tritium concentration in the plasma facing surface layer that is followed by a sharp decrease to a bulk tritium activity which then stays at a uniform level until it reaches the backside layer where it increases again. Increase of the fibre diameter followed by a full destruction of the fibres were observed in the backside layer and could be explained either by mechanical forces applied on the tile during exploitation in the divertor. The increase of the specific surface area and concentration of the hydrogen traps in the CFC material as a result of deformations and destruction of the

fibres might be one of the reasons for increased tritium retention in the backside layers of a tile.

YEAR 2010

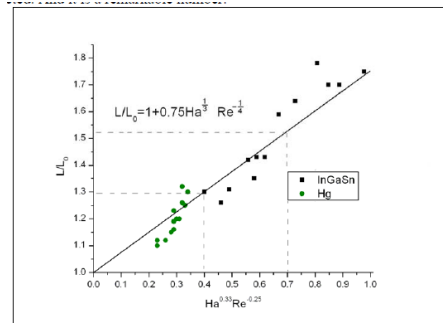
FUSION RELATED LIQUID METAL MHD RESEARCH.

Principal investigator: E.Platacis

WP10-PWI-05-04-04/ ULV/ PS

DEVELOPING AND DELIVERING OF GA INSTALLATIONS FOR TESTS ON ISTTOK AND FTU.

Content: a) Gallium jet power extraction capability; b) Break-up of liquid metal jets; c) Testing of active techniques for jets disintegration.



Shifting of break-up point by slight mechanical perturbation
Increase of the break-up length if a magnetic field is applied to nozzle.

Task WP10-PWI-05-04-01/ULV/PS

SPECTROSCOPY OF GA MULTIJET VAPOR CONCENTRATION AND DYNAMICS IN TOKAMAK PLASMA

Principal investigator: I. Tale

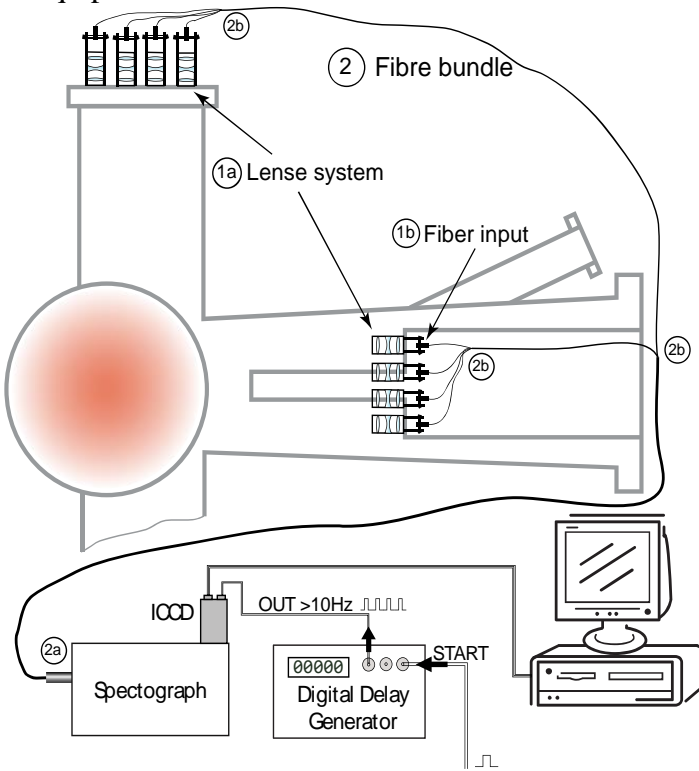
The liquid Ga metal limiter experiment involves collaboration between Associations: ENEA Frascati, Italy, IST Lisbon, Portugal AEUL, Latvia.

According to the final plan the Ga multijet experiments at IST tokamak ISTTOK during 2010 will not be performed. Present task is focused in development of advanced technique for multi-jet liquid metal experiments at FTU ENEA Frascati.

Following the analysis of experience of the Ga-vapor spectroscopy at experiments at ISTTOK the preferred direction for investigation of the Ga vapor distribution is the poloidal plane of tokamak. The liquid Ga jet will be injected in the underneath part of

vessel. The aim of project is development of equipment for investigation of dynamics of metal vapor distribution in poloidal plane during the plasma pulse and equipment for spectroscopy and the spectra acquisition systems. plane of tokamak.

The setup of Ga- vapor spectroscopy involves the *in situ* optical system for collection of the tokamak plasma emission in poloidal plane of tokamak and *remote* system for spectroscopy of plasma emission, spectral data acquisition, and time resolved control of equipment.



Both the vertical port and the horizontal port is equipped by four object lens systems (4x4 plasma emission positions).

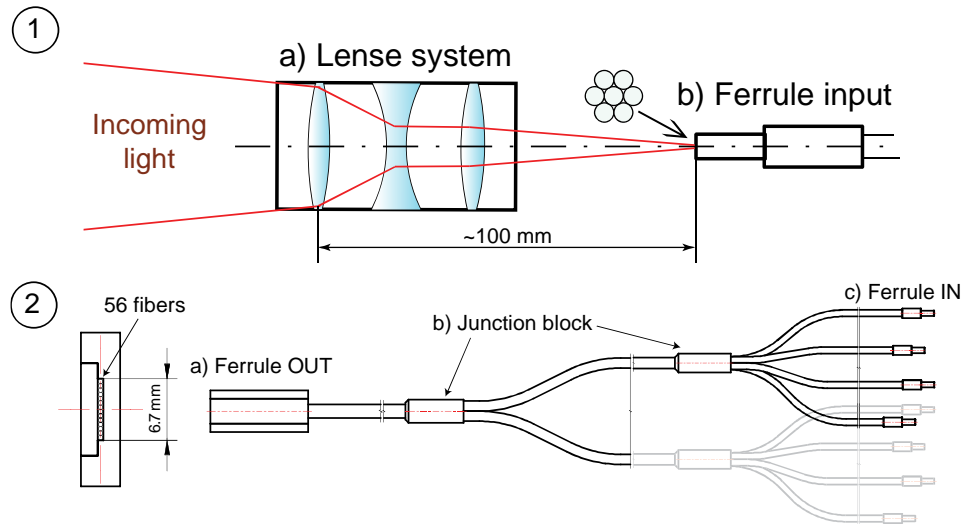
The full observable length of openings in radial and vertical direction is 400 mm, distance from vessel center to objective about 800 mm.

Object lens is represented by three lens combination allowing adjust both the input aperture and the output aperture. The fiber bundle is assembled by the fiber sub bundles.

Time-resolved spectroscopy
Spectrograph Andor Shamrock 303i.

The iStar 720 intensified CCD camera.

Spectral Range (nm) 380 - 980
Active Pixels 690 x 256

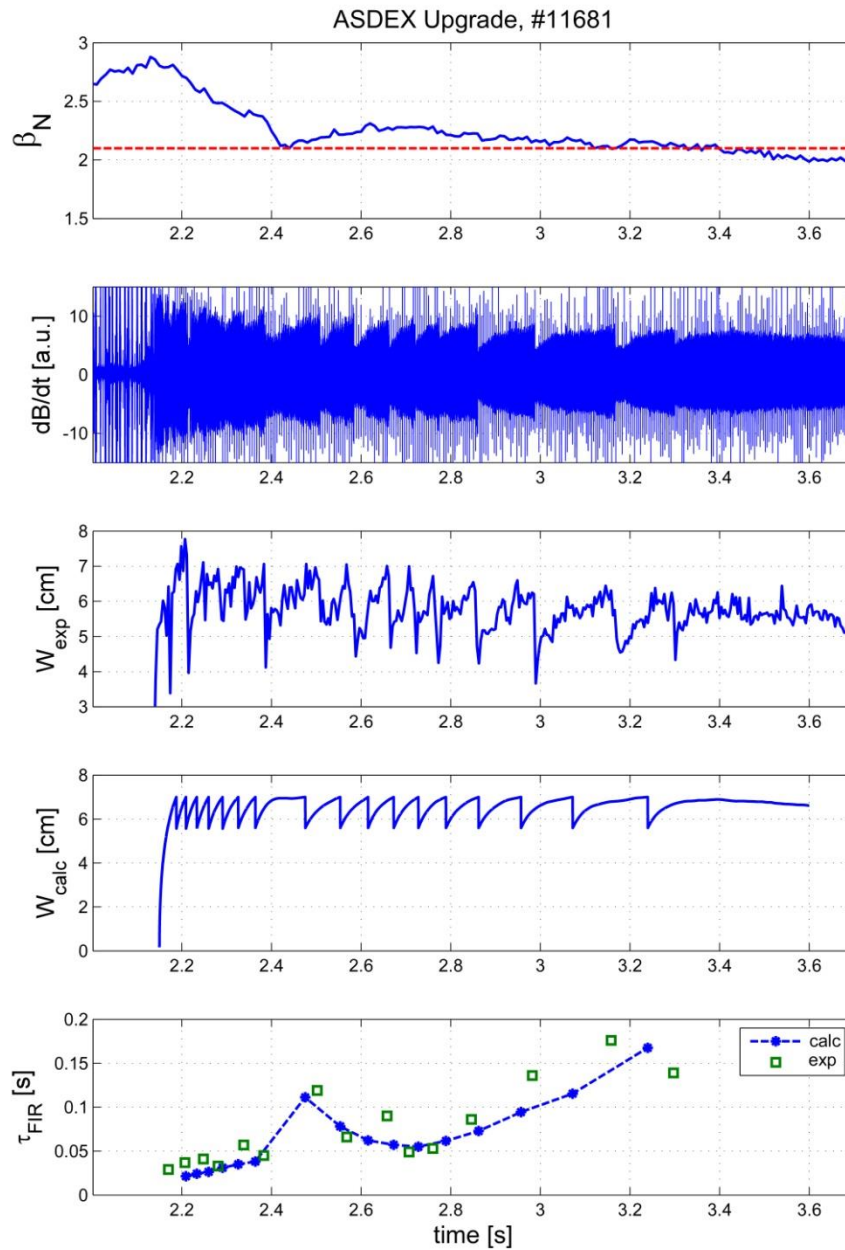


Emission spectrum is detected by ICCD camera. The ICCD camera used ensures reach the exposition – data acquisition time less than 100 ms. Spectral data of plasma emission are accumulated by PC. Time resolved spectra measurements, positioning of the entry ferrules of fiber optics for multiple emission spectra measurements at different plasma positions are controlled by PC. Separat delay generator will be installed for time resolved spectra accumulation during the whole plasma shot.

PLASMA PHYSICS TOPICAL GROUP: TG-MHD

Principal investigator O. Dumbrajs

A phenomenological method for description of temporal evolution of neoclassical tearing modes in the frequently interrupted regime (FIR) is proposed. The method makes it possible to predict the beginning and the end of the FIR regime as well as the frequency of the FIR drops.



Temporal evolution.

O. Dumbrajs, V. Igochine, A. Gude, M. Maraschek, H. Zohm and ASDEX Upgrade Team “Temporal evolution of neoclassical tearing modes in the frequently interrupted regime” Phys. Plasmas 17, 042118 (2010).

The crash phase of the sawteeth in ASDEX Upgrade tokamak is investigated by means of soft x-ray and electron cyclotron emission diagnostics.

V. Igochine, J. Boom, I. Classen, O. Dumbrajs, K. Lackner, G. Pereverzev, H. Zohm and ASDEX-U team, “Structure and dynamics of sawteeth crashes in ASDEX Upgrade” Phys. Plasmas 17, 122506 (2010).

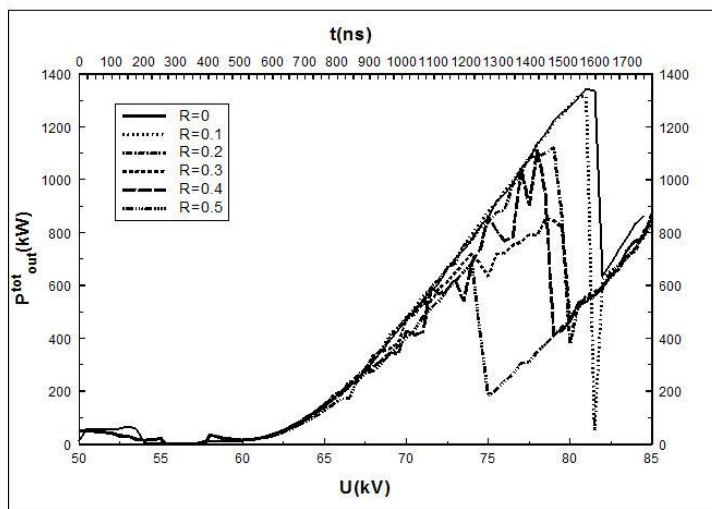
GYROTRONS TOPICAL GROUP: TG-H&CD

Principal investigator O. Dumbrajs

The effect of a slight uptapering of the resonator wall on the efficiency enhancement and the purity of the radiation spectrum in the process of the gyrotron start-up and power modulation are studied.

O. Dumbrajs and G.S. Nusinovich, „To the theory of high-power gyrotrons with uptapered resonators” Phys. Plasmas 17, 053104 (2010).

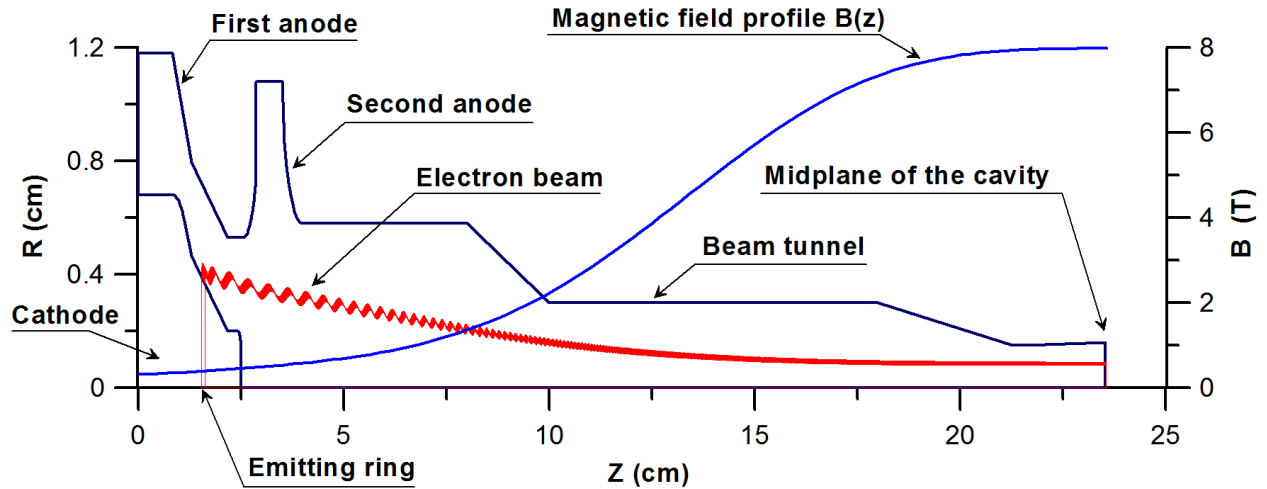
The theory describing the influence of reflections on operation of gyrotrons with radial output is used for evaluating the effect of reflections on the operation of the ITER 170 GHz 2 MW coaxial cavity gyrotron, which is under development, and the 170 GHz 1 MW cylindrical cavity gyrotron as a fall back solution.



The total output power as a function of time and voltage. It is seen that even in the case of relatively small reflection $R=0.2$ the maximal output at the operating voltage $U_{op} = 79kV$ is noticeably smaller than in the case of no reflections.

O. Dumbrajs, „Influence of possible reflections on the operation of European ITER gyrotrons” J. Infrared Milli. Terahz. Waves 31, 892 (2010).

Instead of a regular (cylindrical) part as in the conventional cavities it contains an uptapered section. Such configuration offers a significant increase of the efficiency and improves the overall performance of the tube.



Configuration of the magnetron injection gun (MIG), magnetic field profile and trajectories of the electron beam.

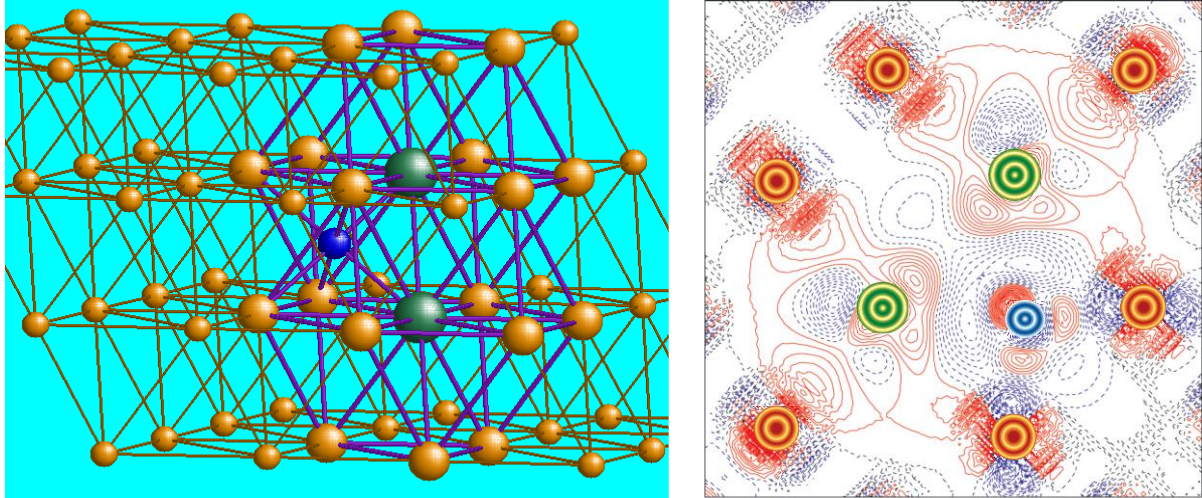
O. Dumbrajs, T. Idehara, and S. Sabchevski, “Design of an optimized resonant cavity for a compact sub-Terahertz gyrotron” J. Infrared Milli. Terahz. Waves 31, 1115 (2010).

MATERIALS MODELING

Principal investigator: E.A. Kotomin

STABILITY OF THE SMALLEST CLUSTERS CONSISTING OF IMPURITY O AND Y ATOMS IN FCC-FE LATTICE

To construct the more stable configuration of solute atoms, we have added to the pair of Y substitute atoms (1-NN neighbors) an oxygen atom positioned at the *O* site and have calculated three-atom configuration (Fig. 6). No binding was found in this nanocluster inside the γ -Fe lattice as compared to Y-O-Y motif existing in bixbyite structure of Y_2O_3 . Significant displacements were observed during relaxation between each pair of Y and O atoms, achieving 0.45 Å for yttrium, whereas Y atoms move from each other by 0.37 Å.



The model of the γ -Fe crystalline lattice with 2 Y substitutes and 1 O impurity atom in the 1st nearest neighbors positions (a) and the corresponding charge redistribution around the 2 Y substitutes and O atom inside the (110) splitting plane (b). The latter is defined as the total electron density of γ -Fe lattice including the two Y substitutes and O impurity atom minus the sum of those for γ -Fe lattice with 2 vacancies, 2 Y and O atom in vacuum.

JW10-FT-3.62. ESTIMATION OF THE TRITIUM DISTRIBUTION IN THE CARBON BASED TILES

Principal investigator G. Kizane

The task JW10-FT-3.62 are related to the estimation of the tritium distribution in the carbon based tiles and are continuation of the EFDA JET Technology Tasks on the tritium in tokamaks.

Goals of the task are to determine depth profiles of tritium trapped in the bulk of CFC tiles, make comparison of tritium activities in the bulk and surface layers, estimate changes of structure of a tile, to investigate properties of the tritium trapped in CFC tiles.

In the year 2010 analysis of tritium was continued for core-drilled cylinders of tile 14BWG4B for tritium analysis in a poloidal and toroidal direction.

Concentration of tritium in the surface layers and in the bulk is connected with the thickness of deposition layer, with energy of implanted tritium ions and with the energy of plasma deposited on a tile. Increase of the space between the sheath graphite planes facilitates the transport of tritium between the planes, while full destruction of fibre sheath leads to the increase of specific surface area and concentration of high energy trapping sites.

Tritium activity in the slice 1 (A1) of Cylinder 2 up to Cylinder 10 of the Line 2 is not uniform, as previously determinate the sequence is the same, concentration of tritium at the septum replace plate is much more less than at the louvers side

Tritium depth profile also is uniform of the Cylinder 9 which is placed near to the louvers side for the lines 1up to the line 5. Amount of tritium is in the range of one order some kBg.g^{-1}

Detailed analysis of the tritium distribution in the cylinders of the first line shows the analogous situation as described previously. The large part of tritium is concentrated in the first slices A1 (1 mm) for all cylinders. In the next slice the tritium amount sharply decreases and stayed less or more uniform in the middle of tile and then slightly increases. Migration of tritium into the bulk of a tile may be expected at high temperatures. The surface of the sloping part of the tile may reach even 1000°C during plasma exposure.

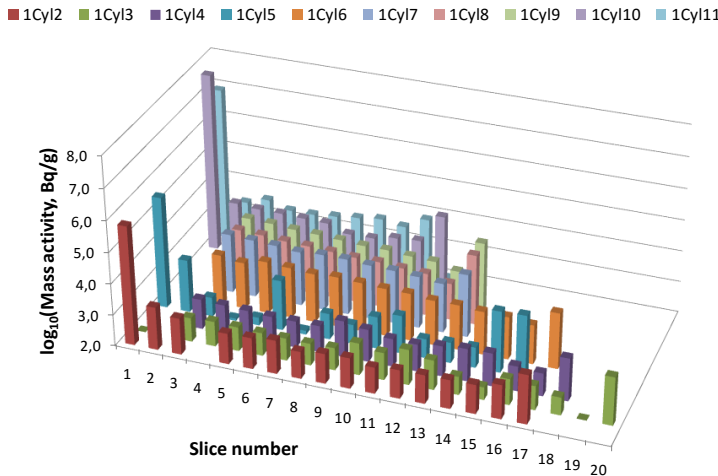


Figure 7. Distribution of tritium in the cylinders from 1 to 12 of the 1st line

Desorption spectra of tritium from plasma exposed surface slices under action of temperature for all three investigated samples are different. The thermo-desorption spectra has additional shoulders for the slices of the cylinders 1 and 5. Common feature for all is that tritium release starts at ≤ 200 °C, the release rate reaches a maximum at <680 °C and decreases rapidly at temperatures above 950 °C.

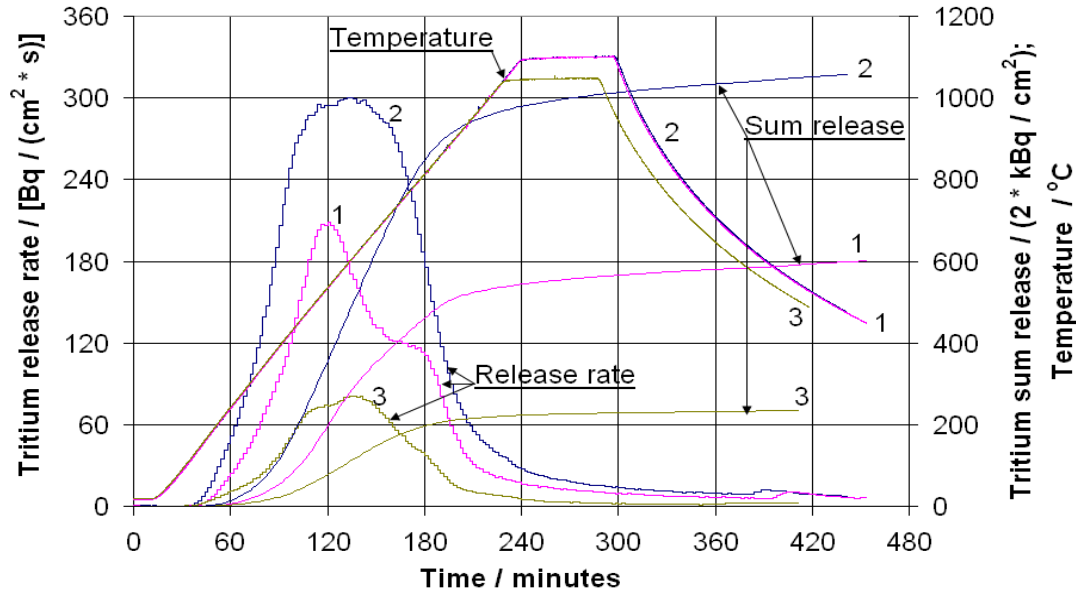


Figure 8. Tritium release by thermal desorption from the A1 discs of cylinders 1 (1), 4 (2) and 5 (3) of tile 14BWG4B.

Main conclusions

The tritium profile in the JET divertor MkII SRP 14BWG4B tile is not uniform both as in the poloidal and as in the toroidal direction of the tile. Distribution of tritium in the JET divertor MkII SRP tile show that the largest amount of tritium is accumulated in plasma facing part in areas shadowed from the plasma interaction, near to the louvers side. For tile 14BWG4B, the plasma-facing surface disks A1 at the louvers have the surface activity of tritium ($10\text{-}65\text{ MBq/cm}^2$) by a factor of 10-100 higher than that ($0.5\text{-}2.1\text{ MBq/cm}^2$) at the SRP. Depth profiles of tritium of the investigated cylinders are similar. Amount of the retained tritium in plasma facing part of the carbon deposited layers is in the range of 10^9 Bq.g^{-1} , whereas in the middle part of the cylinder concentration of the tritium sharply decrease and is nearly constant 10^6 Bq/g^{-1} , but in the rear side of the cylinder the concentration of tritium slightly increases. Tritium release from plasma exposed surface disks starts at $\leq 200\text{ }^\circ\text{C}$, the release rate reaches a maximum at $< 680\text{ }^\circ\text{C}$ and decreases rapidly at temperatures above $950\text{ }^\circ\text{C}$.

Tritium release from neutron irradiated beryllium pebbles

The aim of the programme of the year 2010 was to investigate post irradiation tritium release from pebble bed assembly's (PBA) irradiation experiment beryllium pebbles under action of both temperature ramp and at a constant temperature relatively long time. In the year 2010 laboratory began investigations on tritium behaviour of the HIDOBE-I beryllium pebbles and obtained the first results on the tritium specific activity of pebbles from HIDOBE-I experiments

Tritium release experiments were performed in a setup enabling annealing at temperatures up to 1310-1550 K. Investigations of the tritium release from PBA pebbles with the temperature ramps to 1310-1520 K was realized in order to obtain temperature-

programmed desorption spectra of tritium from the beryllium pebbles, to get general insight into tritium release properties of the beryllium pebbles.

A significant tritium release started at 920 K. Generally, the tritium release took place in a single maximum with two distinct stages – a stage of a gradual increase in the tritium release rate in the temperature range from 920 K to 1178-1223 K, which was a shoulder before a maximum, and a stage starting with an abrupt increase in the tritium release rate and resulting in a maximum at 1253-1287 K. The histograms in the range of the maximum had a fine structure with possible presence of minor peaks. At the temperature above 1327 K, the histograms of the tritium release rate were gradually descending with no apparent transitions at the steps of the temperature program. No significant amounts of residual tritium were found at dissolution of the pebbles in 2 mol/L H₂SO₄ after their annealing under the temperature programs that testifies that a complete release of tritium took place under the given conditions of annealing.

Tritium release from a PBA Be pebble at shorter or longer anneal time at 1083-1089 K has burst release of tritium. The stages of gradual and burst release are related to the tritium release by atomic diffusion and bubble venting respectively. The sharp peaks of burst release are followed by gradually descending curves of tritium release rate that are higher than those before the burst release. That can be explained by the fact that the pores that appeared in the pebble at the burst release increase the outer surface of the pebble and thus increase the rate of the tritium release limited by atomic diffusion from inner part of the pebble.

The first experiments on HIDOBE-1 beryllium pebbles were realized. The specific activity of the pebbles was determinate by dissolution technique. The correlation of tritium amount and irradiation temperature was observed. Tritium mass activity at higher irradiation temperature 750 °C is 3-4 times less mass activity of tritium than at irradiation temperature 450 °C.

Main conclusions

Two distinct stages of tritium release – a stage of gradual increase and a stage of abrupt release peaks are evident in the tritium release of the PBA. These two stages are related to the tritium release by atomic diffusion and bubble venting respectively.

The mass activity of the accumulated tritium in HIDOBE-1 beryllium pebbles correlates with the irradiation temperature.

Radiolysis of lithium orthosilicate pebbles

In close cooperation with Karlsruhe Institute of Technology changes in the composition and microstructure of overstoichiometric Li₄SiO₄ pebbles were investigated after fast electron irradiation.

Three types of pebbles received from the KIT with different diameters and grain sizes were investigated. Lithium orthosilicate (Li₄SiO₄) pebbles were fabricated by a melt-spraying process in a semi-industrial scale facility at Schott AG, Mainz, Germany. The pebbles were irradiated with accelerated 5 MeV electrons at 560 ±20 K, the dose rate of 24.4 kGy/s.

Analysis of the microstructure of the pebbles at etched cross-sections showed the different grain sizes of the samples before irradiation. In lithium orthosilicate samples 2

and 3 was observed the grains of lithium metasilicate as inter- or intracrystalline inclusions. Because of the small grain size, lithium metasilicate cannot be detected in sample 1. In sample 2 the grains seem to be only loosely connected and some of the pebbles were already destroyed during grinding and polishing. This may be caused by an improper heat treatment during crystallization of the previously amorphous pebbles. After irradiation in air, all samples exhibit a fissured microstructure, and the smaller pebbles (samples 1 and 2) nearly appear to be disintegrated. After irradiation in argon, the samples are nearly unchanged the small pebbles seem to exhibit a slightly more porous microstructure with more gaping grain boundaries, but there is hardly any difference in the microstructure of the large pebbles compared to the unirradiated material. The second phase, lithium metasilicate, can also be detected as inter- or intracrystalline inclusions in samples 2 and 3. Nevertheless, the samples irradiated under air appear to be chemically eroded by possible reactions with air, containing H₂O and CO₂.

ESR spectra of all investigated samples after irradiation with doses up to 10.56 GGy exhibit at least three different lines with g-factors of 2.001, 2.011 and 2.016. Those spectra are similar to previously reported ones for irradiated “pure” Li₄SiO₄ and can be interpreted as superposition of signals from so called E' and HC2 centres (ion radicals SiO₃³⁻ and SiO₄³⁻, respectively). Ion radical SiO₃³⁻ (HC2 centre) in ESR spectra is presented with 2 lines ($g_{\perp}=2.009$ and $g_{\parallel}=2.016$) due to anisotropy of g-factor. A very weak and broad multiplex signal was also observed at ESR spectra of irradiated sample 1. This signal can be attributed to electrons localized in anion or oxygen vacancy (so called F⁺ centres). ESR spectra of all three samples irradiated in air atmosphere with a dose of 10.56 GGy contain two symmetric lines with 50.2 mT splitting, typical for localized hydrogen atoms. Beside this, several unidentified lines possibly due to impurities were observed at ESR spectra of samples irradiated with a dose of 10.56 GGy in air atmosphere.

Concentrations of stabilized paramagnetic centres in pebbles irradiated with doses from 1 to 5 GGy are in the range of 10¹⁵-10¹⁶ radical/g and slightly increase with increasing absorbed dose. Concentration of free radicals stabilised in samples irradiated in dry argon with absorbed doses of less than 2 GGy are significantly higher than in case of samples irradiated in air atmosphere. For samples irradiated in dry argon an increase of the absorbed dose higher than 5 GGy cause a decrease of radicals' concentration. On the other hand, a surprisingly high concentration of stabilised paramagnetic centres (10¹⁷-10¹⁹ radical/g) was observed in samples irradiated with a dose of 10.56 GGy in air atmosphere.

In irradiated pebbles the same radiation defects are stabilized that were previously detected in “pure” Li₄SiO₄, but the concentration of stabilized free radicals at doses from 1 to 5 GGy is approximately 2 times higher. ESR measurements of “pure” Li₄SiO₄ irradiated with a dose of 10.56 GGy were not made previously.

Products of radiolysis in irradiated pebbles were investigated by means of XRD and FTIR spectroscopy. While for sample 3 no change in the phase composition, not even after the irradiation in air could be detected by XRD, the diffraction diagram of sample 1 after irradiation in air exhibits significant amounts of impurities. Due to the large amount of phases, only LiOH, LiOH·H₂O and traces of Li₂CO₃ could be verified, however, traces of lithium oxide cannot be ruled out.

In samples 1 and 2 irradiated in air atmosphere, a significant increase of the initial concentration of Li_2SiO_3 as well as characteristic lines for LiOH and Li_2CO_3 were detected with both mentioned methods. As the specific surface area of samples 1 and 2 is 1000 times higher than of sample 3, surface reactions with H_2O and CO_2 are significantly increased in samples with a smaller pebble size. According to FTIR spectroscopy, in all three samples irradiated in air with a dose of 10.56 GGy the concentration of Li_2SiO_3 FORMED DURING IRRADIATION IS APPROXIMATELY 1 WT% OR 4.5 MOL%. ON THE OTHER HAND, THE concentration of metasilicate in samples irradiated in argon is practically unchanged. Concentrations of colloidal lithium and other reducing products of radiolysis and radiation defects were equal to $4.4 \cdot 10^{19}$, $1.2 \cdot 10^{19}$, and $3.1 \cdot 10^{19}$ electron/g for samples Nr. 1, 2 and 3, respectively.

Main conclusions

The degree of decomposition $\alpha_{10.56}$ of the lithium orthosilicate matrix at an absorbed dose of 10.56 GGy calculated from estimated concentration of radiolytic metasilicate is approximately equal to 1.5% for irradiation in air atmosphere and 0.15% for irradiation in dry argon. This is significantly lower than the value $\alpha_{10.56} \approx 5\%$ calculated on base of empiric equation.

Comparison of the obtained data for the investigated pebbles allow to say that pebbles with a diameter of 500 μm , which represent the potential material for the European test blanket module, have a higher radiation stability than the smaller pebbles.

YEAR 2011

FUSION RELATED LIQUID METAL MHD REASEARCH.

Principal investigator: E.Platacis

WP 11-PWI-04-04/AEUL/BS. ADDAPTATION OF LIQUID METAL (LM) STANDS FOR EXPERIMENTS WITH LM JETS AND DROPLETS UNDER HIGH POWER LOADS.

Content: a) A single InGaSn jet in a strong non-homogeneous 2D magnetic field;
b) Behavior of InGaSn jets after touching to a conducting flat plate in the presence of a strong magnetic field.



Scheme for investigation of jets stability in strong non-homogeneous field.
Three jets touching a plate at $B=1T$ and $v=2.07$ m/s.

TASK DESIGN AND IMPLEMENTATION OF TIME RESOLVED LIQUID METAL VAPOUR SPECTROSCOPY AT TOKAMAK

Principal investigator: I. Tale

Background

The liquid Ga metal limiter experiment will be provided in collaboration between three Associations: ENEA Frascati, Italy, IST Lisbon, Portugal AEUL, Latvia.

Goals

Development of the methodology for evaluation of the vapor concentration from emission intensity data.

Testing of the methodology using results of spectroscopy of Ga- vapor emission lines at tokamak ISSTOK.

3. Emission model of Ga vapors in plazma.

Metal impurities in Tokamak are excited and deexcited by collisions with the plasma electrons.

Excitation and deexcitation rate is governed by the electron concentration and temperature.

Electron excitation rate can be averaged over Maxwellian velocity distribution.

$$X_{mn} = 1.6 \times 10^{-5} \frac{f_{mn} \langle g(n,m) \rangle N_e}{\Delta E_{nm} T_e^{1/2}} \exp\left(-\frac{\Delta E_{nm}}{kT}\right)$$

where: f_{nm} - oscillator strength
elements

- spectroscopy tables of

$\langle g(n,m) \rangle$ -averaged Gaunt factor

~ 1 for atoms; ~ 0.2 for ions

$\Delta E_{nm} = E_n - E_m$ - n -th and m -th levels energy
elements

- spectroscopy tables of

N_e - electron concentration in plasma (in cm^3)

- plasma parameter

T_e - electron temperature in plasma (in eV)

- plasma parameter

Electron deexcitation rate

$$Y_{nm} = \frac{N_m^*}{N_n^*} X_{mn}, \text{ where } N_m^*/N_n^* = \left(\frac{g_m}{g_n} \right) \exp \frac{\Delta E_{nm}}{kT_e}$$

Rate for spontaneous decay n - m (Einstein coefficient)

$$A_{nm} = 4.3 \times 10^7 \frac{g_m}{g_n} f_{mn} \left(\frac{\Delta E_{nm}}{kT_e} \right), \text{ sec}^{-1}$$

Intensity emitted per unit volume from the transition n to m on a optically thin plasma

$$I_{nm} = 1.6 \times 10^{19} A_{nm} N_n \Delta E_{nm}, \text{ watt/cm}^3$$

Condition for steady state in a corona model

$$n_0 N_e (\sigma_{0n} v) = N_n A_{n0}$$

Intensity emitted per unit volume for transition n - m

$$I_{nm} = 5.1 \times 10^{-25} \frac{f_{nm} g_0 N_e N_0}{g_m T_e^{1/2}} \left(\frac{\Delta E_{nm}}{\Delta E_{n0}} \right)^3 \exp \left(- \frac{\Delta E_{n0}}{T_e} \right) \text{ watt/cm}^3,$$

Concentration of Ga atoms/ ions in plasma

$$\Rightarrow N_0 = 2 \times 10^{24} \frac{I_{nm} g_m T_e^{1/2}}{f_{nm} g_0 N_e \left(\frac{\Delta E_{nm}}{\Delta E_{n0}} \right)^3 \exp \left(- \frac{\Delta E_{n0}}{T_e} \right)} \text{ cm}^{-3}$$

3.1.2 Basic equations. Shell - shell ionization

Ionization from the ground state over Maxwellian electron distribution for $0.02 \leq T_e / E_\infty^Z \leq 100$.

Ionization rate $S(Z)$, where E_∞^Z

$$S(Z) = 10^{-5} \frac{(T_e / E_\infty^Z)^{1/2}}{(E_\infty^Z)^{3/2} (6.0 + T_e / E_\infty^Z)} \exp \left(- \frac{E_\infty^Z}{T_e} \right) \text{ cm}^3/\text{sec} . \quad N^*(Z) = \frac{N^*(Z-1) \times S(Z-1)}{\alpha_3 N_e}$$

Steady state: $\frac{N_e N(Z)}{N(Z-1)} = \frac{S(Z-1)}{\alpha_3}$, where $\alpha_3 = 8.75 \times 10^{-27} T_e^{-4.5} = 2.8 \times 10^{-31} \text{ cm}^6/\text{sec}$

(electron-ion recombinative rate)

3.2 Estimation of Ga vapour concentration using Ga emission spectroscopy

At present Ga vapor distribution in the tokamak plasma have been performed only during single Ga jet experiments at ISTTOK. Distribution of GaI, GaII and GaIII emission in the poloidal plane have been observed. The distribution shape depends on the Ga ionization step.

Using experimental data of the relative average intensity for GaI, GaII, GaIII distribution of Ga vapor concentration in different ionized states in the tokamak plasma in thermodynamic equilibrium.

We present the results for plasma parameters typical for TOKAMAK Frascati, planned for investigation of liquid metal experiments.

Plasma parameters:

The Gaunthy factor representing the statistic weight of electron levels involved in transitions:

$$\langle g(n,0) \rangle \sim 0.2$$

The electron temperature

$$T_e = 10 \text{ eV}$$

The plasma electron temperature

$$N_e = 0.55 \times 10^{20} \text{ m}^{-3}$$

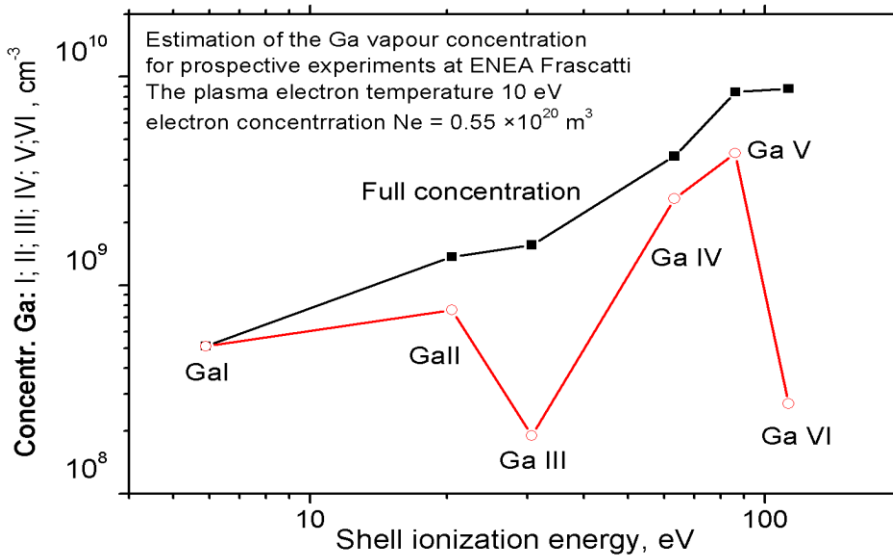
Results.

Concentration of Ga vapours in the outer shell of Ga

Ga I $I_{nm} = 20 \text{ a.u.}$ $N_{\text{GaI}} = 5.1 \times 10^8 \text{ m}^{-3}$	Ga II $I_{nm} = 90 \text{ a.u.}$ $N_{\text{GaII}} = 7.6 \times 10^8 \text{ m}^{-3}$	Ga III $I_{nm} = 5 \text{ a.u.}$ $N_{\text{GaIII}} = 1.9 \times 10^8 \text{ m}^{-3}$
--	--	---

Concentration of Ga vapours in the inner shells (Saha equilibrium)

Ga IV $N_{\text{GaIV}} = 2.6 \times 10^{10} \text{ m}^{-3}$	Ga V $N_{\text{GaV}} = 4.3 \times 10^9 \text{ m}^{-3}$	Ga VI $N_{\text{GaVI}} = 2.7 \times 10^8 \text{ m}^{-3}$
--	---	---



4. Conclusions

- The developed routine for estimation of Ga vapour total concentration in plasma can be applied in the future experiments.
- The routine can be applied for investigations of other liquid metal experiments (Li)
- For Ga experiments the vapour concentration shall be performed up to the Ga IV

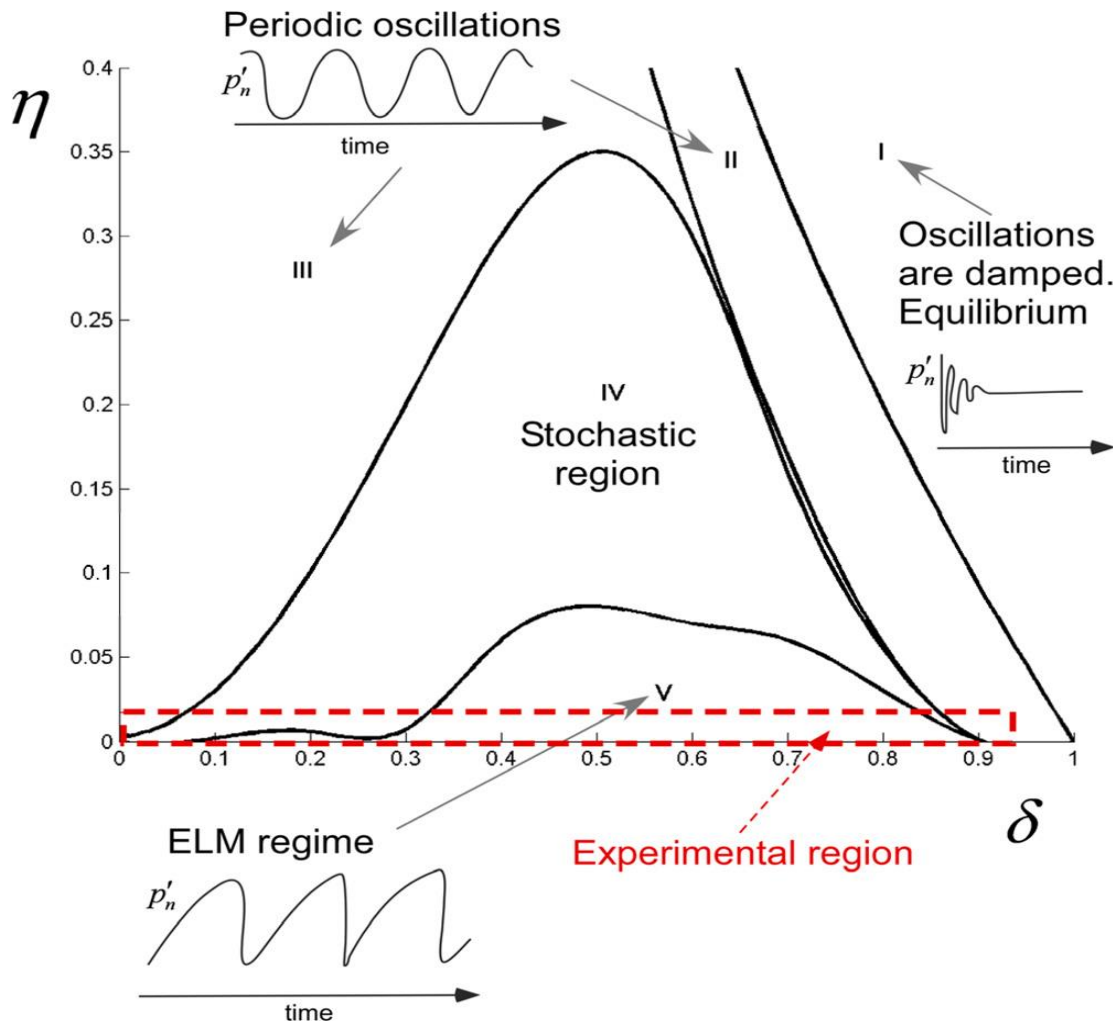
Independent plasma electron temperature distribution is required for investigation of Ga or other material distribution in radial and poloidal planes, planned for installation at the tokamak Frascati.

Spontaneous emission between two Ga atom levels m, n will be observed in different ionization states.

PLASMA PHYSICS TOPICAL GROUP: TG-MHD

Principal investigator **O. Dumbrajs**

Larger scale plasma instabilities not leading to an immediate termination of a discharge often result in periodic nonlinear perturbations of the plasma. A minimal possible model is formulated for description of the system with drive and relaxation processes which have different time scales. The model is based on two equations: the first being responsible for the relaxation dynamics and the second for the drive. Some specific physical examples are presented. The model can be generalized to describe the pellet injection.



Dynamical zones of oscillations.

D. Constantinescu, O. Dumbrajs, V. Igochine, K. Lackner, R. Meyer-Spasche, and H. Zohm, “A low-dimensional model system for quasi-periodic plasma perturbations” Phys. Plasmas 18, 062307 (2011).

A new relaxation instability with complex MHD activities is found in the HT-7 tokamak operational region.

Erzhong Li, Liqun Hu, V. Igochine, O. Dumbrajs, and Kaiyun Chen, „Understanding complex magnetohydrodynamic activities associated with a relaxation in HT-7 tokamak” Plasma Phys. Control. Fusion 53, 085019 (2011).

MATERIALS MODELING

Principal investigator: E.A. Kotomin

2011A. VACANCIES AND Y IMPURITIES IN BCC-FE LATTICE

Stabilization of Y impurity atom inside α -Fe lattice could require more than one Fe vacancy *per* solute atom. In such a case, not only substitute Y_{Fe} atom is stable but also yttrium atom in interstitial sites (Y_i). The reference energy state for the isolated vacancies as well as isolated Y_{Fe} and Y_i atoms could be estimated if the impurity Y atom is positioned in the center of vacancy cluster. Detailed analysis of interaction between the two vacancies revealed their strongest attraction of vacancies positioned in the second nearest neighbor sphere ($2NN$) – 0.23 eV, being smaller than that for $1NN$ (0.14 eV). In the case of $3NN$ and larger inter-vacancy distances, the interaction is lower than 0.05 eV. More than two vacancies form clusters of the smallest possible volume.

Binding energies of multiple vacancies ($N = 1-9$) inside α -Fe lattice.

N	1	2	3	4	5	6	7	8	9
$E_{bind}(N)$, eV	0.0	0.23	0.65	1.38	2.19	3.18	2.94	4.23	5.34

2011B. INTERACTION OF FE VACANCIES AND Y-O-Y CLUSTERS IN FCC-FE LATTICE

We predict location of Fe vacancies in the proximity of impurity atoms. The calculations on different Y-O-Y cluster configurations clearly show that not only the presence of oxygen atom is required to form certain binding between impurity atoms but also the presence of Fe vacancies favors the growth of the Y_2O_3 precipitates inside the iron crystalline matrix. This has been proven by the calculations of interactions inside the $Y-V_{Fe}-Y$ cluster for which the binding energy has been found to be rather large.

JW11-FT-1.19. AMS AND FCM MEASUREMENTS OF TRITIUM IN LASER CLEANED TILES AND TRITIUM DEPTH PROFILES IN JET DIVERTOR TILES

Principal investigator G, Kizane

The goals of the task are measurement of complete poloidal distributions of T deposition (depth distribution) on Divertor tiles and a set of divertor tiles from the 2009 shutdown and assessment of the efficiency of tritium laser cleaning by measuring the T- content by AMS and by FCM of treated and untreated surfaces and cross comparison of results.

Analysis of selected samples of plasma-facing components CFC, in order to support particle transport studies, tritium trapping, development of in-situ detritiation methods and others has been proposed as the JET Fusion Technology activities in the frame of the EFDA 2011 Workprogramme.

In order to obtain wider information on tritium distribution, cooperation was realized between AEUL (Latvia) and MEdC (Romania) and TEKES (Finland) in the frame of the task JW11-FT-1.19.

Distribution of tritium has been analysed in the selected tiles of the JET MkII Septum Replace Plate (SRP) divertor, campaign 2001-2004. Samples of tile 14ING3B (Fig. 4.21) was analysed and analysis of tile 14BWG4B was continued for realization the tasks.

Analysis of surface activity of tritium once more confirm the fact that main part of tritium is accumulated in a deposited layer and substantial difference are between the surface and bulk activity and the last slice at a rear side. Migration of tritium into the bulk of a tile is expected at high temperatures as is clearly demonstrated in the results from the sloping part where the tritium mass activity of the bulk was found to be about an order higher than in other parts of the tile.

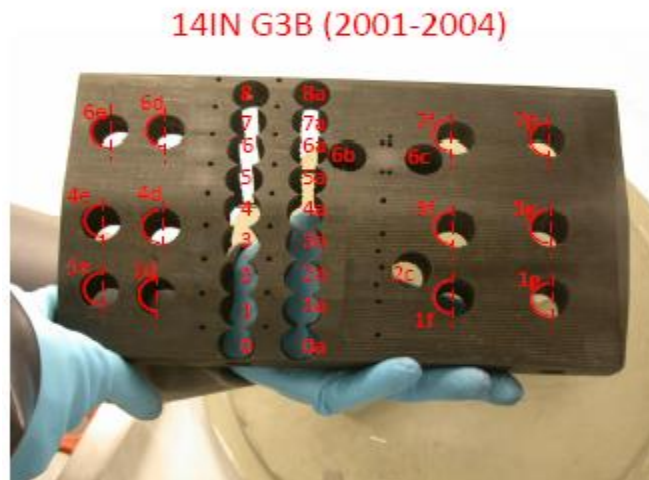


Figure 9. Positions of analysed cylinders of tile 14ING3B, cylinders “e” – without treatment, not detritiated and cylinders “f” laser cleaned.

Laboratory analysed slices cut from both type of cylinders –from cylinders “e” without cleaning, non-detririated samples and from laser cleaned slices from “f” cylinders. Amount of tritium on plasma facing surface slices, in the bulk and in the back side slices are shown in Figs. 10 - 13.

The larger part of tritium is concentrated in the first slices A1 (1 mm) for all analysed cylinders. In the next slice the tritium amount sharply decreases and stayed less or more uniform in the middle of tile and then once more sharply increases in the last slice of the back side.

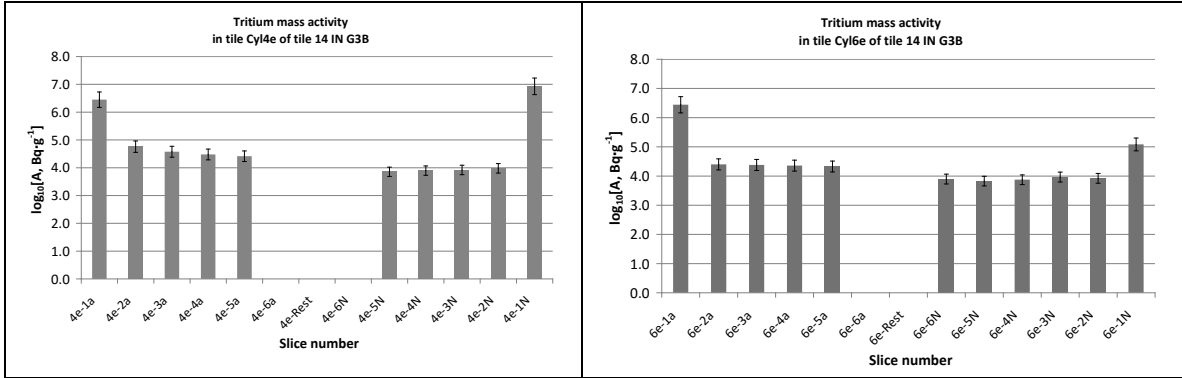


Figure 10. Distribution of tritium in non detririated cylinders Cyl4e and Cyl 6e.

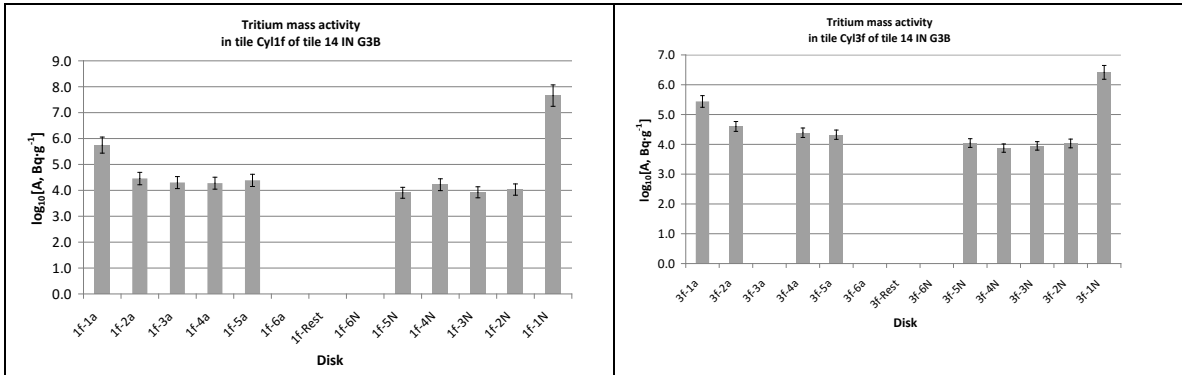


Figure 11. Distribution of tritium in laser cleaned cylinders Cyl1f and Cyl 3f

Obtained results show that an effect of laser cleaning could be observed on the first slice, but as analysis was realized with full combustion technique and in this case the thickness of a slice is 1 mm for analysis, to give precious numerical estimation of detririation degree is difficult, substantially thin slice is necessary to prepare. Additional analyses are necessary in order to explain the large amount of tritium in the last slice of all cylinders. The temperature-programmed desorption spectrum of tritium from oblong sample E1 of tile 14BWG4B obtained by means of the thermal analyser is shown in Figure 11.

In Figure12. the temperature-programmed desorption spectrum of tritium from oblong sample E1 is combined with the results of its thermal analysis. The tritium release in the temperature range of 300-600 °C can be associated with the mass loss of about 0.2% from the initial mass of sample E1, but the tritium release in the temperature range of 600-900 °C was not accompanied by any appreciable mass loss. We may note that the

set-up of the experiment had no zinc bed. Therefore, the possibly released tritiated water and some possibly released tritiated organic compounds may have been retained in the silica gel column and in the cold trap.

The residual tritium amount in sample E1 after the thermal desorption shown in Figure13 was determined by the full combustion method and was found to be 127 Bq, which is about 0.1% of the initial total amount, which is estimated to be about 125 kBq.

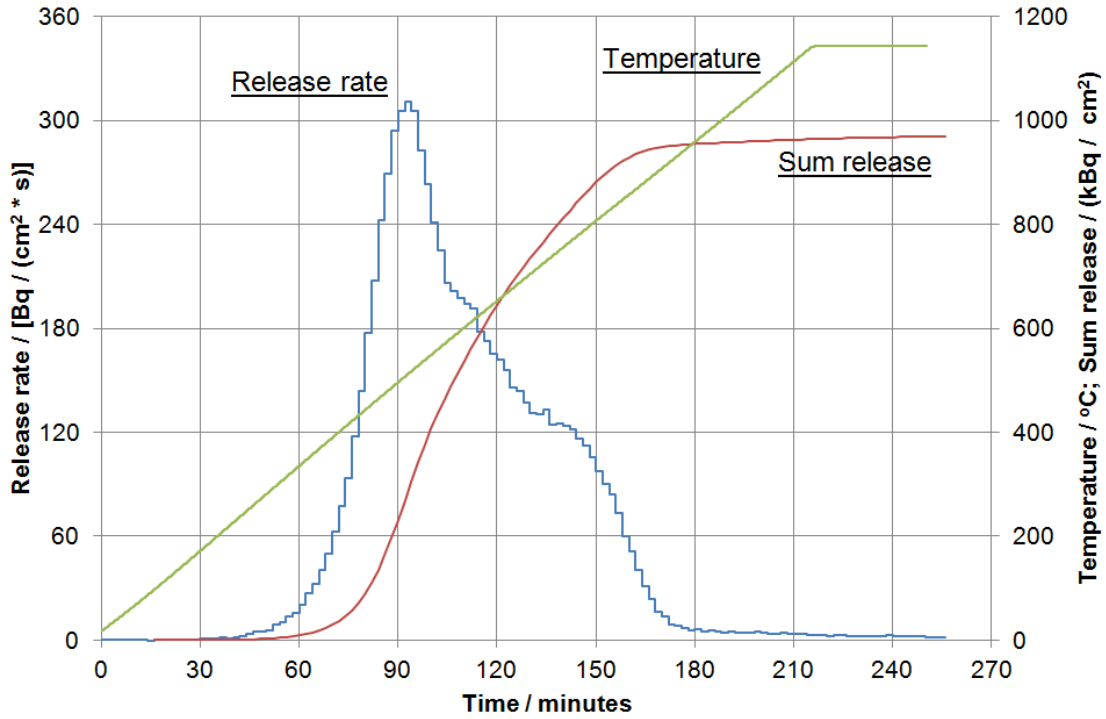
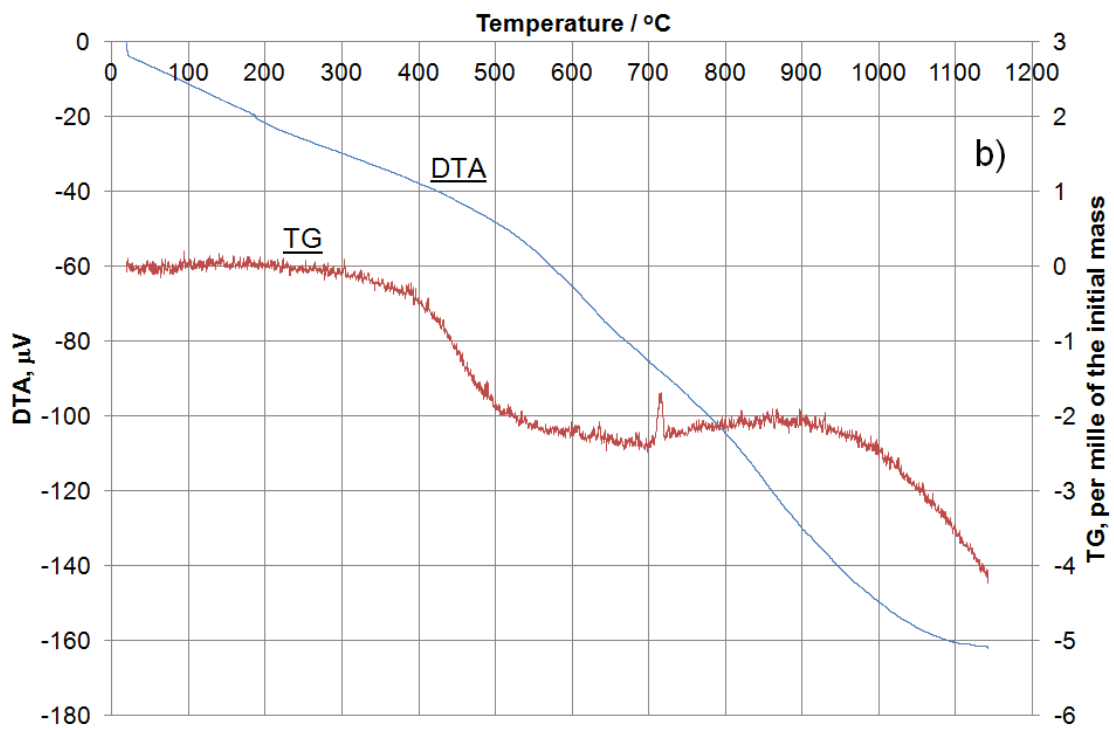
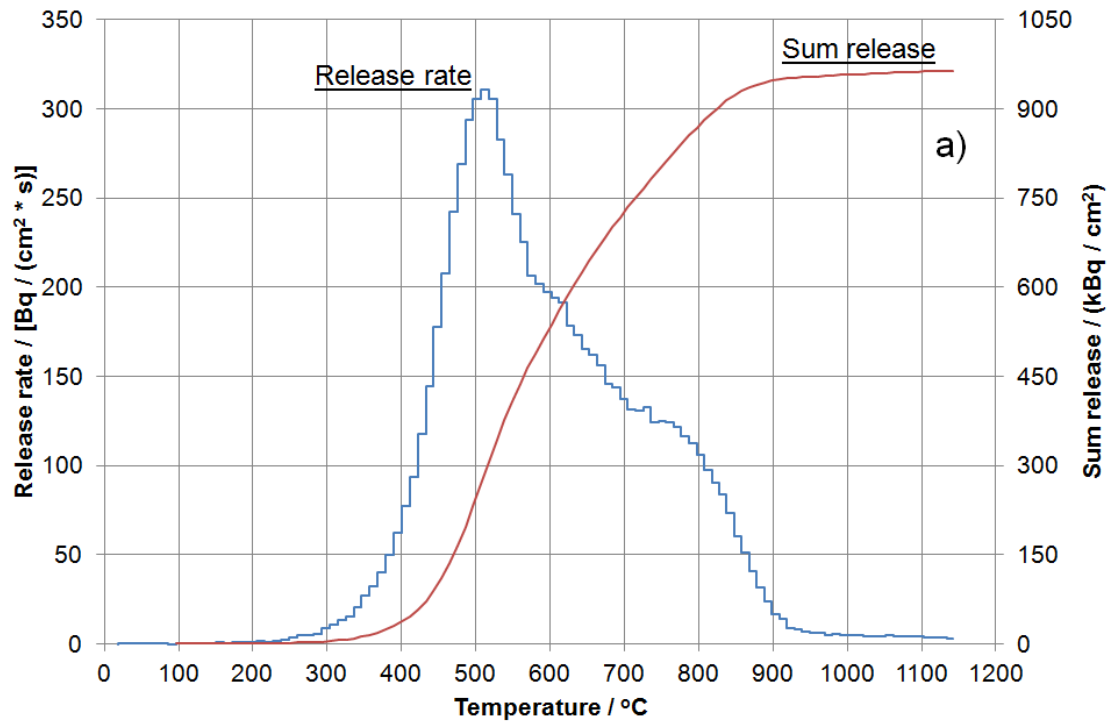


Figure 12. Tritium release by thermal desorption from oblong sample E1 of tile 14BWG4B.



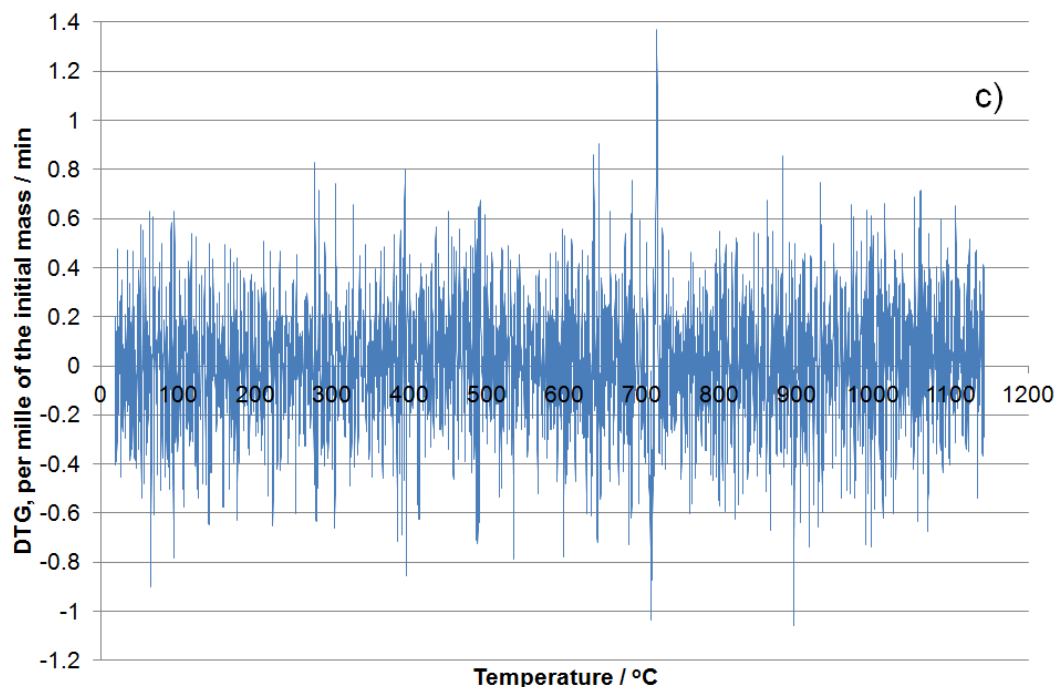


Figure 13. Tritium release by thermal desorption from oblong sample E1 of tile 14BWG4B (a) and its simultaneous curves of differential thermal analysis (DTA), thermogravimetry (TG) (b) and differential thermogravimetry (TG).

Regarding the possible effect of magnetic field on the tritium release, the pairs of adjacent oblong samples C4&C5, A1&A2 and A5&6 of tile 14BWG4D were analysed and compared. All samples from the plasma exposed surface. Adjacent samples may be thought to be similar in respect of their tritium release properties. However, the oblong samples were dissimilar not only by their initial total tritium activity, which was in the range of 0.5-3.5 MBq·cm⁻², but also by their tritium fractional release under the similar conditions. This dissimilarity of the samples limits the ability to draw quantitative conclusions about the magnetic field effect on the tritium release.

The degrees of detritiation achieved in the annealing process are summarized in Figure 14. as function of the maximum temperatures of the samples. The highest degrees of detritiation of 55-66% were achieved only in a magnetic field of 1.7 T. The medium degrees of detritiation of 22-32% were achieved with the electron irradiation in a magnetic field of 1.7 T in most cases at lower maximum temperatures of the samples than those with the electron irradiation without magnetic field or with simple heating without electron irradiation. Therefore, a trend that magnetic field of 1.7 T had a facilitating effect on the tritium release may be concluded from the experimental results.

Regarding the choice of the time of the electron irradiation of 30 min in comparison with 180 min, we may conclude from the tritium release curves that the fractional release rate diminished significantly by the end of the 30 min electron irradiation time in the case of samples 2, 4, 5 and A2, but the fractional release rate remained high by the end of the 30 min electron irradiation time in the case of samples 3, C1, C2, C4, C5, A1, A3-A6. Therefore, we may suggest that prolongation of the electron irradiation would have considerably increased the degree of detritiation of samples 3, C1, C2, C4, C5, A1, A3-A6

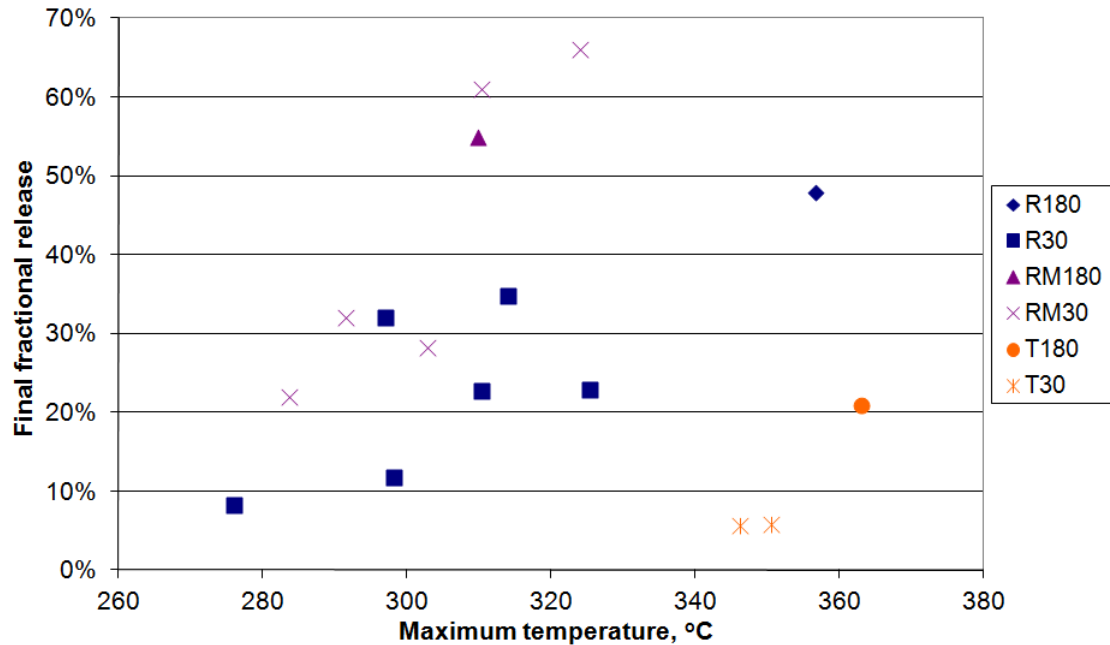


Figure 14. Final values of the tritium fractional release as a function of the maximum temperature at annealing. Explanation of the legend: R180 and R30 – the 5 MeV fast-electron irradiation for 180 and 30 min respectively without magnetic field; RM180 and RM30 – the 5 MeV fast-electron irradiation for 180 and 30 min respectively in a magnetic field of 1.7 T; T180 and T30 – only thermal treatment for 180 and 30 min respectively without electron irradiation and without magnetic field.

Tritium release from neutron irradiated beryllium pebbles F4E-2009-GRT-030-A3

In order to estimate behaviour of beryllium pebbles under exploitation conditions relevant to the ITER and DEMO, the HIDOBE-1 (**H**igh **D**ose Irradiated **B**eryllium) experiment had been performed in the frame of the European Programme for development of the helium cooled pebble bed (HCPB).

Be pebbles as neutron multiplier will be under action of a high temperature, neutron flux and high magnetic field. The range of temperature at the operating conditions of the HCPB of different designs is given different - up to 920 K (**647 °C**), 700-1050 K (**427-777°C**) or up to 1170 K (**897°C**), but the latest information is that the maximum interface temperature of 823K (**550 ° C**) is chosen. Tritium release and retention is dependent on beryllium properties (structure, impurities, grain size, diameter of a pebble, porosity etc.), on irradiation conditions (neutron flux, temperature, content of purge gas etc.), on chemical impurities.

Mass activity of tritium in the pebble correlates with irradiation temperature, if we compare amount of accumulated tritium at the highest irradiation temperature - 750 °C with tritium amount accumulated at 425, 550 and 650 °C, but at the same time at temperatures 425, 550 and 650 °C the activities of tritium are similar, influence of irradiation temperature isn't substantial.

Abundance ratio of tritium chemical forms might be assumed to be similar. Only slight differences that do not exceed confidence level are observed for the pebbles synthesized in the year 2003. Higher amount of molecular tritium was observed in pebbles produced by improved method in 2003.

Tritium accumulated in the HIDOBE-I beryllium pebbles has been localized in forms of the gas T_2 and T^0 and ions T^+ . The main chemical form of the tritium accumulated in the HIDOBE-I beryllium pebbles is molecular tritium T_2 - $94 \pm 2\%$, atomic tritium T^0 only $2 \pm 2\%$ and tritium in ionic form $6 \pm 1\%$.

Tritium release under action of temperature

Post irradiation tritium room temperature to 1310 K and anneals at a constant temperature of 1 h on the beryllium pebbles were performed.. Tritium release begins for all of investigated HIDOBE-I beryllium pebbles at temperatures 850-900 °C and after 900 °C starts fast tritium release process. Amount of accumulated and retained tritium is very dissimilar for one batch; but for different batches it differs even 22-58 times each from another pebble. Tritium release from pebbles at 1039 °C temperature for 1 h long time with lower tritium activity (1-3 GBq) goes more effective. Residual tritium had been determined by dissolution method and was only some kBq. Tritium release even from three beryllium pebbles of one batch is very dissimilar. Figure 15 shows tritium release histograms from three pebbles of the same batch. 9SPc/3.

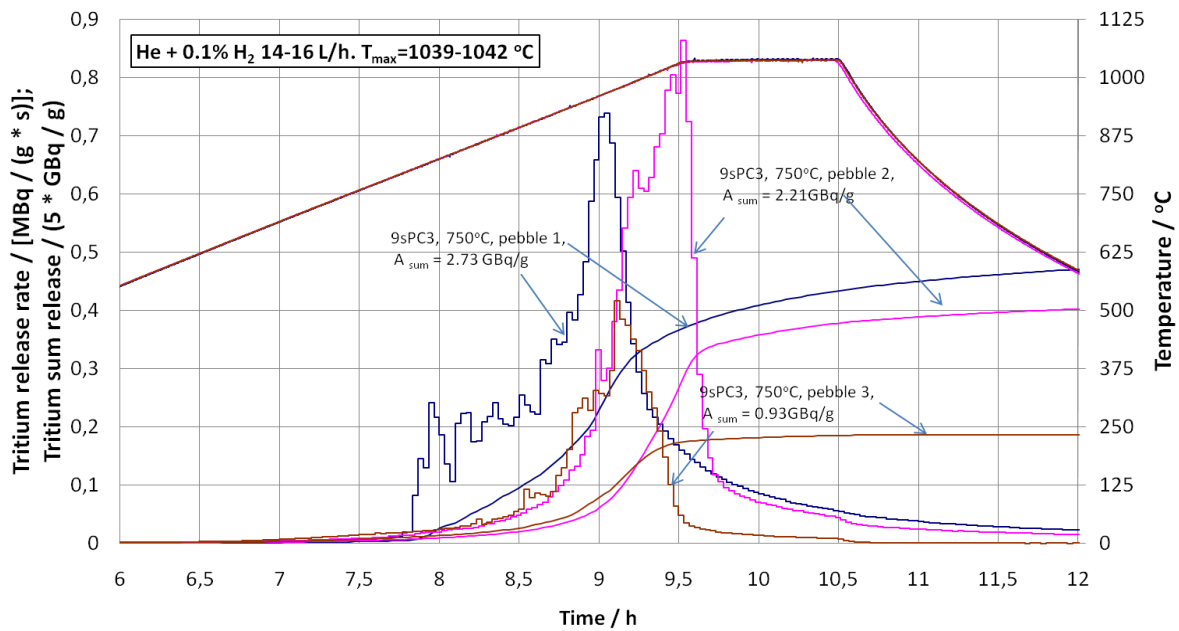


Figure 15. Tritium release rate and tritium sum release from the HIDOBE-01 beryllium pebbles having lower level tritium activity heated at the given temperature. The blue curves – the HIDOBE Be pebble of 1.12 mg having the tritium sum release 2.73 GBq/g. The pink curves – the HIDOBE Be pebble of 1.04 mg, the tritium sum release 2.21 GBq/g. The brown curves – the HIDOBE pebble the tritium sum release 0.93 GBq/g.

Main conclusions

Tritium content in irradiated pebbles depends on irradiation temperature: at lower temperatures more tritium is left in the pebble. Most of the tritium is accumulated as a molecular T_2 (89-93%), whereas chemically bonded to oxygen T^+ is 5-10% of tritium. Atomic tritium T^0 does not exceed 4-7% of the total content. Investigated pebbles were

different by their mass (0.67-1.34 mg), by their initial total tritium activity and by their tritium fractional release under the given conditions. Tritium thermo-desorption process is considerably different even within one type of pebbles. For estimation of desorption mechanisms and reasons for such differences more measurements are needed.

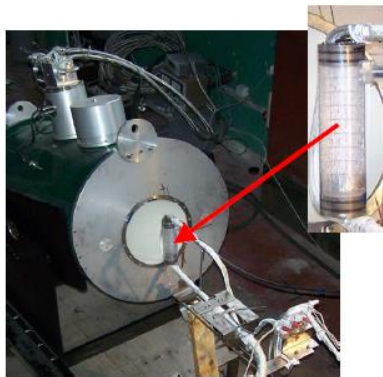
YEAR 2012

FUSION RELATED LIQUID METAL MHD RESEARCH.

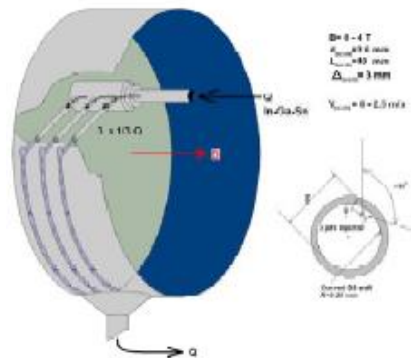
Principal investigator: E.Platacis

WP12-PEX-04-TO3-01/UNIVERSITY OF LATVIA/BS STABILITY OF METAL DROPLETS /JETS IN TOKAMAK ENVIRONMENT.

Content: a)Introduction; b)Stability of liquid metal jets trajectory in strong non homogeneous magnetic fields; c)Influence of a non-homogeneous magnetic field on the stability of the break-up length; d)Pathway of a LM jet over a solid substrate in the presence of a strong magnetic field.



Jet in a strong non-homogeneous field.



Experiment with jets over curved substrates

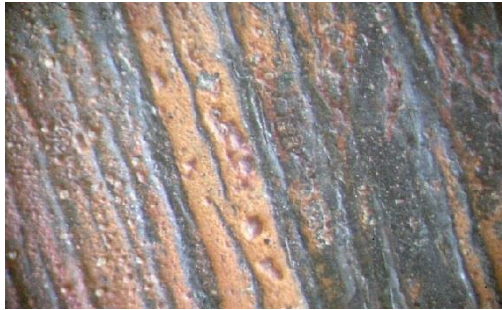
POST MORTEM ANALYSIS OF BARE STEEL EROSION, IMPURITY DISTRIBUTION USING LIBS SPECTROSCOPY

Principal investigator: I. Tale

By exploiting PWI-dedicated devices, P92 or EUROFER samples should be exposed to monoenergetic particle fluxes, at energies ranging beyond 1 keV to measure the erosion rate as a function of the energy. Because of the vessel opening schedule of ASDEX Upgrade, Association UL supports realization the investigations of corrosion effects in EUROFR by interaction with liquid PbLi flux in a strong up to 4T magnetic field and temperature up to 550⁰ C.. The preliminary experiments are performed using LIBS spectroscopy.

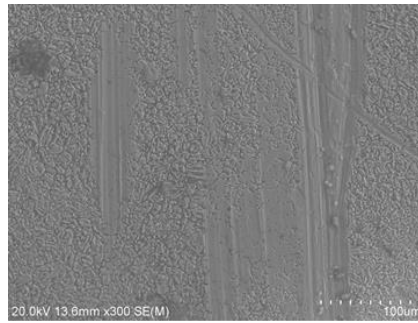
Post mortem analysis of bare steel erosion, impurity distribution using LIBS spectroscopy are performed.

EUROFER SEM images



T=550C, B=5 T.

Roughness: up to 25 μm



T=515C, B=1,8T.

Roughness: ~ 0,15 μm

Double laser beam LIBS spectroscopy has been provided for following atoms, not presenting in EUROFER elements together with Fe:521,8 nm.

	Emission line wavelength, nm		
H	656.23		
Li I	548.4	610.35	670.72
Pb	405.7	569.2	
O	557.2		

Main results.

Linear scan of sample T=550C, B=5 T represented by two characteristic surface regions: emission of Fe-line, emission of considerable LI I- , weak Pb- and O- lines.

During repetition of linear scans results in diminish first, the Pb- line, and continuous diminish simultaneously the LI I- and O- lines simultaneously restoring the characteristic emission spectrum of EUROER.

Principal similar results are obtained for sample $T=515\text{ C}$, $B=1,8\text{ T}$. However, even using of focused ablation laser beam during the first scan the ratio Li I-, O- / Fe lines intensity fluctuate from pulse-to pulse.

Conclusions;

Presence of oxygen in liquid FeLi flux results in formation of Li- and Pb- oxide layer.

Presence of oxide layer can be responsible for selective erosion of EUROFER.

Non homogenous PbLi flow in magnetic field can be important factor for formation of oxide layers.

PLASMA PHYSICS TOPICAL GROUP: TG-MHD

Principal investigator O. Dumbrajs

In a low dimensional model which describes the dynamics of the plasma pressure gradient and of the amplitude of the displacement of the magnetic field in tokamaks we study the Hopf bifurcation. We analyze the fast-slow dynamics which appears for small normal heat diffusion and we corroborate the results with those observed in experiments.

D. Constantinescu, O. Dumbrajs, V. Igochine, K. Lackner, and H. Zohm

“Bifurcations and fast- slow dynamics in a low-dimensional model for quasi-periodic plasma perturbations” Romanian Physics Report.

GYROTRONS TOPICAL GROUP: TG-H&CD

Principal investigator: O.Dumbrajs

J. Cepitis, O. Dumbrajs, H. Kalis, A. Reinfelds, and U. Strautins „*Analysis of equations arising in gyrotron theory*” **Nonlinear Analysis: Modelling and Control** **17, 139 (2012)**

The paper provides a survey of the analytical and numerical results obtained by our group in the last decade.

O. Dumbrajs, T. Idehara, and S. Sabchevski, “**Design of an optimized resonant cavity for a compact sub-Terahertz gyrotron**” **J. Infrared Milli. Terahz. Waves** **31, 1115 (2010).**

Two versions of gyrotron equations are investigated by means of implicit difference schemes and method of lines.

A. Reinfelds, O. Dumbrajs, H. Kalis, J. Cepitis, and D. Constantinescu, „*Numerical experiments with single mode gyrotron equations*” **Mathematical Modelling and Analysis** **17, 251 (2012).**

This paper is devoted to the analysis of the instability of operating modes in high-power gyrotrons with cylindrically symmetric resonators. This instability manifests itself in destruction of the azimuthally uniform wave envelope rotating in a gyrotron resonator having a transverse size greatly exceeding the wavelength. The appearance of azimuthally nonuniform solutions can be interpreted as simultaneous excitation of modes with different azimuthal indices.

O. Dumbrajs, G.S. Nusinovich, and T.M. Antonsen, Jr., “Regions of azimuthal instability in gyrotrons” Phys. Plasmas 19, 063103 (2012).

Possibilities of arising of aftercavity interaction are analyzed in the ITER 170 GHz 2 MW coaxial cavity gyrotron and the 170 GHz 1 MW cylindrical cavity gyrotron

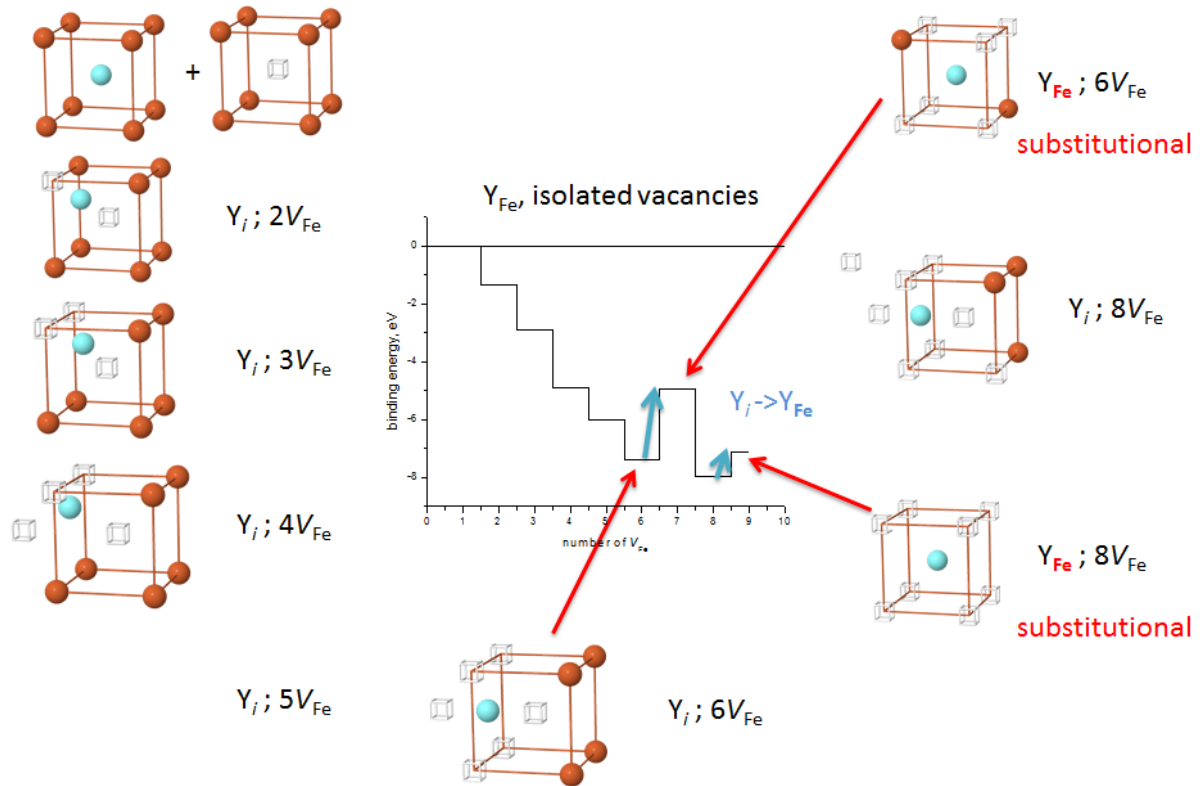
O. Dumbrajs and T. Idehara „Analysis of aftercavity interaction in European ITER gyrotrons and in the compact sub-THz gyrotron FU CW-CI” J. Infrared Milli. Terahz. Waves 33, 1171 (2012).

MATERIALS MODELING

Principal investigator: E.A. Kotomin

2012A. INTERACTION BETWEEN VACANCIES AND SINGLE Y IMPURITIES IN BCC-FE LATTICE

Various configurations of a single Y solute atom incorporated in different vacancy clusters have been calculated. As the reference energies, there have been used isolated vacancies and isolated Y_{Fe} . In all the configurations, Y atom has been positioned in the middle of vacancy cluster and all the corresponding defect complexes have been found energetically stable. Incorporation of additional vacancy to the cluster containing Y_i atom and six vacancies in octahedral coordination around it has been found to be energetically unfavourable. Although the complex of Y_{Fe} atom and eight vacancies in cubic coordination around it has been found to be stable too, the binding energy for this configuration is smaller, than that for clusters containing six and eight vacancies with interstitial Y_i .



2012B. INTERACTION BETWEEN VACANCIES AND Y IMPURITIES IN FCC-Fe LATTICE

For *fcc* Fe phase, the binding energy between Fe-vacancies significantly increases in the case of four vacancies in comparison to the configurations with two or three Fe vacancies. The largest binding energies were found for the configurations with a single Y atom and several vacancies. The binding energies for the configuration between two Y atoms and vacancy increase with the increase of the distance between two Y atoms, and in the case of the 4NN attraction was observed between two Y atoms inside the lattice.

Interactions between clusters consisting of different number of vacancies

Configuration	E_{form} (eV)	Binding energy (eV)
$1V_{Fe}$	2.37	-
$2V_{Fe}$ (1NN)	4.50	0.25
$3V_{Fe}$	6.76	0.37
$4V_{Fe}$	8.18	1.32

JW12-FT- 1.20 COMPLETE POLOIDAL DISTRIBUTION OF TRITIUM RETENTION IN JET DIVERTOR TILES MEASURED BY AMS AND FCM+SD ANALYSING METHODS

Principal investigator G.Kizane

JW12-FT-1.20 are related to the estimation of the tritium distribution in the carbon based tiles – tungsten uncoated, coated. Both tasks are continuation of the EFDA JET Technology Tasks on the tritium in tokamaks. Besides mentioned tasks laboratory additionally investigated microstructure and content of tiles.

The tasks were realized in cooperation with association of EURATOM and Romania, MEdC, as well as with Finland, TEKES and Estonia.

Tungsten coated and uncoated tiles of the MkII-HD divertor configuration used in JET during the experimental campaign in 2007-2009 were compared. Tile 2OWG7B and 2ONG8A tungsten coated and uncoated tile 2IWG1A had been analysed. Tile 2OWG7B and 2ONG8A have ~ 25 μm tungsten coating with molybdenum interlayer.

Analysis of surface activity of tritium once more confirms the fact that main part of tritium is accumulated in a deposited layer. Thickness of the first analysed layer is about 1 mm for full combustion technique. In the next slice, which is 2-3 mm deeper from plasma facing part, tritium amount sharply decrease up to order of 1-1.5 magnitude.

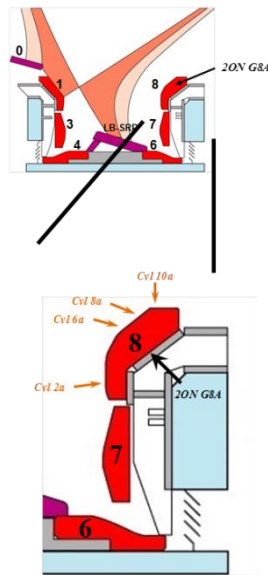
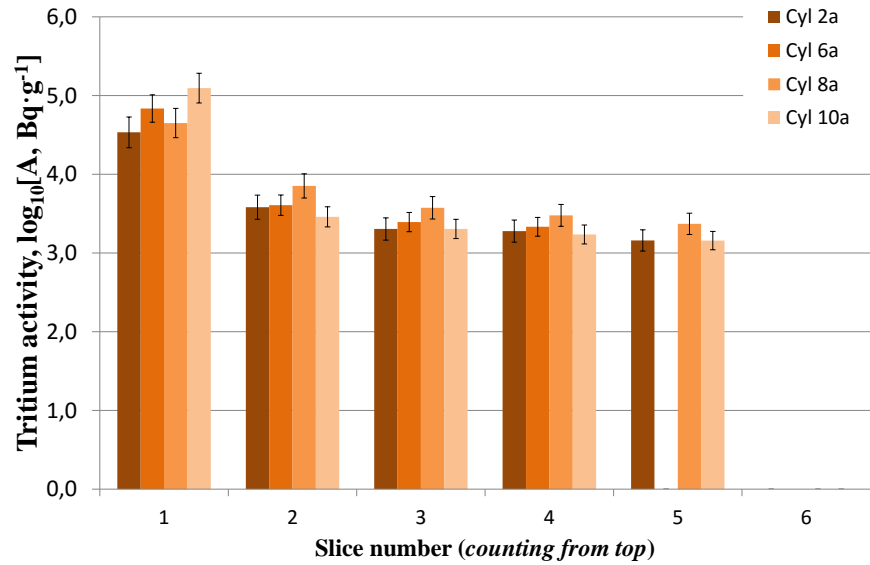


Figure 16. Tritium mass activity comparison in tungsten coated tile 2ON G8A and scheme of positions of the cylinders

Distribution of tritium amount depends on position of tile against plasma reaction zone. Anyway the difference between activity of tritium amount for cylinders Cyl 2a, 6a and 8a of tungsten coated tile 2ON G8A is not substantially different, but in the first slice of Cyl 10a amount of tritium is the larger. It is understandable as the Cyl 10a is not placed straight against plasma zone. In the bulk of tile 2ON G8A in the slices 2, 3, 4, 5, which are 2-9 mm deep from plasma facing surface, for all investigated cylinders Cyl 2a, 6a, 8a and 10a tritium amount has one order magnitude.

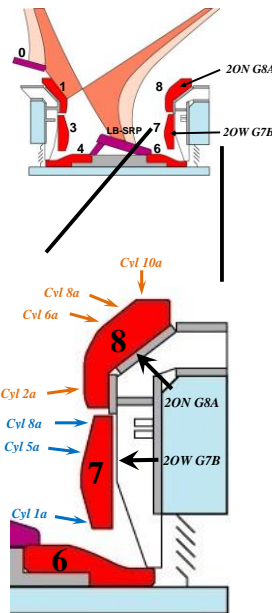
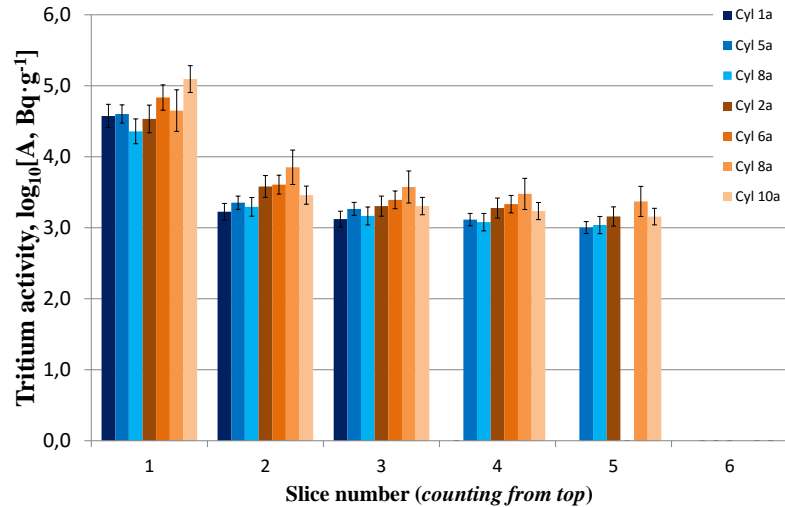


Figure 17. Tritium mass activity comparison in tungsten coated tiles 2OWG7B (blue colour) and 2ON G8A (orange colour)

Tritium amount in tungsten coated tiles 7 and 8 (2OWG7B and 2ON G8A) is one magnitude. Comparison of tritium amount in tile 7 and 8 shows clearly, that tritium is more accumulated in tile 8 -2ON G8A. Observed that in both cases as in the first slice and in the bulk of tile tritium accumulated more in tile 2ON G8A.

Samples of uncoated divertor tile 2IWG1A used in the same JET experimental campaign in 2007-2009 with an MkII-HD divertor configuration was analysed in comparison to W-coated tiles, resulting in following:

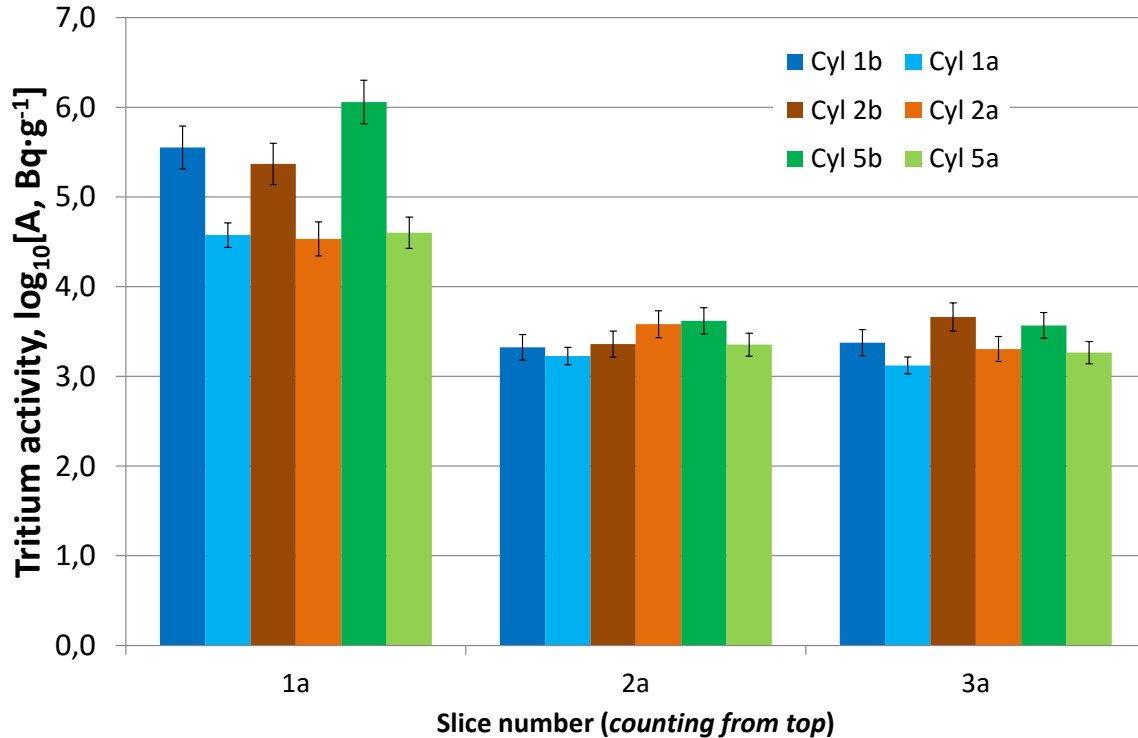


Figure 18. Tritium mass activity comparison in cylinders of uncoated and tungsten coated tiles:

- cylinders Cyl 1b, Cyl 2b, Cyl 5b of uncoated tile 2IW G1A tile
- cylinder Cyl 2a of tungsten coated tile 2ON G8A
- cylinders Cyl 1a, Cyl 5a of tungsten coated tile 2OW G7B

As observed in this and previous studies for uncoated divertor tiles, there is up to 3 orders of magnitude difference between the tritium activity in plasma exposed surface upper layer and the bulk. For the W-coated tiles retrieved from the same divertor area this difference appears to be smaller –about 1-2 orders of magnitude – compare with the bulk activity of tile.

Experimental work provides confirmation that tungsten coating of divertor tiles has a beneficial effect reducing the tritium retention on both, on the plasma exposed area of as well as in the bulk of tile. Therefore, from the point of view of tritium retention, tungsten can be efficiently used in the divertor region of any fusion machine such as ITER or DEMO.

Microstructure of MkII-SRP divertor tiles comparing with amount of accumulated tritium

In order to understand tritium accumulation in bulk of CFC related with microstructure of a tile we chose for analysis floor base wide tile 4 - 14BWG4B and vertical inner narrow tile 3 - 14ING3B.

X-ray diffractometry was used for structure analysis. It is known that changes of the reflex intensity show heterogeneity and crystallinity of sample. In diffractograms

observed diffraction reflex at $26.5^{\circ}2\theta$ characterises graphite structure in CFC material. The mentioned reflex is observed in all analysed CFC slices.

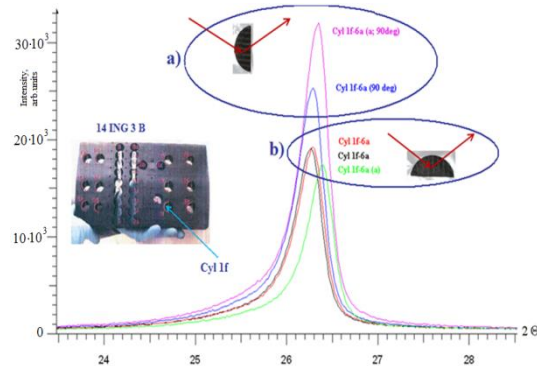


Figure 19. X-ray diffractograms of slice 1f-6a from tile 14ING3B

Material is more amorphous in parts of tile where the amount of accumulated tritium is higher. Differences in structure depend on plasma processes in vacuum camera and are linked to a position of tile in vacuum chamber and also of a geometry of tile.

The structure of material was also investigated with Raman spectroscopy. Raman spectra were taken for the half-slice from the middle part of tile – half-slice 3f-6a, tile 14ING3B. If in the spectrum is a single high-frequency line at about 1580 cm^{-1} it is attributed to large single crystal graphite. In case of analysed CFC two peaks are observed in spectra. The G-peak, at about 1580 cm^{-1} , is due to the bond stretching of all pairs of sp^2 atoms in both rings and chains (C-C bonds of graphite). A peak at about 1350 cm^{-1} (D-peak) is due to the breathing modes of sp^2 atoms in rings.

The presence of the D-peak in Raman spectra points to disorder related structures in material. That matches with results of X-ray diffractometry, which shows a presence of amorphous structures in the investigated tiles. The differences between Raman spectra of samples could be explained with different plasma exposure to different parts of the tile (**Figure 19 and 20**).

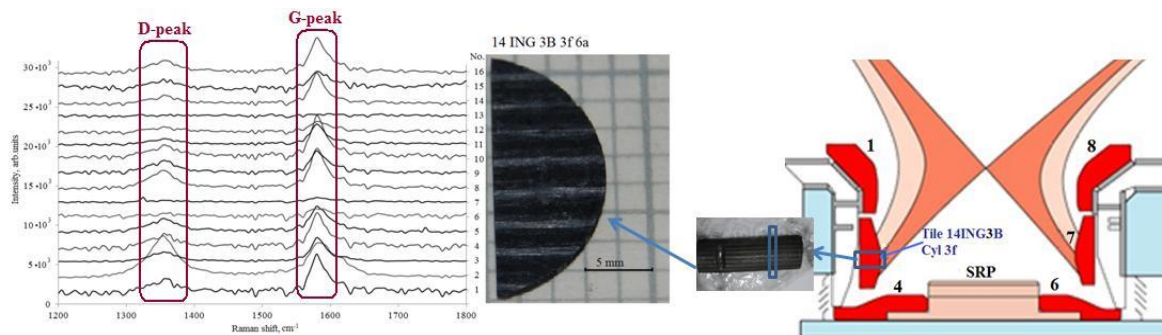


Figure 20. Raman spectra of the slice 6a from cylinder 3f of tile 14ING3B and position of these in the divertor

In the sloping part of tile 14BWG4B tritium activity is higher as in cylinders of the SRP and of the shadowed part.

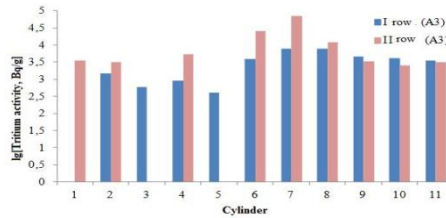


Figure 21. Tritium activity in slices of tile 14BWG4B into depth 4-5 mm from PFS

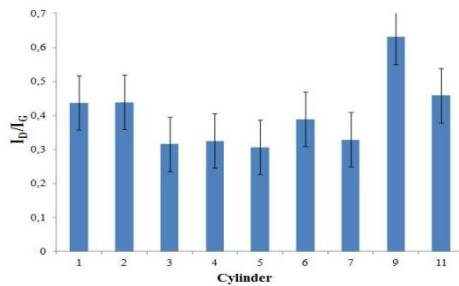


Figure 22. Intensity ratio I_D/I_G in slices of tile 14BWG4B in depth 2-3 mm from plasma facing surface

Intensity ratios I_D/I_G calculated from Raman spectra are lower in sloping part as in shadowed area and SRP part (Figure 21), which points to structure changes in severe parts of tiles, that is analogous to tritium distribution.

Main conclusions

Structure, including microcrystalline structure, of the tiles is not homogeneous and depends on a position of a tile, against plasma interaction. Consequently, it might be assumed that different mechanisms of tritium migration and deposition are possible in different parts of tile.

Distribution of tritium amount depends on position of tile against plasma reaction zone

Tritium in high dose neutron irradiated HIDOBE-01 beryllium pebbles

At low irradiation temperature (425°C, 525°C) about 90% of produced tritium has remained in the bulk of the pebble .Chemical form analysis shows that most of tritium is accumulated as molecular T_2 . At 750°C most of the tritium is released already during the irradiation (~99%) and remaining tritium is mostly chemically bonded, could be more likely to the oxygen containing compounds.

Tritium bulk distribution was measured for pebbles irradiated at low temperatures, at high temperatures (750 °C) there were insufficient tritium concentration for this method. Tritium bulk distribution measurements indicate that except for the surface layer where

tritium concentration is comparably low in remaining bulk of the pebbles tritium is evenly distributed.

At low irradiation temperature (425°C) all of produced tritium remains in the bulk of the pebble. At 650°C tritium release during the irradiation has started and only 37% has remained in the bulk of the pebbles. At 750°C ~95% of the tritium is released already during the irradiation. In contrast to 0.5 mm pebbles most of the remained tritium is molecular. Therefore it might be concluded that from 1.0 mm pebbles at this temperature not all of gaseous products are released during irradiation. Tritium distribution in the bulk of the 1.0 mm pebbles after irradiation at 650°C was found to be uneven– tritium concentration increases towards centre of the pebble.

Influence of chemisorption products on radiolysis of lithium orthosilicate

Research work was done in cooperation with Karlsruhe Institute of Technology, Institute for Applied Materials.

Lithium orthosilicate pebbles with excess of SiO₂ (90 mol% Li₄SiO₄, 10 mol% Li₂SiO₃) are the European Union's designed reference tritium breeder for the Helium Cooled Pebble bed blanket module. On surface of Li₄SiO₄ pebbles after annealing (T_{max}=1243 K, t_{max}=168 h) in air may accumulate chemisorption products of CO₂ and H₂O vapour, i.e, Li₂CO₃ and LiOH. The aim of these investigations was to estimate influence of chemisorption products on the radiolysis of Li₄SiO₄ pebbles. Due to high surface area and small grain size, nano-structured Li₄SiO₄ powders with different composition and different surface area was selected as investigation materials to compare with pebbles as reference.

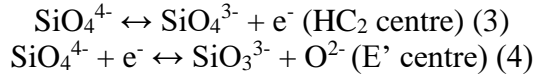
To identify accumulated RD and products of radiolysis (RP) of chemisorption products in nano-structured Li₄SiO₄ powders, "pure" Li₂CO₃ and LiOH powders were irradiated (absorbed dose 56 kGy, dose rate 14 kGy·h⁻¹). To investigate thermal stability of accumulated RD, irradiated nano-structured "pure" Li₄SiO₄ powder were thermally treated from 473 to 580±5 K for 30 minutes.

To simulate processes which occurred in Li₄SiO₄ pebbles in irradiation process at high temperature in air, annealed nano-structured Li₄SiO₄ powder with SiO₂, with relevant composition as in pebbles, was selected as investigation material. The powder was thermally treated up to 570 K for 4 hours and irradiated with gamma rays (absorbed dose 56 kGy, dose rate 14 kGy·h⁻¹) at air.

Formation of radiation defects in lithium orthosilicate

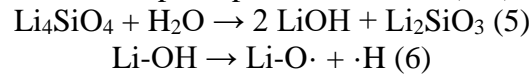
Using chemical scavenger method, it has been determined that under action of accelerated electrons (D_{abs.}=11 GGy) at 570±20 K and at dry argon in annealed Li₄SiO₄ pebbles with SiO₂ accumulated both, simple (3.0 10¹⁸ radicals g⁻¹) and multi-electron centres (3.0 10¹⁹ radicals g⁻¹). Multi-electron centres in pebbles mainly consist from aggregates of primary electron type RP, i.e. colloidal lithium (Li_n), but simple centres from localized electrons in oxygen vacancies, so called F⁺ and F⁰ centres. Both electron type centres possess paramagnetic properties and therefore could be observed in ESR spectra. In ESR spectra Li_n forms characteristic ultra-fine signal with g-factor from 2.001 to 2.004, but F⁺ centres broad multiplex signal with g-factor 2.002.

In obtained ESR spectra of irradiated Li_4SiO_4 pebbles three other signals with contiguously lying values of g-factors: 2.001, 2.011 and 2.016, and different width were observed. It has been suggested that ESR signal of Li_n in obtained spectra was not observed due to aggregation of RP. All three observed signals in ESR spectra were attributed to characteristic RD which accumulates in “pure” Li_4SiO_4 and has been investigated in previous researches. ESR signal with a g-factor 2.002 ($\Delta H=10$ mT) was related to electron type E' centres (ion radical SiO_3^{3-}), in contrast to the 2.009 and 2.013 signals, which could be attributed to hole type HC_2 centres (ion-radical SiO_4^{3-}). Both E' , and HC_2 centres are primary RD of Li_4SiO_4 (3-4.) and Li_2SiO_3 phase. However due to high irradiation temperature and recombination processes, concentration of RD is quite small - $4.0 \cdot 10^{15}$ radicals g^{-1} (99 % E' and 1 % HC_2 centres).



From obtained ESR results it can be suggested that concentration and type of RD in pebbles depends not only on absorbed dose and irradiation temperature, but also on irradiation atmosphere. For example, by replacing dry argon with air, concentration of RD increases several times – up to $5.0 \cdot 10^{17}$ radicals g^{-1} , and amount of HC_2 centres increases from 1 % to 25 %. As well as air atmosphere influence also type of accumulated RD.

In ESR spectra of pebbles were observed not only characteristic signals of E' and HC_2 centres, but also two symmetric lines ($g_1=2.193$ and $g_2=1.898$) with 50.2 mT splitting. In previous research two symmetric signals were attributed to localized hydrogen ($\text{H}\cdot$), which is characteristic RD of chemisorption products of H_2O (5-6).



Therefore increase of characteristic silicate RD concentration at irradiation process in air could be explained as side effect of radiolysis of chemisorption products of H_2O vapour and CO_2 . To understand formation and radiolysis of chemisorption products on surface of Li_4SiO_4 pebbles at these irradiation conditions, influence of temperature ($T_{\max} \leq 570$ K) and air were investigated separately.

Influence of air atmosphere and chemical additions

Formation of chemisorption products of H_2O vapour and CO_2 on surface of Li_4SiO_4 pebbles depends not only on irradiation temperature, but also on contact surface area with air. Therefore to increase contact surface area, nano-structured “pure” Li_4SiO_4 powder was selected for investigation.

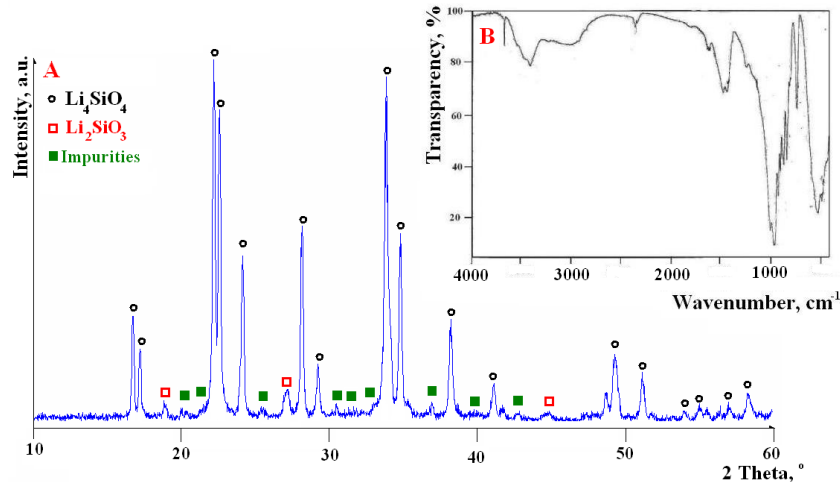


Figure 23. p-XRD patterns (A) and FR-IR spectra (B) of obtained nano-structured “pure” Li₄SiO₄ powder

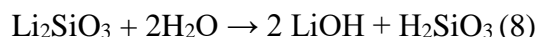
At storage stage from dry air on surface of nano-structured “pure” Li₄SiO₄ powder chemisorbed H₂O vapour and CO₂ (2.2±0.3 wt%). Formation of chemisorption products, i.e. LiOH and Li₂CO₃, was determined by p-XRD and FT-IR. Beside to characteristic signals of lithium silicates in both methods were also observed signals of impurities, for example, in FT-IR spectra was observed bond vibrations of C-O ($\nu=1440\text{ cm}^{-1}$) and O-H ($\nu=2800\text{-}3500\text{ cm}^{-1}$).

Mostly in irradiated Li₄SiO₄ containing ceramics these two quite small signals could be attributed to hole type RD - peroxide radical ($\equiv\text{Si-O-O}\cdot$). For all that in ESR spectra of irradiated “pure” LiOH and Li₂CO₃ powders from 338 to 348 mT were also observed similar signals. Thus it has been suggested that formation of signals in ESR spectra of “pure” Li₄SiO₄ powders could be related not only to peroxide radical, but also to accumulated RD or RP of chemisorption products.

On basis of obtained results it was concluded that air essentially influence radiolysis of ceramic of nano-structured “pure” Li₄SiO₄ powder. From obtained ESR results it was suggested that formation and type of RD in nano-structured powder is linked not only to irradiation atmosphere, but also on additions of SiO₂.

Additions of SiO₂ to nano-structured Li₄SiO₄ powder practically do not influence specific surface area, and therefore decrease of concentration of RD most likely could be related to chemical properties of SiO₂. It has been suggested that SiO₂ on surface of Li₄SiO₄ powder particles forms layer which could disturb and prevent chemisorption process of H₂O vapour and CO₂. Using TG-DTA it has been determined that 2.0 wt% of SiO₂ in Li₄SiO₄ decreases sorption of gases from air up to 7 times - from 14.0 to 2.0±0.3 wt%.

Annealing of Li₄SiO₄ powder with 2.0 wt% SiO₂ at air also decreases concentration of RD up to 25 % - from $2.7 \cdot 10^{18}$ to $2.0 \cdot 10^{18}$ radical g⁻¹, yet signals of H· in ESR spectra forms again. It has been suggested that SiO₂ on surface of particles, at high temperature in air, transforms in Li₂SiO₃ phase and due to angulations of particles decreases specific surface - from 22 to $17\pm 2\text{ m}^2\text{ g}^{-1}$. Therefore decrease of RD was attributed to change of contact surface with air, but formation of H· was explained by chemical properties of Li₂SiO₃ (8).



Beside of radiolysis of chemisorption products of H₂O vapour and CO₂, radiolysis of Li₄SiO₄ pebbles is affected also by temperature ($T_{\text{max}}=570\pm 20\text{ K}$). To understand influence of irradiation temperature on radiolysis, “pure” Li₄SiO₄ powder was selected as investigation material, due to high concentration of RD.

Using chemical scavenger method, it has been determined that under action of gamma rays in “pure” nano-structured Li₄SiO₄ powder mostly forms multi-electron centres. Obtained results correlate with ESR results, and therefore it has been suggested that multi-electron centres in “pure” nano-structured Li₄SiO₄ powder mainly consists from E'

centres, due to small absorbed dose. Electron type E' centres are thermally un-stable and mainly recombine from 450 to 620. Previously with thermally stimulated luminescence method it was showed that E' centres in recombination process formed excited states of SiO_4^{4-} ions or L-centres.

Using ESR method it has been observed that up to 650 K accumulated HC_2 centres, unidentified signals and atomic hydrogen, in nanostructured powders also were unstable and recombine. $\text{H}\cdot$ and hole type HC_2 centres recombine up to 470 K, but unidentified RD recombine at temperature range from 460 to 590 K. Therefore at 570 K in radiolysis of Li_4SiO_4 pebbles should accumulate only E' centres. However at air irradiated pebbles not only E' centres, but also HC_2 centres and H^0 accumulates. It has been suggested that this effect may be related to chemisorption process of CO_2 and H_2O vapour on surface of Li_4SiO_4 pebbles at high temperature.

To understand influence of irradiation temperature and air on radiolysis of Li_4SiO_4 pebbles, annealed Li_4SiO_4 powder with SiO_2 was selected as investigation material. The nanostructured powder was deselected due to relevant composition as in pebbles.

Using TG-DTA it has been observed that up to 570 K from air on surface of annealed nano-structured Li_4SiO_4 powder with SiO_2 accumulates up to 12.0 ± 0.3 wt% of H_2O and CO_2 . In thermal treatment process both, H_2O vapour and CO_2 , in the Li_4SiO_4 powder form Li_2CO_3 and LiOH , respectively. However in obtained p-XRD characteristic patterns of chemisorption products are quite small.

It has been suggested that this effect could be related to X-ray amorphous of Li_2CO_3 and LiOH . In same time, after irradiation ($D_{\text{abs.}}=56$ kGy) at air, intensity of chemisorption products patterns increases essentially. It has been assumed that increase of intensity is related with radiation induced crystallization of chemisorption products. Radiation induced crystallization of amorphous compounds has been previously reported.

In ESR spectra of thermally treated and in air irradiated Li_4SiO_4 powder signals with g-factor 1.898, 1.998, 1.999, 2.002, 2.010, 2.015, 2.026, 2.036 and 2.193 were observed. Most intensive three signals were attributed to E' and HC_2 centres, but other to chemisorption products of LiOH and Li_2CO_3 . It has been observed that radiolysis of chemisorption products essentially affects the radiation stability of the Li_4SiO_4 powder and increases the concentration of RD up to 50% - from $2.0 \cdot 10^{18}$ to $3.0 \cdot 10^{18}$ radicals g^{-1} . Summarizing obtained results it has been concluded that radiolysis of annealed Li_4SiO_4 pebbles with SiO_2 at high temperature ($T_{\text{max}}=570 \pm 20$ K) is affected by air, i.e. chemisorption products of H_2O vapour and CO_2 . First, under action of high temperature on surface of pebbles form X-ray amorphous chemisorption products of H_2O vapour and CO_2 , i.e. LiOH and Li_2CO_3 . Second, under action of accelerated electrons chemisorption products form RD, which are radiation and thermally unstable. However, radiolysis of chemisorption products essentially decreases radiation stability of Li_4SiO_4 pebbles and increase concentration of RD up to several times.

Therefore it can be concluded that Li_2CO_3 layer which forms after annealing ($T_{\text{max}}=1243$ K, $t_{\text{max}}=168$ h, air) on surface of Li_4SiO_4 pebbles can reduce the radiation stability of tritium breeder. As well as under long term exploitation condition in HCPB module on surface of Li_4SiO_4 pebbles may increase concentration of Li_n and so could be affected tritium diffusion and caused tritium accumulation.

Main conclusions

One of options to resolve this problem is annealing of HCPB module before tritium breeder exploitation above 973 K at inert atmosphere to desorb chemisorbed gases from surface of pebbles. Second option is a change of the ceramic composition. Pebbles with Li_4SiO_4 as main phase have appropriate tritium breeder parameters, i.e. high lithium density, high melting point and good tritium release behaviour. Therefore it may be favourable to change the secondary phase and to replace Li_2SiO_3 with a less reactive and more mechanically stable lithium metatitanate (Li_2TiO_3) phase. The Li_2TiO_3 also has smaller decomposition degree, and thus it could increase radiation stability of Li_4SiO_4 pebbles.

YEAR 2013

FUSION RELATED LIQUID METAL MHD RESEARCH.

Principal investigator: E.Platacis

WP13-PEX-03B-T05-01/UNIVERSITY OF LATVIA/BS. REPORT FOR TASK AGREEMENT

TASK AREA: NOVEL PFC MATERIAL SOLUTIONS - LIQUID METALS
TASK TITLE: FIRST SIMULATIONS CONCERNING LIQUID METALS IN TOKAMAKS DIVERTOR - CPS AND FREE FLOWING LIQUIDS.

1. First simulations concerning liquid metals in tokamaks divertor

Contribution of AEUL .MHD experiments on LM Jets passing over curved substrates

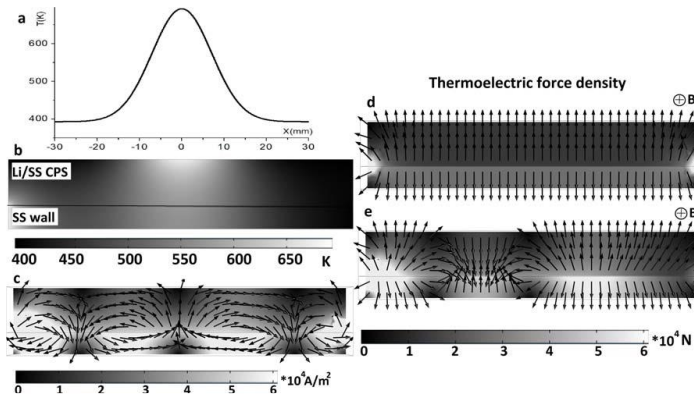
2. CPS-Modelling the convection in the porous structure.

A. To quantify the influence of EM forces on renewal of surface by capillary forces

B. To identify the main parameters affecting MHD flows in CPS



PbLi MHD loop.



Thermoelectric effects in

Summary.

The reasons for the long standing interest in free-surface liquid metal (LM) flows are well discussed. The moving free surface PFC offers the potential to solve the problems of erosion and thermal stresses, of absorbing impurities and possibly helium, of an effective heat exhaust. However, as the main performance goal for advanced limiters and divertors the acceptance of heat fluxes of $> 50 \text{ MW/m}^2$ should be considered. Different schemes have been proposed, with a rather different relation to the mentioned tasks. In the frame of EFDA the idea is prevailing that most advanced and promising are the capillary porous systems CPS where the LM is brought to contact with plasma by capillary forces. The MHD interaction becomes avoided due to the low velocity and small size of the capillary channels. Latest results gained on FTU can be found in [1]. Aiming at thermal loads as high as 10 MW/m^2 with up to 5s of plasma pulse duration an advanced version of the liquid lithium limiter, named Cooled Lithium Limiter (CLL), is proposed. Initially heat loads as high as 2 MW/m^2 for 1.5s have been withstood without problems, using water as a coolant. Lithium related investigations have been performed also at IPUL. In [2, 3, 4] the influence of a poloidal magnetic field on super-thin ($h \approx 0.1 \text{ mm}$) film flow of liquid metal at a very small linear flowrate $q \leq 1 \text{ mm}^2/\text{s}$ is considered. The creeping flow is driven by gravity and must protect the surface of a properly cooled divertor plate. As in the previous case, the liquid lithium must absorb plasma particles (hydrogen isotopes), which otherwise hit the wall and return as neutral atoms cooling the plasma edge. At the same time, liquid lithium can be replenished thus providing stationary low recycling plasma regime. Questions of the power extraction capability were not addressed. The potentially expected value $\approx 10 \text{ W/m}^2$.

We are proposing to pay attention to the potentially crucial role of thermoelectric (TE) phenomena at any application of lithium, because of its extremely high absolute thermoelectric power (20 mikroV/K). A CPS related example was considered [5]. It was demonstrated that TE currents may create forces with a significant effect on the Li flow within CPS, the liquid metal surface can be deformed, the metal can be even pushed away from the zone of the TEM forces. A Gaussian shape heat impulse in a constant magnetic field was numerically modeled (Fig.1).

According to another approach the plasma should be faced by a liquid metal in a fast motion. The high power load capability should be considered as the most distinguishing feature of these developments, especially, if high-Z materials (Ga, Sn, etc.) are introduced and high velocities ($v > 5 \text{ m/s}$) allowed. Estimates show that loads of the order of 50 MW/m^2 and even higher could be expected. Already in 1986, an essential result was achieved on the small tokamak T-3M, namely, it was shown that after a contact with a high-Z liquid metal the plasma remained alive [6]. The plasma touched upon a screen formed by InGaSn droplets. The discharges remained practically unchanged. The jets were replaced by droplets with the aim to avoid the MHD interaction. However, the generation of fast droplets turned out to be a technically difficult task; the development of this promising option was stopped. Essential are the results obtained during the joint proof-of-principal experiments on ISTTOK, where the plasma was interacting directly with a Ga jet [7, 8]. After touching with plasma (approx. 10 cm below the touching point), the jet is breaking up in droplets because of the Rayleigh instability. Interruption of the path for electric currents which can be induced along the jet is the purpose of this breakup action. The workability of the developed Ga setup was confirmed, the Ga-technology under tokamak relevant conditions mastered. It was shown once more that the interaction of plasma with Ga did not influence essentially the discharge. However, most important are the conclusion about the ability of liquid metal jets to absorb and transfer a high

indeed power. During 25 ms of discharge, the plasma was contacting with about 1 cm³ of Ga. During this short time 2.4 kW of power were extracted by a $v \approx 2$ m/s jet [8]. It means that the corresponding power extraction capacity equal to 2.4 kW/cm³. It is a high indeed value and it is attributed to a jet of a rather moderate velocity. It is essential that the jet continuity is preserved. Doubts were previously expressed that at such high loads the LM body should “explode” because of the non-homogeneous heat deposition, because of gas inclusions, etc. Finally, the old and general problem of spatial stability of such free flying jets was actualized: during the discharge, a definite deflection of the jet was detected. A possible explanation for this deviation was given in [9]. The responsible for the deflection electric currents could be generated by the non-homogeneous floating potential inside the plasma.

We propose to control the path of fast moving LM by curved substrates. It should be considered as a novel approach to the problem of spatial fixation of free surface LM flows. The relation to practice is also visible. For power extraction processes inside the chamber the introduction of curved surfaces is a logical step forward since practically all the plasma facing components are of a curved shape. However, we suggest to go even further and consider flows over curved substrates also at formulation of proposals for LM protection of high loaded divertors

We are referring to a following 2013 experiment [10,11]. The most impressive information is presented in Fig.2. A cylindrical ($R = 95$ mm) container was placed in the bore of a superconducting magnet. Three parallel $d = 2.3$ mm InGaSn jets were targeted towards the inner SS wall of this container. The $\approx 30^\circ$ angle of incidence should be considered as rather blunt. The velocities were varied from ~ 20 cm/s to ~ 60 cm/s. Exposed to a magnetic field of up to 4 T, the jets remained apart, running stably in parallel over the full length (~ 200 mm) of their path. If the jets were targeted towards a properly wetted Cu insert of the same curvature, the MHD interaction resulted in a full disorganization of the flow. To avoid a similar unwanted interaction, finally, each of the jets was directed along an apart standing insulated rail. Again, in a field of 4 T, the path of each jet remained stable over the full length of the rail (Fig.3).

Today it is difficult to give a clear explanation of such an intriguing behavior of the jets, as well as of the stability of such a specific form of MHD motion. Only very common and indefinite arguments can be used. Indications have been presented that also in the case of free-flying jets the influence of an orthogonal field is stabilizing. Gaining of additional evidences about the positive influence of substrates curvature, it should be considered as one of the tasks. However, the main aim seems to be clear - promotion towards a better understanding of the physics of the phenomenon. There are no grounds to expect for a fast outcome here. At the same time, the results must be made reliable enough for the initiation of definite engineering ideas. The already acquired experience will be used as a base for such a promotion. During the long enough time of development, different versions of LM jet protected divertors have been considered. As a base for comparison, we propose the scheme described in [12]. The general motivation could also be taken from this publication, namely, to get a stable system of jets, which are able to absorb heat fluxes of up to 50 MW/m². In a similar composition, the free flying jets could be replaced by rail-supported jets. Better performances might be expected. The high power load capability of the installation would remain practically unchanged. At the same time, the system stability could be essentially enhanced.

Interesting tendencies in the development of free surface MHD flows were demonstrated already in [13]. Experiments on InGaS were performed in fields up to 4 T. An attempt was made to generate a stable motion in a flat open bed in the presence of a

coplanar to the bottom field. Unexpected flow destroying perturbations were observed, probably caused by Hartmann-type interactions inside the flow. On the other hand, at the generation of jet-type flows the influence of the field was clearly stabilizing. In the uniform 4 T field, the initial most impressive information is concentrated in Fig.1. In parallel jets were injected. The nozzles were directed orthogonal to the field. Being subjected to the field, the 20 cm long jets started to run in a surprisingly stable way, appearing simply string-like. After targeting the outlet plate, the “traditional” splashes were also damped. Essential results on this subject can be found in [12]

It was stated that jets passing over substrates with differently prepared surfaces are behaving differently. In the above mentioned initial case the surface was badly contacting. The jets were targeted also towards a properly treated well-wetted Cu insert. Under such conditions, a good electrical contact between the LM and the substrate must also be ensured. As expected, without the field, the jets were tending to form a filmlike cover under the influence of capillary forces. In the presence of a strong field, the picture becomes unstable, fragmentary. The induced forces were able even to separate the flow from the substrate, to lift small sub-volumes, etc. It is an additional example to focus attention on problems related to the generation of film-like motions under strong fields. It is the base for the definition of one of the concrete tasks– investigation of possibly best boundary conditions for generation of stable film –like MHD flows.

However, under the conditions of the tokamak environment, the acting surfaces most probably will be properly “treated”, good-wetted and contacting, etc. Neighboring jets could start interacting in the above-described way. To avoid the potential consequences of such kind of interaction, we propose to guide each of the jets by its own separate standing isolated rail (Fig.3). To relate the described system to a real divertor, a specific configuration of the magnetic field in this region should be mentioned. The guided by the field particles are approaching the surface of the divertor at an approx. 150° angle and will be faced by the bodies of the jets. The metallic parts of the rails will remain safe in the shadow of the neighboring jets.

As already mentioned, presently it is difficult to give a clear explanation of the somewhat strange MHD behavior of the LM jets. Certain analogies could be useful. As the closest neighbor a free flying jet should be considered. It is not easy to define a single numerical parameter, which would describe the stability of a jet in a general enough way. Under definite conditions, each jet breaks up in droplets because of the Rayleigh instability. The break-up length could be considered as one of the parameters, characterizing in a definite sense the jet stability. With an acceptable accuracy, the length of the continuous part of an LM jet “L” can be described by the dependence $L/d = 4.2 \cdot Wb^{1/2}$, where d stays for the nozzle diameter. The Weber number $Wb = \rho v^2 d / \sigma$ (with

ρ being the density, v the velocity; σ the surface tension, and d the nozzle diameter) characterizes the ratio of the inertial forces to the surface tension forces. The break-up length of a jet can be defined by different semi-empirical expressions. Usually a linear dependence of $L/d = k Wb^{1/2}$ is considered. The physical parameters of liquid as well as the conditions of experiment can slightly affect the coefficient of proportionality k named also as the coefficient of stability. In general, values $k \approx 4.0$ have been accepted for the so-called quasi-turbulent regime. For liquid metals we are proposing [14] the value $k = 4.2$ in a close agreement with the mentioned general value. The conclusion is that with regard to Rayleigh instability the liquid metal jets do not stand out for some specific features.

Basing on the existing experience, an assumption can be made that the basic influence of the field on jet-type flows is stabilizing. Then the break-up length must also grow if a magnetic field is applied. And indeed, already in [12] it was suggested to express the breakup length with a magnetic field by the dependence $L = \alpha L_{\text{no field}}$, where α is a coefficient related to the Hartmann number, which varies from 1.05 to 1.14, as the velocity varies from 3 to 2.1 m/s. It is difficult to agree with the suggestion to relate the coefficient α simply to the Hartmann number. As the first approximation, the relation Ha/Re could be considered as the leading parameter, however, the dependence of L/L_0 on Ha/Re was more complex, already non-linear. Efforts to bring all of the results together [14] have resulted in the following fully empirical dependence: $L/L_0 = 1 + 0.75 \cdot Ha^{1/3} \cdot Re^{-1/4}$.

$1/4$. An opportunity appears to form some pattern of the jet behavior under reactor relevant conditions. Let us consider a Ga jet at $d = 5$ mm, $v = 5$ m/s, $B = 5$ T. The corresponding increase in length caused by the field would reach 45%.

The main components of the designed experimental setup are shown in Fig.4. Our cryogen-less superconducting magnet (5 T, in the bore with $D = 30$ cm; $L = 100$ cm) was activated. In the bore of the magnet a cylindrical container will be placed, first at all in the region of a uniform field, later also in the inlet region of a non-uniform field. Inside the container, different varieties of curved guiding substrates will be positioned. The system will be connected to our stationary InGaSn loop ($p \approx 2.5$ bar; $q \approx 100$ cm³/s). A specially designed MHD for experiments PbLi loop should also be mentioned [15]. The isothermal ($T=350^\circ\text{C}$) loop equipped with a induction pump on permanent magnets was adapted for tests in up to 5T fields of the mentioned superconducting magnet (Fig.4.).

During the years under consideration IPUL was actively working in accordance with the Memorandum of Understanding with the Institute of Plasma Research, Bhabha Atomic Research Center, India. This collaboration was registered at EFDA. The main blanket related results have been published in {16,17,18}.

References

- [1].G. Mazzitelli, M.L. Apicella, G. Apruzzese, F. Crescenzi, F. Iannone, G. Maddaluno, V. Pericoli-Ridolfini, S. Roccella, M. Reale, B. Viola, I. Lyublinski, A. Vertkov. Experiments on FTU with an actively water cooled liquid lithium limiter.
- [2] F.Muktepavela, E.Platacis, A.Sobolevs, A.Shishko, A.Zik Difficulties of creation of thin lithium film on the stainless steel substrate. The 3d International Symposium on Lithium Applications for Fusion Devices, ISLA2013, October 9-11, 2013, C.R.ENERGIA Frascati
- [3] Platacis E., Sobolevs A., Shishko A., Muktapavela F. Experimental studies of liquid lithium film flow in magnetic field. 9th International Conference on Fundamental and applied MHD, Thermo acoustic and Space technologies. Riga – Latvia. June 16-20 , 2014. V2. pp 16-19.
- [4]. E. Platacis, A. Flerov, A. Klukin, S. Ivanov, A. Sobolevs, A. Shishko, L. Zaharov, M. Gryaznevich. Gravitational flow of thin film of liquid metal in strong magnetic field. Submitted to Fus.Eng.& Des., under revision.
- [5] Kaldre I., Lielausis O. Role of thermoelectromagnetic foci in capillary porous system proposed for liquid metal cooling of fusion reactor components. 9th International Conference on Fundamental and applied MHD, Thermo acoustic and Space technologies. Riga – Latvia. June 16-20 , 2014.V2. pp 1-5.
- [6] A.F. Kolesnichenko, E.V. Murav'ev, V.N. Dem'janenko, B.O. Karasev, I.V. Lavrent'ev, O.A. Lielausis, A.V. Tananaev. Research and development liquid metal

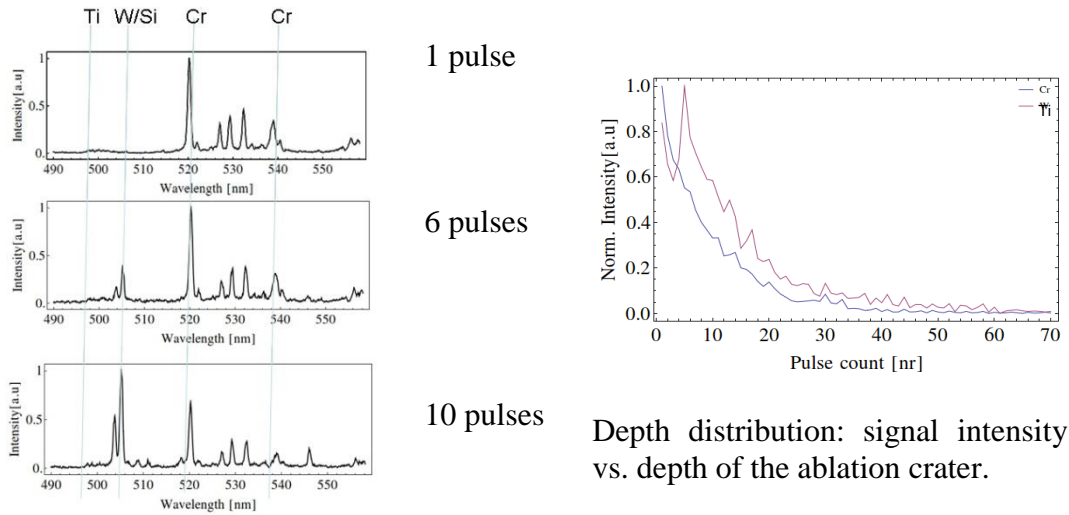
- system for a tokamak reactor. *Fusion Eng. & Design*, 1989, No.8, pp.283-288.
- [7] R.B. Gomes, C. Silva, H. Fernandes, P. Duarte, O. Lielausis, A. Klyukin, E. Platacis. Dynamic behavior of a liquid gallium jet under the influence of the Tokamak ISTTOK plasmas. *The 19 Intern. Conf. on Plasma Surface Interaction*, P2-83, May 24-28 (2010) Sam Diego, USA.
- [8] R.B. Gomes, C. Silva, H. Fernandes, P. Duarte, I. Nedzelskiy, O. Lielausis, A. Klyukin, E. Platacis. ISTTOK tokamak plasmas influence on a liquid gallium jet dynamic behavior. *Journal of Nuclear Materials*, 415, S989-S992, (2011).
- [9] L. Benos, N. Pelekasis, R. Gomes. Interfacial stability of liquid metal flow in the presence of an electromagnetic field. *The 3d International Symposium on Lithium Applications for Fusion Devices, ISLA2013*, October 9-11, 2013, C.R. ENEA Frascati.
- [10] O. Lielausis, A. Klyukin, E. Platacis. MHD experiments on LM jets passing over curved substrates. *The 3d International Symposium on Lithium Applications for Fusion Devices, ISLA2013*, October 9-11, 2013, C.R. ENEA Frascati.
- [11] Lielausis O., Platacis E., Klyukin A., Peinbergs J. LM jet and film flows over solid substrates in strong magnetic fields. *9th International Conference on Fundamental and applied MHD, Thermo acoustic and Space technologies. Riga – Latvia. June 16-20, 2014. V2. pp 20-24.*
- [12] A.Y. Ying, M.A. Abdou, N. Morley, T. Sketchley, R. Wooley, J. Burris, R. Kaita, P. Fogarty, H. Huang, X. Lao, M. Narula, S. Smolentsev, M. Ulrikson. Exploratory studies of flowing liquid metal divertor options for fusion-relevant magnetic fields in MTOR facility. *Fusion Eng. & Des.* 72 (2004) 35-62.
- [13] I. Bucenijs, O. Lielausis, E. Platacis, A. Shishko. An experimental study of liquid metal film and jet flows in a strong magnetic field. *Magnetohydrodynamics. Vol.30 N.2 1994, pp 179-187*
- [14] O. Lielausis, A. Klyukin, E. Platacis, A. Mikelsons, R.B. Gomes, H. Fernandes, C. Silva. Stability of liquid metal jet in the context of fusion applications. *Proc. Int. Conf. on Fundamental and Applied MHD, PAMIR 2011, vol. 1, p. 257-260 (Borgo-Corsica-France September 5-9, 2011*
- [15] Ivanov S., Shishko A., Flerov A., Platacis E., Romanchuks A., Zik A. MHD PbLi loop at IPUL. *9th International Conference on Fundamental and applied MHD, Thermo acoustic and Space technologies. Riga – Latvia. June 16-20, 2014. V2. pp 76-80.*
- [16] Bhattacharyya, R.; Patel, A.; Ellappan, R.; Swain, P. K.; Kumar, S.; Ivanov, S.; Shishko, A.; Platacis, E.; Ziks A. : Liquid metal MHD experimental activities for LLCB TBM development. *Fusion Engineering and Design* 88 (2013) 2244–2250.
- [17] Swain, P.K.; Satyamurthy, P.; Bhattacharyya, R.; Patel, A.; Shishko, A.; Platacis, E.; Ziks, A.; Ivanov, S.; Deshpande, A.V. : 3D MHD lead–lithium liquid metal flow analysis and experiments in a test-section of multiple rectangular bends at moderate to high Hartmann numbers. *Fusion Engineering and Design* 88(2013) 2848-2859
- [18] Patel, A.; Bhattacharyya, R.; Swain, P.K.; Satyamurthy, P.; Sahu, S.; RShishko, A.; Platacis, E.; Ziks, A.: Liquid metal MHD studies with non-magnetic and ferro-magnetic structural

Principal investigator: Dr. I. Tale

Laser-induced breakdown spectroscopy (LIBS) had been performed for the W/Cr/Ti samples on different substrates: sapphire, quartz, and silicon wafer with Cu interlayer. Nd:YAG pumped diode laser with pulse width of 9 ns, repetition rate of 1 kHz, and laser power density of 0.85 J/cm² with 1064 nm wavelength has been used for sample ablation. The material ablation rate was in average 7 nm per laser pulse. The samples were ablated in the vacuum chamber with the pressure of 10⁻⁵ Torr.

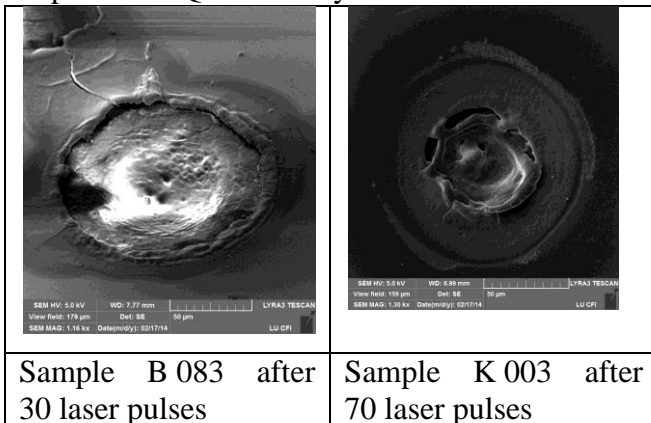
The typical results for the samples with different substrates are the following:

Sample K 003; W/Cr/Ti content 83/15/2; substrate: silicon wafer with Cu interlayer.



Depth distribution: signal intensity vs. depth of the ablation crater.

Similar LIBS Depth profiles have been obtained for samples on substrates Cu+Si, Sapphire and Quartz. Analysis of the LIBS crater SEM analysis



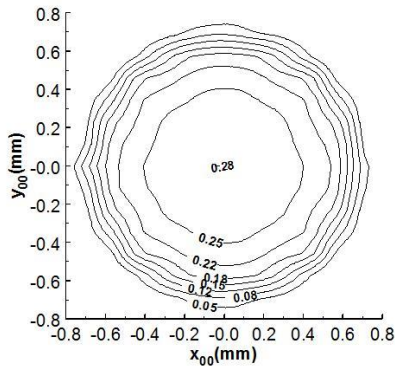
The decrease of the signals on the depth distribution plots can be explained with unsuccessful beam focussing and on the 90° to the ablation laser beam. Due to the low intensity required for the minimal ablation rate, the plasma plume had disappeared inside the crater forming, and the light became undetectable. Experiments have been performed

using defocused picosecond laser beam to increase the diameter of the crater, avoid boiling and increase the resolution of the determination of the element concentrations and material ablation rate. The W/Cr/Ti layer depth does not depend on the substrate material.

PLASMA PHYSICS TOPICAL GROUP: TG-MHD

Principal investigator O. Dumbrajs

The theory describing the operation of gyrotrons with tilted and shifted electron beams has been developed. Effects of the tilt and shift are studied for a 1 MW, 170 GHz gyrotron, which is presently under development in Europe for electron cyclotron resonance plasma heating and current drive in the International Thermonuclear Experimental Reactor (ITER). It is shown that one should expect significant deterioration of gyrotron operation in such gyrotrons when the tilt angle exceeds $0.4-0.5^\circ$ and the parallel shift of the beam axis with respect to the axis of a microwave circuit is larger than 0.4-0.5 mm. At the same time, simultaneous tilting and shifting in a proper manner can mitigate this deteriorating effect.



Efficiency as a function of transverse coordinates in the case of parallel displacement.

O. Dumbrajs and G.S. Nusinovich “Effect of electron beam misalignments on the gyrotron efficiency” Phys. Plasmas 20, 073105 (2013).

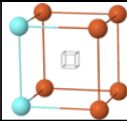
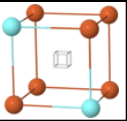
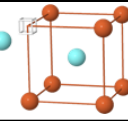
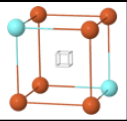
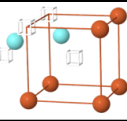
MATERIALS MODELING

Principal investigator: E.A. Kotomin

2013A. INTERACTION BETWEEN VACANCIES AND DIMERS OF SINGLE Y IMPURITIES IN BCC-FE LATTICE

The bonding between isolated Y_{Fe} atom and $V_{Fe}-Y_i-V_{Fe}$ complex has been analysed. At the distances of the $3NN$ and smaller, Y_{Fe} transforms $V_{Fe}-Y_i-V_{Fe}$ complex into $Y_{Fe}-V_{Fe}-Y_{Fe}$ configuration. The strongest attraction has been observed for the defect aligned along the

[111] direction. Starting from the 4NN the interaction becomes weaker and does not exceed 0.15 eV. Interaction between the two V-Y_i-V complexes is attractive too. At three closest distances, without overlapping vacancies, binding energy between the complexes is about 1.3-1.4eV.

models					
NN distance	1	2	3	3	2
E_{bind} , eV	0.30	1.03	0.27	1.16	1.3

2013B.DEPENDENCE OF INTERACTION BETWEEN V_{FE} AND Y IMPURITIES ON SIZE OF FCC-FE SUPERCELL

Calculations of multiple defects require the increase of supercell (SC) size. In order to increase the size of the SC, it has been necessary to perform additional analysis if the results of the calculations performed on the increased SCs reproduce the earlier results received in smaller SCs. The test calculations performed for 5×5×5 SC have reproduced both qualitatively and semi-quantitatively the results received for 4×4×4 SC. Further variation of cut-off energy has not been required and the cut-off energy value of 800 eV has been fixed in further calculations since it was found to be optimal previously. It has been also necessary to perform the calculations of point defects in *fcc*-Fe lattice, in order to check if those results received in the calculations of 4×4×4 supercell are reproducible within 5×5×5 SC. In order to do this, the binding energies received within the calculations of 4×4×4 and 5×5×5 SCs between Y and vacancy have been compared. The corresponding results are present below, clearly showing that the absolute values of E_{bind} between defects slightly decrease with SC increase which could be explained by the decreased influence of defect periodic images.

Bonding in Y_{Fe}-V_{Fe} pairs in γ -Fe lattice

Supercell	4×4×4	5×5×5
Configuration	E_{bind} , eV	E_{bind} ,
1NN	1.67	1.42
2NN	-0.21	-0.07
3NN	0.30	0.14
4NN	0.40	0.30

JW13-FT-1.21. AMS AND FCM + LSC INVESTIGATION OF FUEL RETENTION IN VARIOUS JET TILES

Principal investigator G.Kizane

The task of the EFDA JET Technology project JW13-FT-1.21 “AMS and FCM + LSC Investigation of Fuel Retention in Various JET Tiles” is estimation of influence of tungsten layer on a surface of a tile on tritium accumulation, on a profile of tritium. The project was realized in cooperation with EURATOM associations of Romania, MEDC and Finland, TEKES.

The accumulation of fusion fuel in the vacuum vessel materials of fusion devices, especially in a divertor region, has always been one of the major problems for various fusion devices. In order to reduce the fuel retention the constructions as well as materials of a divertor are constantly upgraded.

Tungsten W coating for carbon fibre composite (CFC) material is proposed as the latest upgrade for pure CFC material divertor used in JET. The 15 – 25 μm W coating with molybdenum Mo or rhodium Rh interlayers are meant to decrease the sputtering of plasma facing materials and to decrease accumulation of fusion fuel on the surface and in the bulk of divertor materials.

Analysed tiles are from the JET campaign 2007 – 2009 of divertor MkII-HD and from the campaign 2010 – 2012 of divertor MkII-HD ILW. Samples from tungsten non-coated tiles are following - MkII-HD divertor – 2BNG4C, 2BNG6D, 2ONG7A and 2ONG8B. Samples from tungsten coated tiles of divertor MkII-HD (ITER Like Wall)-2BNG6C, 2ONG7A*, 2ONG8B* (* further in the text means that samples are from campaign 2010-2012).

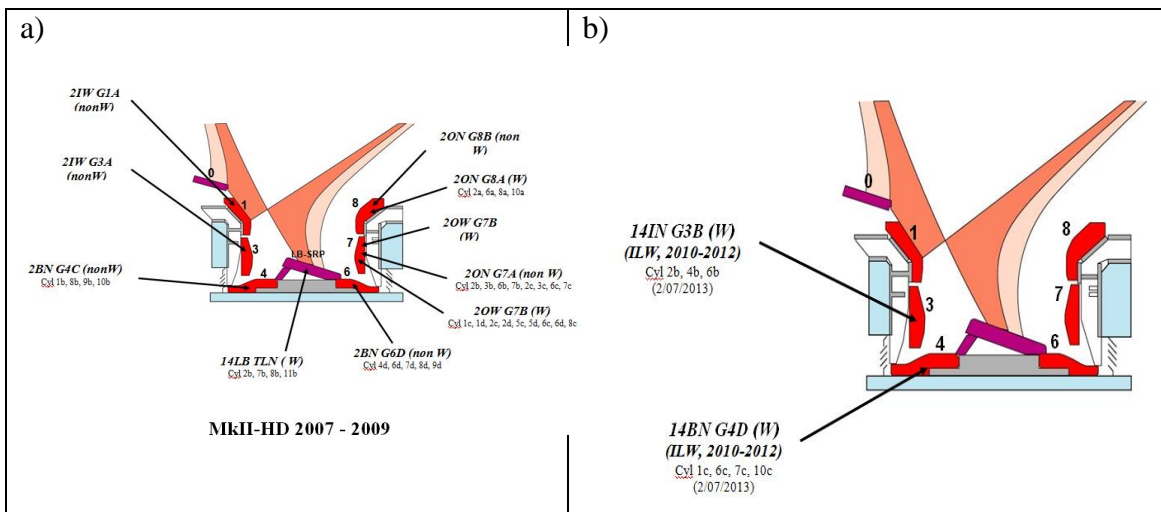


Figure 24. Cross-section of the divertor MkIIHD and analysed tiles: a) campaign 2007-2009, b) 2010-2012.

Comparison of tritium accumulation in W-coated (200 μm tungsten coating for 2007 - 2009 or ~ 25 μm tungsten coating for 2010 - 2012 samples with molybdenum or rhodium interlayer) and non-coated CFC tiles of JET divertors was made. As tungsten has higher density and is less affected by sputtering than carbon, it should decrease the total amount of accumulated tritium and prevent its transport in the tiles.

Samples of vertical tile 14ING3B top layer have tritium mass activity of $(0.13 \div 0.21) \cdot 10^5 \text{ Bq} \cdot \text{g}^{-1}$ whereas horizontal “floor” tile 14BNG4D sample activity increases from $0.15 \cdot 10^5 \text{ Bq} \cdot \text{g}^{-1}$ to $0.37 \cdot 10^5 \text{ Bq} \cdot \text{g}^{-1}$ towards the central load-bearing tile of the divertor.

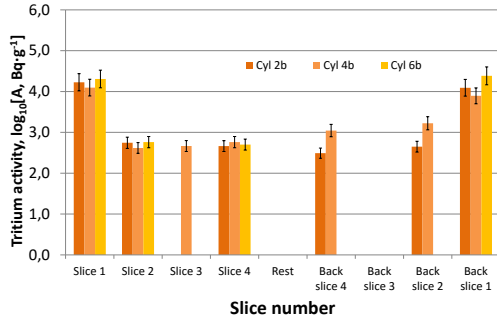


Figure 25. Tritium mass activity in Tile 14ING3B (W-coated, ILW, 2010-2012) cylinders Cyl2b, Cyl4b and Cyl6b (combusted in 2013)

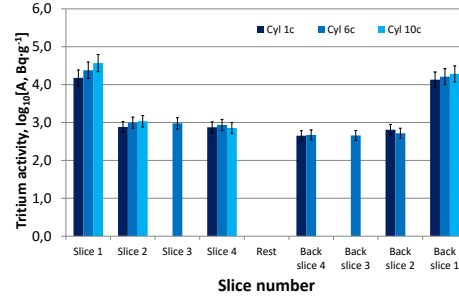


Figure 26. Tritium mass activity in Tile 14BNG4D (W-coated, ILW, 2010-2012) cylinders Cyl1c, Cyl6c and Cyl10c (combusted in 2013)

The bulk activity of 14ING3B and 14BNG4D tile samples gradually decreases until roughly 1 mm in depth of tile and remains constant at $(0.46 \div 0.56) \cdot 10^3 \text{ Bq} \cdot \text{g}^{-1}$.

The W-coated tile 2BNG6C has a homogeneous surface tritium activity with average values being $4.7 \cdot 10^4 \text{ Bq} \cdot \text{g}^{-1}$ and bulk activity – $4.6 \cdot 10^3 \text{ Bq} \cdot \text{g}^{-1}$.

Samples of W-coated tile 2ONG7A* has average surface tritium activity $1.8 \cdot 10^4 \text{ Bq} \cdot \text{g}^{-1}$ with bulk tritium activity of $10^3 \text{ Bq} \cdot \text{g}^{-1}$ level.

W-coated tile 2ONG8A* show average activity of $5 \cdot 10^4 \text{ Bq} \cdot \text{g}^{-1}$ at the top layer and approximately the same bulk activity as in tile with no tungsten coating – $3 \cdot 10^3 \text{ Bq} \cdot \text{g}^{-1}$.

The obtained results for non-covered CFC tile 2BNG4C show that average surface tritium activity is in range of $(0.7 \div 6.7) \cdot 10^5 \text{ Bq} \cdot \text{g}^{-1}$ while volume activity is at a level of $3.7 \cdot 10^3 \text{ Bq} \cdot \text{g}^{-1}$.

For the floor tile 4 it can be concluded that by coating divertor with W coating, surface activity reduced by a factor of 20, also reducing bulk tritium activity by more than 4 times. As a result of less divertor material erosion and further tritium accumulation in erosion materials, bulk activity is also diminished as the total amount of tritium on the surface layer available for volume diffusion processes is reduced.

For the divertor floor tile 6, being in a “shadowed” zone of direct plasma interaction, accumulation of erosion materials on the surface is of a great importance. Tile with no coating 2BNG6D had average surface tritium activity $5.5 \cdot 10^5 \text{ Bq} \cdot \text{g}^{-1}$ rapidly changing by a factor of 30 for samples in “open” part of the tile to “shadowed” part where direct plasma has almost no interaction with the tile surface.

As for tile 7, the non-coated tile 2ONG7A has average surface tritium activity $5.4 \cdot 10^4 \text{ Bq} \cdot \text{g}^{-1}$ with bulk tritium activity of $1.7 \cdot 10^3 \text{ Bq} \cdot \text{g}^{-1}$.

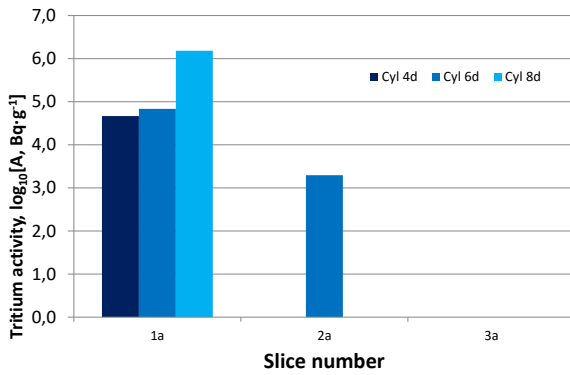


Figure 27. Tritium mass activity comparison in: Tile 2BNG6D (non W-coated) cylinders Cyl4d, Cyl6d, Cyl8d, combusted in 2013 JET MkII-HD divertor (2007 - 2009)

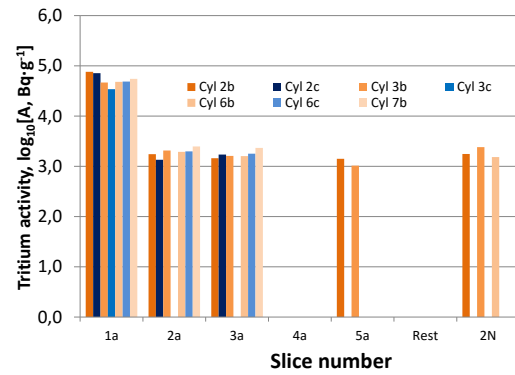


Figure 28. Tritium mass activity comparison in Tile 2ONG7A (non W-coated) cylinders Cyl2b, Cyl2c, Cyl3b, Cyl3c, Cyl6b, Cyl6c, Cyl7b, combusted in 2013 JET MkII-HD divertor (2007 - 2009)

W coating reduces the total amount of tritium collected, but the effect is much less significant than for tile 4 being under more frequent plasma interaction during fusion, the bulk activity remains almost the same. Therefore it could be concluded that kinetic collision-like tritium access through the surface of divertor tiles is much less influential for the bulk activity. It can be assumed that tritium bulk activity levels are mainly driven by diffusion processes rather than a rapid kinetic process during the plasma interaction with the divertor.

The reducing effect of tritium accumulation is even smaller for the tile 7 samples. While coating slightly decreases the tritium surface activity for a tile that has small direct plasma-facing surface interaction time, the bulk activity remains similar to previously described tiles.

Main conclusions

As observed in previous researches, the difference of tritium activity in the upper layer of divertor can reach even the magnitude of 5 powers with average bulk activity level of $10^4 \text{ Bq}\cdot\text{g}^{-1}$. While tungsten-coated materials as showed have a steady difference of less than 2 magnitudes with slightly lower bulk activity ($3\cdot 10^3 \text{ Bq}\cdot\text{g}^{-1}$).

W coating is unarguably effective in reducing tritium accumulation on the surface and in the bulk of divertor tiles. It is clearly shown in performed experiments that tungsten coating decreases the accumulation of tritium in the top layer. This is due to smaller penetrability of tungsten for tritium and lesser sputtering material in which tritium has been previously collected on carbon fibre composite divertor tiles. The efficiency of this process varies and the best results would be achieved for the tiles that have more plasma-facing surface interaction time and higher energy load. The research also shows that W coating barely affects the tritium bulk activity and most likely comparably slower processes of diffusion are happening that would need detailed studies.

JW13-FT-1.21 Preparation for the analysis of long chain hydrocarbon in JET flake/dust material using TGA/DTA coupled to QMS & FTIR

The goal of the EFDA JET task JW13-FT-1.23 “Preparation for the analysis of long chain hydrocarbon in JET flake/dust material using TGA/DTA coupled to QMS & FTIR” is to analyse and compare properties of decomposition of dust/flakes, fullerene C₆₀, n-eicosane, n-triacontane, n-tetracontane, pentacontane and hexacontane in inert and in air atmosphere in order prepare to analyse real plasma exposed samples from JET vacuum vessel containing tritium and other impurities.

In the year 2013 analysis of inactive carbon dust prepared from whole inactive carbon fibre composite (CFC) tile, fullerene C₆₀, separate long chain hydrocarbons and mixtures prepared from inactive CFC dust with additions of long chain hydrocarbons, as well as analysis of real deposited and collected carbon dust from the JET vacuum vessel inner divertor “Pot D” of the year 2010 were realized.

The inactive Joint European Torus (JET) dust sample was prepared from a carbon tile. From an inactive JET carbon tile that was not installed in JET machine and thus contained no tritium and no beryllium, 1.5 mm thick slices were mechanically cut with a saw and then broken up to simulate flakes removed/recovered from JET machine. Different sizes of flakes and associated dust were collected. The dust resulting from the flake preparation was collected for analysing in University of Latvia.

High purity substances for mixtures were delivered by Sigma-Aldrich. The delivered substances were an allotrope of carbon fullerene C₆₀ (sublimed 99.9%) and five long-chain hydrocarbons with 20-60 carbon atoms in chain: n-Eicosane (99.9%), n-Triacontane (99.1%), n-Tetracontane (99.2%), Pentacontane (99.9%) Hexacontane (99.9%). The active dust sample was collected from JET inner divertor, “Pot D” in 2010.

Analysis of inactive JET dust material show that particle size in CFC dust material varies from nanometre size up to hundreds of micrometres. The shape of particles was characterized using SEM. The particles can be divided in two groups: separate particles and non-separated. The ‘non-separate’ particles are more than 100 µm large parts of CFC tile material, containing fibres. The separate particles are as flakes, particles of irregular shape and cylindrical type particles. There are two types of cylindrical particles. One type of cylindrical particles is with rough surface and diameter more than 10 µm and the others are with smooth surface and diameter below 10 µm. The length of cylindrical particles varies around 10-100 µm.

The particles of irregular shape are also with smooth and rough surface. Size of such particles varies from few to several tens of micrometres. The smallest particles are flake like with a size below 1 µm. The variety of shape and size of particles is in wide range and can represent the dust and flakes formed in the vacuum vessel of JET reactor.

The inactive dust material was analysed with infrared and Raman spectroscopy. In FT-IR spectra in a region 900-1000 cm⁻¹ is a broad signal of C=C double bond. Signals in the spectra around 2850-3000 cm⁻¹ show a presence of sp³ hybridized carbon bonds representing signature of sp³ aliphatic groups. Symmetric deformation vibration of CH₃ groups appears at around 1455 cm⁻¹. In spectrum of inactive CFC dust material this signal is close to background level. The presence of graphite as the main phase was approved by Raman spectroscopy. In the Raman spectra of CFC dust material the most intensive is a

peak at 1580 cm^{-1} . This peak, called G-band (from Graphite), is due to the bond stretching of both aromatic and aliphatic C-C pairs. A broad peak at 1350 cm^{-1} , D-band (Disorder-related) is due to the breathing of aromatic rings and/or the presence of disorder. One more band that appears in case of disordered graphite is a D'-band at ca. 1620 cm^{-1} . In Raman spectra of inactive CFC dust the D'-band is observed as a shoulder of G-band. The centre of D'-band (1617 cm^{-1}) was obtained by fitting the Raman spectrum with three Lorentz peaks. The ratio between intensities of D- and G-band (I_D/I_G) is one of several parameters used to characterize the material – as larger is the value of intensity ratio as more disordered is the material. For CFC dust the I_D/I_G value is not closing to one, it is 0.32 meaning that the material consists mostly from well-structured graphite with the disordered structures for examples on the edges of crystallites. In p-XRD pattern in 2Θ range from 20° to 60° graphite reflexes are observed. The 002 diffraction peak was fitted with a Gaussian line. Asymmetry observed for 002 diffraction peak is probably due to both fibre particle and pyrolytic components. Position of 002 maxima 26.32° . The interplane distance is deduced from the position by the diffraction relation and $d=0.338\text{ nm}$ for the inactive dust. That is not differing much from expected graphite value of 0.335 nm , showing that the crystalline part of CFC dust material consists mostly from graphite. The linear dimension of the particles calculated from Scherer relation is 330 \AA . A reference ESR spectrum was taken for the inactive CFC dust materials and the obtained g-value 2.001 is close to a free electron g-value. No other signals were observed showing that material contains no other paramagnetic centres.

The thermal properties of the inactive CFC dust material were investigated with thermogravimetry (TG) in combination with differential thermogravimetry (DTG) and differential thermal analysis (DTA). The samples were heated with controlled heating rate in inert and air atmosphere. The slow heating rates ($0.5; 1\text{ Kmin}^{-1}$) allowed following precisely to mass changes, faster heating rates ($5\text{ and }10\text{ Kmin}^{-1}$) give more intensive signals. The samples were heated in opened ceramic pans (diameter 5 mm , height 5 mm). The kinetic parameter – activation energy (E_a) was calculated with Ozawa-Flynn-Wall (OFW) method, using 5 different heating rates. The basic principle of OFW method is that at a constant conversion, the plot $\lg\beta$ versus $1/T$, obtained from a series of experiments performed at several heating rates, results as a straight line whose slope allows evaluation of E_a . The conversion fraction (α) is calculated from the mass change of material during one process. At each temperature α is calculated from mass loss as the difference between initial mass and the mass at exact temperature divided with a difference between initial mass and the mass at the end of the process. E_a is calculated for each value of α individually. In the average, all calculated E_a of oxidation complies with the graphite oxidation activation energy equal to 2.01 eV . The calculated oxidation activation energy for the CFC dust material is $1.99\pm 0.16\text{ eV}$. In case of sublimation in inert atmosphere (N_2), the process is more affected by particles size; the smaller particles are decomposing and subliming faster than the bigger particles. The activation energy for sublimation of CFC dust material is $1.7\pm 0.6\text{ eV}$. Furthermore the values of E_a are decreasing while α increase, meaning that sublimation process is affected not only by size of particles but by volume of initial sample as well. From these reasons for using the kinetic parameters, like of E_a oxidation for describing the CFC dust containing materials, a heating in air atmosphere was proposed.

The set of analytical methods was used to characterize the inactive CFC dust material as the reference material for inactive mixtures containing CFC dust and active dust collected from JET vacuum vessel.

Analysis of additives of fullerene C₆₀ and long-chain hydrocarbons

Plasma-wall interaction in uncovered places may lead to formation of carbon based compounds like fullerenes and long-chain hydrocarbons. In order to analyse such dust and flakes, pre-analysis of several long-chain hydrocarbons and fullerene C₆₀ was performed to use the obtained results for next steps – analysis of mixtures prepared from inactive CFC dust material and chosen additions. Each component was analysed with FT-IR and Raman spectroscopy and with TG/DTA. Three of long-chain hydrocarbons with lowest boiling points - n-Eicosane, n-Triacontane and n-Tetracontane, were analysed with gas chromatography (Shimadzu GC 2010 gas chromatograph). In the chromatogram three separate peaks were observed.

In FT-IR spectra three types of bond are observed for all analysed long chain hydrocarbons. The observed bonds are in agreement with described in literature: CH₂ and CH₃ stretching modes at 2850, 2920, and 2954 cm⁻¹, an HCH scissor at 1474 cm⁻¹, a CH₃ asymmetric bending mode at 1464 cm⁻¹, a methyl symmetric and methylene wagging mode at 1370 cm⁻¹, and a methylene rocking doublet at 719 and 729 cm⁻¹. The advantage for using transmittance FT-IR for analysing mixtures containing long chain-hydrocarbons is the high qualitative sensibility to stretching and bending deformations of C-H bonds. The disadvantage is the fact that signal intensity is more dependent of the amount of C-H bonds overall the sample, not from length of chain. In Raman spectra of long-chain hydrocarbons characteristic signals at frequencies of single bonds to hydrogen and carbons are observed and are in agreement with literature: terminal rocking of methyl group at 835-975 cm⁻¹, -CH₃ in unbranched alkyls at 1056-1060 cm⁻¹ and -CH₂- at 1070-1140 cm⁻¹, -CH₃ in unbranched alkyls at 1135-1150 cm⁻¹, -CH₂- at 1295-1305 cm⁻¹ and -CH₂- at 1443-1473 cm⁻¹ [9].

In FT-IR spectrum of fullerene C₆₀ four allowed modes at 526, 575, 1182 and 1429 cm⁻¹ are observed. In Raman spectrum the most intensive signal is at 1425 cm⁻¹, the Raman active modes at 534, 709, 772, 1425, 1575 cm⁻¹ are observed as well but with comparable weaker intensities. In p-XRD pattern of C₆₀ eight reflexes, in interval from 10 to 35 degree, are observed: 111; 220; 311; 222; 331; 420; 422 and 511. Only a 331 reflex is partially overlapping with graphite 002 reflexes. That shows that it is possible to distinguish the presence of crystalline fullerene C₆₀ in graphite containing sample.

The thermal analysis was performed for each separate substance and for mixtures prepared from long-chain hydrocarbons and fullerene C₆₀. Separate long-chain hydrocarbons and fullerene C₆₀ were heated with two heating rates in air atmosphere to compare the mass change and heat effects, like melting and decomposition heat. With slow heating rate 1 kmin⁻¹, the detection of mass change is more precise. With a faster heating rate 10 Kmin⁻¹ the heat effects (changes in DTA signal) are more clearly observable. The melting temperatures of five separately analysed long-chain hydrocarbons were compared with theoretical and given by producer. Heating separate n-triacontane and n-tetracontane and additional endothermic peak appears just before melting, that could be because of phase changes in structure of these hydrocarbons.

The enthalpies of melting were calculated to obtain if this parameter can be used to quantitate the amount of long-chain hydrocarbons present in CFC dust. Calculated melting enthalpies can be used as additional information to determine presence of hydrocarbons in mixtures. However the results are not exactly fitting to theoretical values the combination of obtained melting temperature and calculated enthalpy can be used for detecting presence of long-chain hydrocarbons in mixtures.

For further investigations it was assumed that dust collected from JET vacuum vessel contain basically carbon and additions of hydrocarbons.

There were made mixtures with addition of separate long chain hydrocarbons. The mixtures were made by adding one or several long-chain hydrocarbons to CFC. One set of mixtures was made in such way that to 95 mg of CFC was added 5 mg of either one of hydrocarbons or fullerene C₆₀. For precise observation of mass change slow heating rate 1 Kmin⁻¹ was used. It was obtained that in mixture containing CFC dust materials and an addition, until decomposition of additive practically no mass change can be observed. As the decomposition of additives is exothermic, it enhances decomposition of CFC dust particles as well. A slight slope in mass change of CFC appears just after decomposition of additive, consequently presence of long-chain hydrocarbons and fullerene C₆₀ enhances decomposition of CFC dust material. Thus it was concluded that the heating rate can be increased to obtain the heat effects, but not too much to still obtain the mass exchanges.

Mixtures containing exact amount of long chain-hydrocarbons were heated in nitrogen atmosphere with heating rate 10 Kmin⁻¹. The complete decomposition of additives took place with sharp decrease of mass at decomposition temperature, but the DTA signals were less intensive. Heating a mixture of long-chain hydrocarbons in same conditions, several endothermic peaks were observed, but because of overlapping, it was not possible to distinguish precisely each hydrocarbon from its melting temperature. Mixing together long chain hydrocarbons and heating them in air, the same tendency appear – the melting temperatures are overlapping.

As an optimum for thermal analysis of mixtures containing comparably small ($\leq 2\%$) amount of long-chain hydrocarbons and fullerene C₆₀, a heating rate 5 Kmin⁻¹ was preferred, optimal mass of analysed sample was found to be around 5 mg. In this case it is possible to distinguish the melting processes between separate additives.

Analysis of deposited and collected carbon dust

Dust collected from JET vacuum vessel in 2010 “Pot D” were analysed with SEM and EDX. The particle size is comparable with dust material prepared from inactive CFC tile. Particle size varies from nanometre-size to several hundred μm . From the shape particles can be separated in flakes, layered pieces, particles with irregular shape, with smooth, layered or porous surface. The groups can be generalized in two main groups: flakes – particles that exhibit a layered structure, representing the archaeological deposition and dust – particles with globular or irregular shape. Size of flakes can be up to 0.5 mm, thickness is mostly several tens of μm . Surface of flakes is either smooth or with cracks. The cross-section of flakes represents several with several distinguishable layers. Dust particles with size around 10-50 μm contain impurities – oxygen, nickel, boron, chromium, beryllium. From Raman spectra it is obtained that dust and flakes contain graphite (a G-peak at 1585 cm⁻¹) and disordered graphite structures (D-peak at 1350 cm⁻¹).

¹). The broadening of G-peak and intensity ratio I_D/I_G value close to 1 points to presence of amorphous carbon. In other type of Raman spectra photoluminescence background is observed. Increasing photoluminescence background in visible Raman spectrum is a typical signature of increased H content. The sp^2 and sp^3 hybridized carbon clusters contain different structural units with C=C double bonds and C-H chains, which induce different energy states in band tail and form different radiative recombination centres. Nevertheless in Raman spectrum increasing luminescence level and graphite peaks dominate over other signals, a shoulder in spectrum observed around 840 cm^{-1} might correspond to terminal rocking of methyl group at $835\text{-}975\text{ cm}^{-1}$. In Raman spectrum of deposited layer on side surface of inner divertor vertical tile No.3 the luminescence background is even dominating over the graphite signals (D- and G-peak). Leading to a conclusion that in dust and flakes collected from JET vacuum vessel contain graphite and hydrogenated carbon particles, but a deposited layer on surface of divertor tile could be hydrogenated amorphous carbon film. Surface of deposited layer is rough, contains bubble-like structures and is light reflecting, showing that it might contain metallic impurities.

The structure of CFC tile was investigated also in direction from plasma facing surface to bulk of material. Making mapping starting from $5\text{ }\mu\text{m}$ to $65\text{ }\mu\text{m}$ from plasma facing surface, no periodical change in shape of spectra is observed. The characteristic parameter, intensity ratio between D- and G-peak varies from 0.2-0.5. That allows concluding that formation of amorphous hydrogenated carbon films forms more intensively on the surface of divertor tiles and already in few micrometres in bulk of CFC material, spectra of graphite material are close to reference.

On tungsten covered surfaces, in places where due to plasma wall interaction, the tungsten layer has been ablated, presence of tungsten oxide is observed. In Raman spectrum it appears as a broad, intensive signal at around 800 cm^{-1} . Tungsten oxide may form in temperatures above 800 K.

Although the main changes in structure and content takes place on plasma facing surface, the presence of hydrogen containing compounds in bulk of material is observed. Thermal desorption spectroscopy show that in lower temperatures substances with small mass (2, 4) are released, higher masses (12-18) are released in higher temperatures, over 1300 K, with heating rate 4 K s^{-1} .

Main conclusions

Plasma-wall interaction in uncovered places of a tile may lead to formation of carbon based compounds like fullerenes and long-chain hydrocarbons. In order to analyse such dust and flakes, pre-analysis of several long-chain hydrocarbons (LCH) and fullerene C_{60} was performed to use the obtained results for analysis of mixtures prepared from inactive CFC dust material and chosen LCH -n-triacontane, n-tetracontane and n-pentacontane as well as C_{60} . Using set of analytical methods allow to detect LCH and C_{60} in CFC dust materials.

The dust and flakes collected from JET vacuum vessel contain graphite and hydrogenated carbon particles, but a deposited layer on surface of divertor tile could be a hydrogenated

amorphous carbon film. Surface of deposited layer is rough, contains bubble-like structures and is light reflecting, showing that it might contain metallic impurities.